Vibrational Spectroscopic and Related Studies of

Lipid/Protein Interaction in Lung Surfactant Models

by

GUANGRU MAO

A Dissertation submitted to the

Graduate School-Newark

Rutgers, The State University of New Jersey

in partial fulfillment of the requirements

for the degree of

Doctor of Philosophy

Graduate Program in Chemistry

written under the direction of

Professor Richard Mendelsohn

and approved by

_____

_____

_____

_____

Newark, New Jersey

May, 2010

Copyright page:

ABSTRACT OF THE DISSERTATION

Vibrational Spectroscopic and Related Studies of

Lipid/Protein Interaction in Lung Surfactant Models

By GUANGRU MAO

Dissertation Director:
Professor Richard Mendelsohn

Lung surfactant, a lipid/protein complex located at the air/alveolar lining of the mammalian lung, facilitates the work of breathing and prevents alveolar collapse. Lung surfactant associated proteins SP-A and SP-D are also involved in pulmonary innate immune response. The deficiency or dysfunction of lung surfactant may lead to pathological conditions of lungs.

The "squeeze out" hypothesis was proposed in 1960s to explain the mechanism of the surface tension lowering functions of lung surfactant. It suggests that non-DPPC components are squeezed out during expiration from the monolayer and form a multilayer structure attached underneath the monolayer at high compressions. This multilayer structure serves as a surfactant reservoir to supply surfactant for the following surface expansion. Multilamellar structures have been observed in alveolar surface film and with lung surfactant models; however, its composition is not known thoroughly. In this thesis, substrate-supported films were transferred from air/water interface by a novel technique termed "COVASP", which transfers films under continuous surface

compression. Model lung surfactant systems containing DPPC, DPPG, SP-C and cholesterol were used in this study. The COVASP films with a broad surface pressure coverage were characterized by IR imaging. The relative composition of multilayers was probed by the IR absorbance of characteristic vibrational modes for each component. The results showed that both phospholipids and SP-C were present in multilayers, but DPPC was concentrated to a lesser extent compared to DPPG and SP-C.

The application of COVASP-IR imaging was further extended to evaluate the synthetic biomimetics of lung surfactant SP-C for potential therapeutic use. A class of N-substituted polyglycine molecules with helical structures has been synthesized as SP-C mimics by our collaborators. The ability of these peptoids to form multilayers was studied by COVASP and AFM and was compared to native SP-C. It is found that palmitoylated peptoid was able to form multilayers with lung surfactant model used, but only at a higher peptoid concentration. In addition, the extent of multilayer formation was also lower when compared to SP-C.

As a component of pulmonary innate immune system, SP-A directly binds to a series of bacteria and microbes. LPS, constituents of bacterial outer membrane, are ligands of SP-A. The mode of interaction between SP-A and LPS was studied by IRRAS. It is speculated that SP-A interacted with LPS acyl chains in a Ca^{2+} dependent manner. Truncated SP-A was also studied and was compared to its hyperpermeabilizing mutant D215A/PL SP-A. D215A/PL SP-A was more stable at the air/water interface, which may contribute to its hyperpermeability.

Acknowledgement

I would like to express my sincerest gratitude to my advisor, Dr. Richard Mendelsohn, for his advice and encouragement throughout my Ph. D. study. This thesis would not be accomplished without his guidance and support.

I would like to thank my committee members, Dr. Russel M. Waters, Dr. Huixin He and Dr. Roger Lalancette for their efforts and time in reading and correcting my thesis.

I am very thankful to Dr. Kevin Keough at Memorial University of Newfoundland, Dr. Francis X. McCormack at University of Cincinnati and Dr. Annelise Barron at Stanford University for their generous supply of proteins and peptoids. I am also grateful to Dr. Huixin He for her suggestion on AFM study.

Special thanks go to Dr. Carol R. Flach. I appreciated her help with experiment design and her intelligent insights into data interpretation. My appreciation extends to all the members of Dr. Mendelsohn's research group, especially to Dr. Lin Wang, Dr. Chunhong Xiao and Dr. Guojin Zhang for their help during my early days in the laboratory.

I also thank all the faculty and stuff members at our chemistry department. Thank them for making my days at Rutgers both educational and enjoyable.

At last, I wish to express my love and gratitude to my parents, my husband, my sister and my friends. Thank them for their unconditional love, support and their belief in me!

Table of Contents

viii

Lists of Tables

List of illustrations

Chapter One: Introduction

Lung surfactant is a lipid/protein mixture that forms a thin layer at the air/water interface in mammalian lungs. It functions to lower the alveolar surface tension, facilitate the work of breathing, and prevent lungs from collapse. Deficiency or dysfunction of lung surfactant leads to disease states of lungs, such as neonate respiratory distress syndrome (nRDS) and acute respiratory distress syndrome (ARDS). In addition to their surface tension lowering functions, the lung surfactant associated proteins SP-A and SP-D are also found to be involved in the host defense mechanism. Study of the interactions between lung surfactant proteins and lipids will help to understand the breathing mechanism and improve the design and evaluation of therapeutic agents. Knowledge of surfactant proteins and their ways of recognizing invading organisms will facilitate the study of innate immune effects.

1.1 Lung surfactant

1.1.1 Lung anatomy

Figure 1-1 shows the schematic structure of human lungs and the location of lung surfactant. Human lungs are composed of a conducting zone and a respiratory zone. When fresh air is breathed through nose and mouth, it is pulled through the conducting zone, which includes trachea, bronchi, bronchioles and
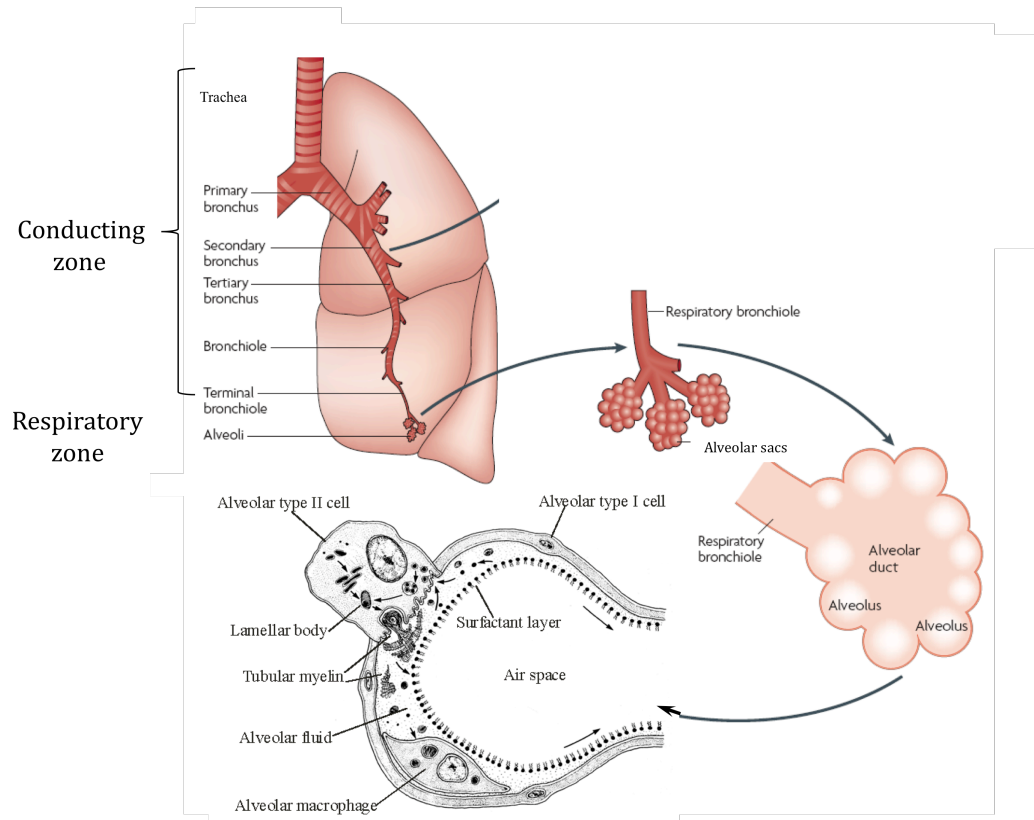
Figure 1-1. Schematic graph of human lung structure (*1, 2*).

terminal bronchioles, and eventually reaches the respiratory bronchioles and alveolar sacs of the respiratory zone. Alveolar sacs are made up of clusters of alveoli, which are bubble-shaped and possess high curvature. They are tightly wrapped in blood vessels. Gas exchange occurs in the alveoli. Oxygen diffuses from the alveoli to the capillaries, while carbon dioxide leaves the capillaries and diffuses into the alveoli. The alveoli are lined with alveolar epithelium comprised predominantly of two specialized epithelial cell types, the terminally differentiated squamous alveolar epithelial type I cells and the surfactant producing cuboidal alveolar epithelial type II cells. Type I cells constitute approximately 93% of the alveolar epithelial surface area and type II cells comprise the remaining 7%. Lung surfactant secreted outside of the type II cells enters the aqueous alveolar liquid and forms a thin layer at the alveolar/air interface. It functions to reduce the surface tension at the interface and prevents alveoli from collapse at the end of expiration.

The lung contains approximately 1500 miles of airways and around 300 million alveoli with diameters of ~70-300 μm and represents a total surface area of 140 m^2. Besides its main function of air exchange, the lung also possesses the largest surface area of any organ exposed to the external environment and is constantly challenged by airborne pathogens. Lung surfactant associated proteins SP-A and SP-D are involved in the pulmonary innate immune response to protect the lung.

1.1.2 Lung surfactant composition

The history of lung surfactant discovery was recently summarized (*3*). The composition and functions of lung surfactant have been frequently reviewed (*4-6*). Lung surfactant composition is highly consistent across species. As shown in Figure 1-2, it consists of ~90% lipids and ~10% surfactant associated proteins.

1.1.2.1 Lipids

Phospholipids form the bulk of the lipid class; and other lipids present include cholesterol, triacylglycerol, and free fatty acids. Phosphatidylcholine is the most abundant component of surfactant and is always found in a quantity of 70-80% of the total amount of lipid. Approximately 50-70% of the PC class is saturated, mostly in the dipalmitoylated form (DPPC). The anionic PG comprises approximately 8% of lipid class. Other phospholipids present include phosphatidylethanolamine (PE, ~5%), phosphatidylinositol (PI, ~3%), phosphatidylserine (PS), along with lysophosphatidylcholine, and sphingomyelin which are present in small quantities (less than 2%). The plasmalogen analog of PC has also been identified as an important minor constitute in pulmonary surfactant. Cholesterol accounts for 2.4 weight % of total composition of surfactant.

Phospholipids are mainly responsible for the surface tension lowering properties of surfactant. DPPC is the main component that can lower the alveolar surface tension to near zero. Some of the other lipid species are considered to
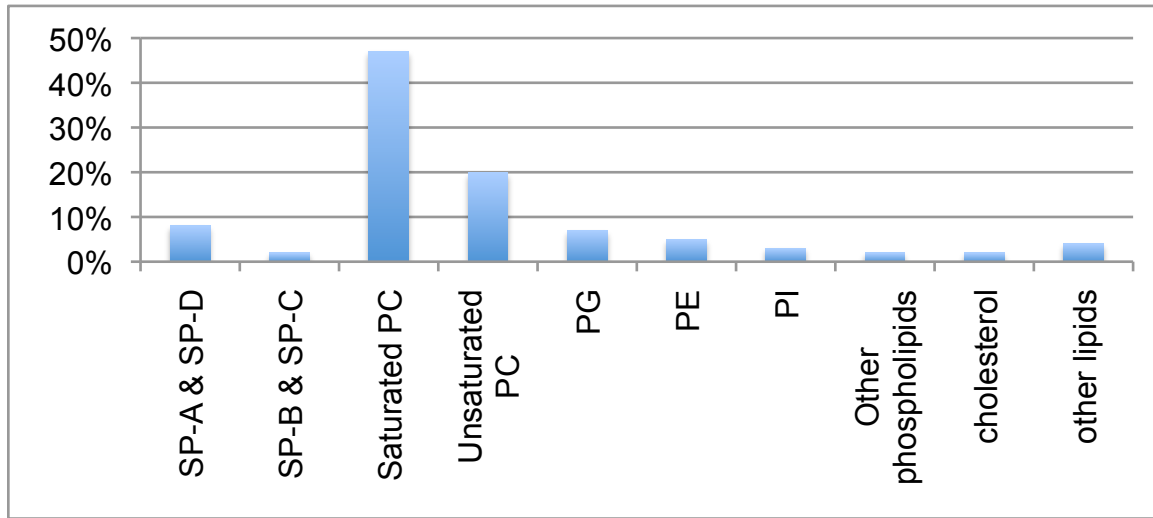
Figure 1-2. Composition of Lung surfactant.

increase the fluidity of the lipid films and facilitate their adsorption to the interfaces.

Even though they only account for 10% of lung surfactant, specific surfactant associated proteins are critical to impart to surfactant phospholipids dynamic properties necessary for full functionality (7). Four surfactant-associated proteins have been discovered and named sequentially in the order of their discovery as SP-A, SP-B, SP-C and SP-D. These four proteins are either exclusively synthesized or mainly found in lungs. They are usually associated with surfactant lipids.

1.1.2.2 SP-A and SP-D

SP-A and SP-D are hydrophilic proteins. SP-A, which is variably glycosylated, consists of 248 amino acids and has a molecular weight of 28-36 kDa, while SP-D contains 355 amino acid residues and has a molecular weight of ~43 kDa. SP-A and SP-D both belong to the Ca^{2+}-dependent carbohydrate-binding collagenous lectin (collectin) family. Their primary structure comprises four domains: an N-terminal domain, a collagenous domain, a neck domain, and a carbohydrate recognition domain (CRD). Three monomers trimerize through the neck and collagen domains, and the resultant trimers further aggregate to oligomers by disulfide bond formation within the N-terminal regions (8). Six SP-A trimers assemble in parallel and in register to form a structure resembling a
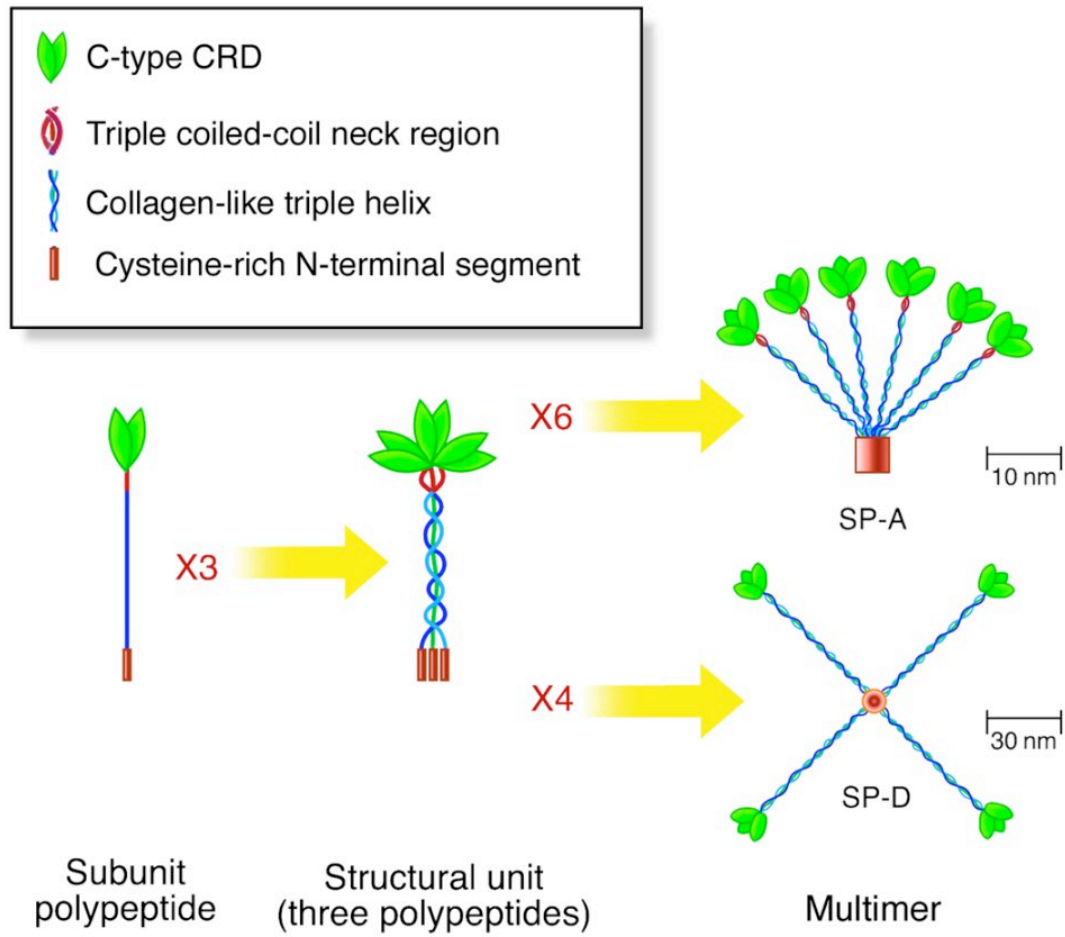
Figure 1-3. Oligomers of SP-A and SP-D (*9*).

bouquet of tulips (*10*), whereas four SP-D trimers arrange radially to form cruciform (*11*). Figure 1-3 depicts the oligomers structures of SP-A and SP-D (*9*).

SP-A is mostly associated with lipids in the lung. It regulates lipid adsorption and monolayer formation. Besides functioning to facilitate the surface activities of lipids, SP-A and SP-D play important roles in host defense against inhaled pathogens. SP-A is the object of interest in this thesis. The crystal structure of a recombinant SP-A comprised of the neck and CRD domains has been determined by X-ray crystallography (*8*). As shown in Figure 1-4, the secondary structure of the CRD of this recombinant SP-A includes three α-helices and 11 short strands of β-sheet, while the neck region consists of a single α-helix. Two classes of calcium binding sites have been identified in the CRD region, the primary and the auxiliary binding sites, which are situated on opposite sides of the highly flexible 198-203 loop. The phospholipid binding domain of SP-A overlaps with the carbohydrate binding domain. When Ca^{2+} is present, the SP-A CRD is considerably less polar than that of SP-D, consistent with the preference of SP-A for hydrophobic ligands.

1.1.2.3 SP-B and SP-C

Compared to SP-A and SP-D, SP-B and SP-C are smaller proteins and they are extremely hydrophobic. The most important functions of SP-B and SP-C are their ability to enhance the surface activity of lung surfactant lipids. Both SP-B and SP-C accelerate the adsorption of surfactant lipids and promote the
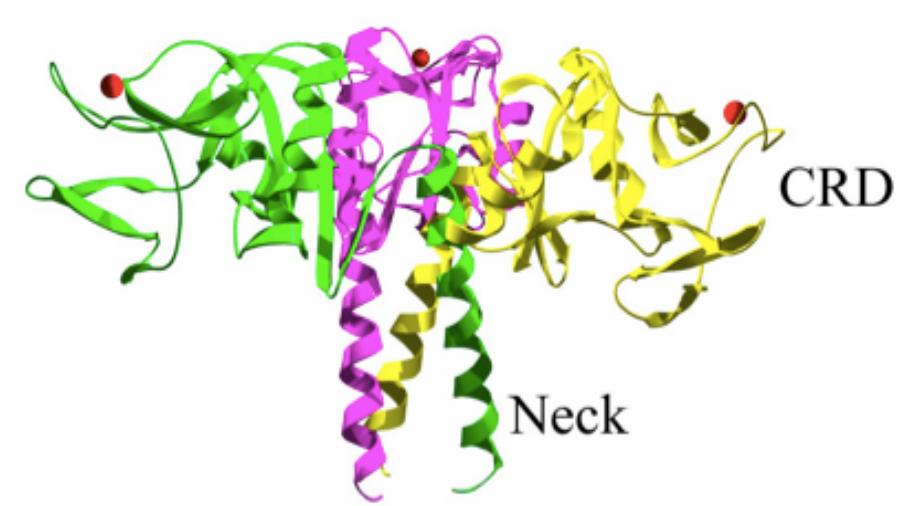
Figure 1-4. Crystal structure of a recombinant SP-A (*8*).

readsorption of excluded materials back to monolayers. SP-C function is investigated in the current work. In particular, SP-C-dependent multilayer formation at high surface pressures that leads to DPPC enrichment in monolayers is studied in this thesis.

The sequence and structure of SP-C is shown in Figure 1-5. SP-C contains 35 amino acid residues and has a molecular weight of 21 kDa. SP-C is extremely hydrophobic. It has two positive charges at positions 11 (lysine) and 12 (arginine) and the cysteine residues at positions 5 and 6 are palmitoylated. The structure of SP-C in solution was determined by NMR (*12*). SP-C forms an α-helix between positions 9 and 34, which includes two segments of seven and four consecutive valines separated by a single leucine residue. The N-terminal segment is disordered. The length of the α-helix is about 37 Å and the helical segment of residues 13-28, which contains exclusively aliphatic residues with branched side chains, is 23 Å long and about 10 Å in diameter. The length of the SP-C α-helix is optimally suited for interaction with DPPC bilayers in the liquid-crystalline phase, but it is too short to span gel-phase bilayers. The palmitoylation of cysteines may serve important purposes. For example, the acyl chains of SP-C might help the protein anchor itself to membrane, orient protein in bilayers and monolayers, and form lipid reservoir attached to monolayers.

1.1.3 Lung surfactant extracellular metabolism

Exhalation happens passively in lungs. Surface tension exists due to the

H₃C   CH₃
| |
(H₂C)₁₄ (CH₂)₁₄
| |
O=C   C=O

                   10   20   30

L R I P C C P V N L K R L L V V V V V V V L V V V V I V G A L L M G I
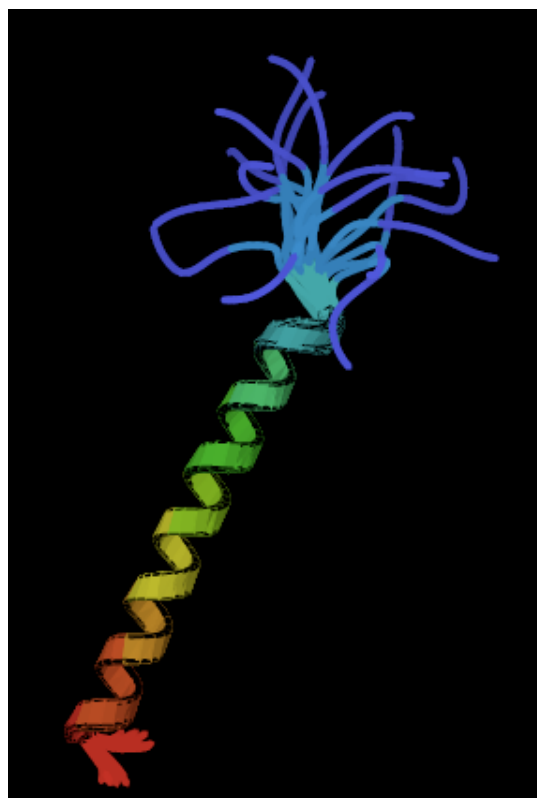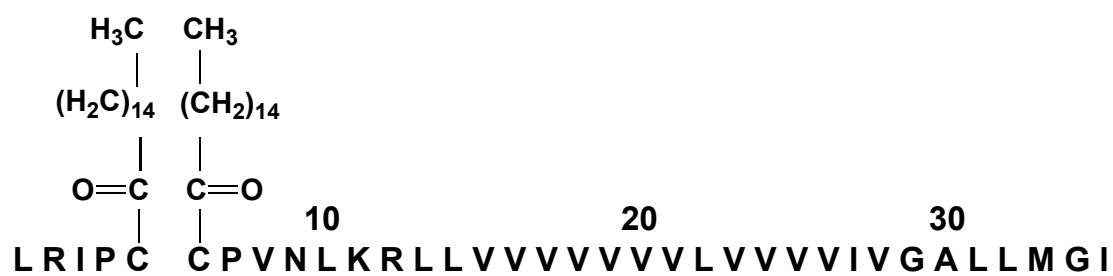
Figure 1-5. Sequence (top) and structure (bottom) of SP-C.

attraction between molecules in the moist alveolar fluid and is responsible for the tendency to make the alveolar bubbles contract and eventually disappear. The presence of lung surfactant lowers the surface tension and prevents alveolar collapse during expiration when the alveolar surface area decreases. As shown in Figure 1-6, lung surfactant synthesized by type 2 cells is stored in lamellar bodies (LBs), where surfactant is packaged as densely packed bilayers. LBs are then secreted outside of type 2 cells and undergo transformation to form tubular myelin (TM), an ordered array of tubules of nearly rectangular cross section. Surfactant gets adsorbed to the interface from TM. During the process of inhalation and expiration, surfactant components are lost from the interface and taken up by the type 2 cells for recycling.

1.1.4 Functions of lung surfactant

1.1.4.1 Surface activities of lung surfactant

Lung surfactant forms a monolayer at the alveolar air/water interface, with bilayer lipid structures attached to it. These bilayer structures are thought to be in contact with the monolayer and serve as the lipid reservoir from which insertion of lipids and possibly proteins is achieved upon inhalation (*13*). As shown in Figure 1-7, such monolayers with attached multilayer structures of lung surfactant surface film were confirmed by TEM (*14*).

The functional surface tension of surfactant monolayers in lung is between 1-25 mN/m during exhalation and inhalation. Among components of lung surfactant
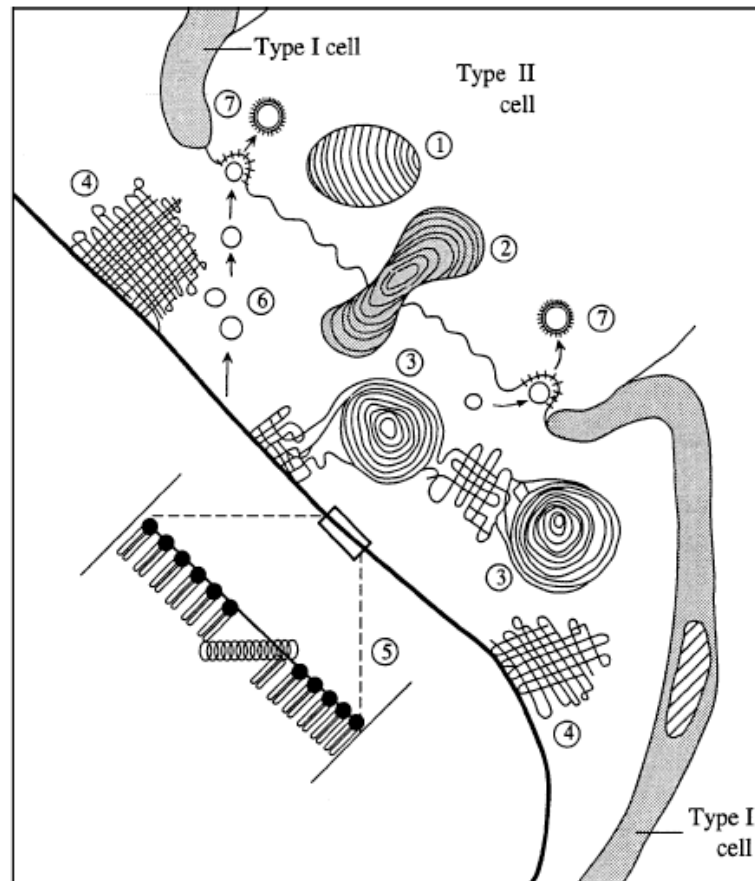
Figure 1-6. Extracelluar lung surfactant metabolism (*5*). Lung surfactant is produced by type II cells and stored in lamellar bodies ① and secreted into the alveolar space ②. The surfactant is transformed ③ into tubular myelin ④, from which the monolayer ⑤ is formed. After the surfactant is used, it is taken up again ⑥ by the type II cells and reused ⑦.
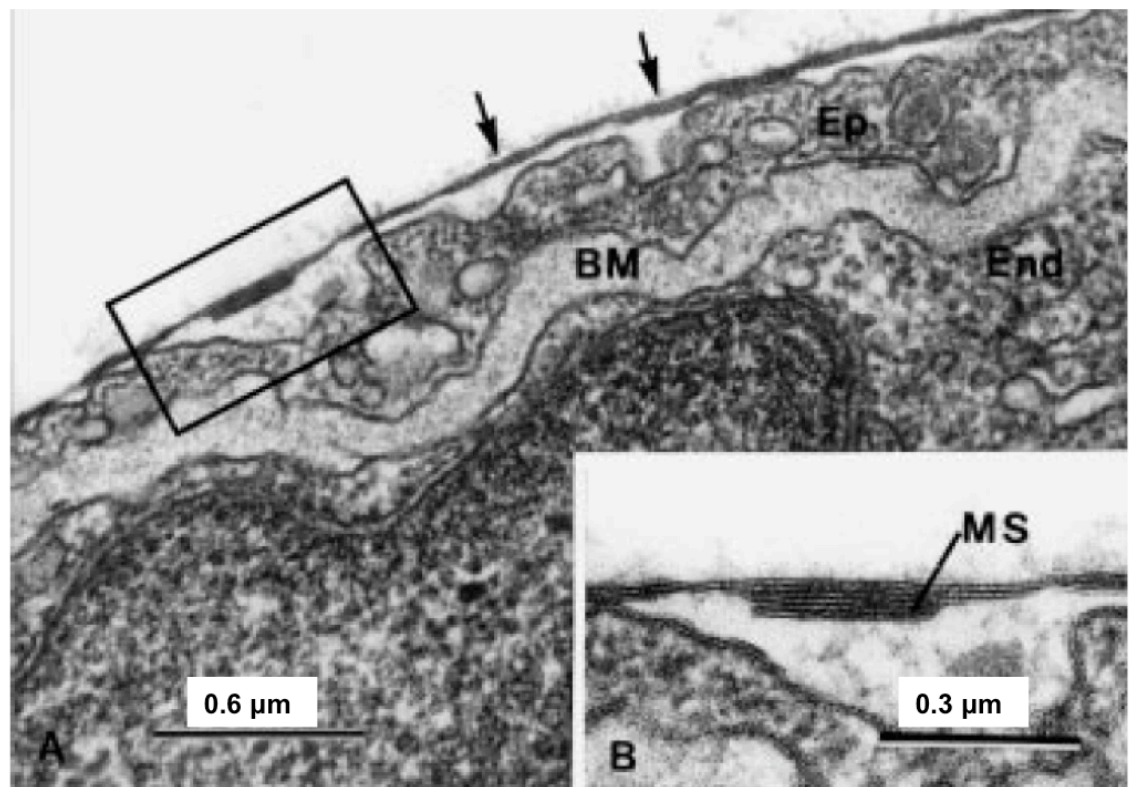
Figure 1-7. TEM picture of lung surfactant surface film (*14*).

DPPC is the only one able to reduce the surface tension to lower than 20 mN/m (*15*). Thus DPPC has to be enriched in the monolayer during expiration when alveolar surface decreases. Such DPPC enrichment is studied with lung surfactant model systems; it is suggested that it occurs either through selective DPPC adsorption or squeeze-out of non-DPPC components. Both mechanisms are supported by the experimental evidence.

The selective adsorption model states that surfactant is sorted during its adsorption to the interface from TM and DPPC is selectively adsorbed to form a DPPC-rich film (*16*). Selective DPPC insertion is mostly supported by captive bubble surfactometer (CBS) studies. In CBS, near zero surface tension was achieved at much lower area reduction of the air bubble than expected for the lipid mixture and SP-A was involved in such adsorption (*17*). SP-A preferentially interacts with DPPC (*18*) than with other lipids and appears to function with the liquid condensed and liquid fluid boundaries of monolayers (*19*).

The squeeze-out model proposed by Clements (*20*) states that the surfactant monolayer has similar composition to the surfactant in the alveolar fluid, and that DPPC is enriched in monolayer when non-DPPC components are squeezed out during film compression. SP-B and SP-C are thought to optimize such squeeze out processes. Protrusions of bilayer heights were observed with AFM for lipid mixtures containing SP-B and a minimal SP-B concentration was required for bilayer formation (*21*). Phospholipid mixtures also formed reversible stacks of lipid bilayers in the presence of SP-C. Time-of-flight secondary ion mass spectrometry (TOF-SIMS) and fluorescence light microscopy (FLM) revealed that

these structures were enriched in SP-C (*22*). Such multilayer formation in SP-C containing phospholipid mixtures was also observed by atomic-force microscopy (AFM) and IRRAS study showed that SP-C orientation changes from 80° in monolayers to nearly transmembrane orientation in multilayers (*23*).

In this thesis, we studied the DPPC enrichment process and squeeze-out hypothesis by cospreading a lung surfactant model system in a Langmuir trough and transferring the film to solid substrates. Semi-quantitative information about the composition of multilayers was acquired by IR intensity measurements of its components.

1.1.4.2 Innate immune response of lung surfactant

Innate Immunity is the host defense mechanisms that are present before infection, which respond rapidly to invading microbes in a broad, nonspecific manner. In the lung, the principal components of the innate host defense system include muco-ciliary clearance in the nasal passages and conducting airways, phagocytic cells such as alveolar macrophages, and an array of host defense proteins including SP-A and SP-D (*24*). Most inhaled particles and organisms are trapped and removed in the conducting airway before they reach alveolar space. Some particles and microorganisms in the inspired air manage to escape the airway defense mechanisms and reach alveolar surfaces. The alveolar macrophages and surfactant proteins in alveoli respond innately to these pathogens.
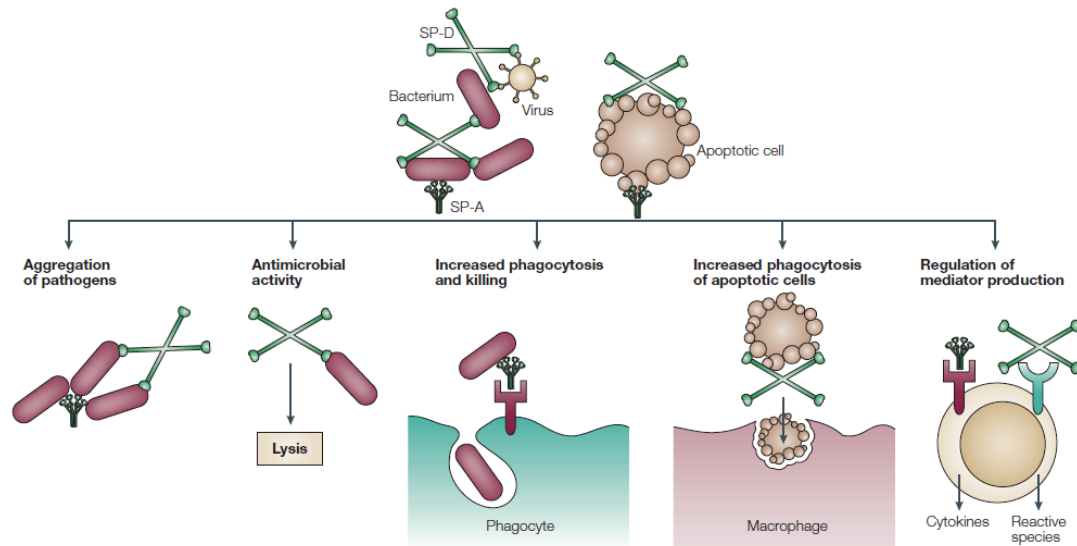
Figure 1-8. Innate immune functions of SP-A and SP-D. SP-A and SP-D bind to a variety of bacteria, viruses, allergens and apoptotic cells and thereby function as opsonins to enhance the uptake of these cells and particles. Binding of the collectins to pathogens occurs by various mechanisms. Some pathogens are aggregated by SP-A and/or SP-D. SP-A and SP-D also have direct effects on immune cells and modulate the production of cytokines and inflammatory mediators (*25*).

SP-A and SP-D forms the first line of host defense in alveoli against inspired pathogens. Their functions in innate immunity are reviewed recently (*24-27*). SP-A and SP-D directly interact with a variety of microorganisms including bacteria, viruses, fungi and allergens (Figure 1-8) (*25*). They enhance the uptake of pathogens by macrophages and contribute to their clearance through different mechanisms (*26*). SP-A and SP-D are also found to modulate pulmonary inflammation (*28*).

We have confined our study of the innate immunity of lung surfactant within the scope of biophysics and focused on the interaction between SP-A and its ligands. SP-A and SP-D recognize pathogen-associated molecular patterns (PAMPS) on foreign organisms. As the major constituents of the outer membrane of Gram-negative bacteria, lipopolysaccharides (LPS) are the ligands of SP-A. The modes of interaction between SP-A and different LPS strains are studied by IRRAS in the thesis.

1.1.5 Surfactant therapy

Exogenous lung surfactant has been used to treat babies with nRDS to help to open and maintain their lungs open until they are able to synthesize endogenous surfactant. Most surfactant preparations in current use for surfactant therapy are extracts from animal lung surfactants. They contain most of the surfactant lipids and hydrophobic surfactant associated proteins SP-B and SP-C (*29*). Even though this natural lung surfactant is effective for nRDS therapy, there

are concerns with this approach. Inherent with any animal source, extraction of natural surfactant has high batch-to-batch variation. It is costly with limited supply, and there is also the potential risk of transmission of animal infectious agents. Synthetic surfactant preparations composed of lipids were then proposed for the surfactant therapeutic intervention. However, they were found to be significantly inferior to those natural preparations containing proteins (*30*). It is of importance to investigate efficient analogs of hydrophobic proteins SP-B and SP-C to improve synthetic surfactant preparation.

Analogs of SP-B and SP-C have been designed based on protein sequence and structure to mimic their surface-related properties. Figure 1-9 shows some current peptide mimics of SP-B (*29*). KL$_4$ is the first SP-B inspired synthetic peptide. It simulates the sequence pattern of the SP-B C-terminal. It promotes the rapid transfer of phospholipids into the air-liquid interface and stabilizes the compressed lipid/peptide films. Peptide SP-B 1-25 contains the 25 N-terminal residues of SP-B. It can mimic many of the membrane and monolayer-perturbing properties as well as the surface activities of native SP-B. The dimeric form of SP-B 1-25 shows enhanced behavior compared with the monomer. Mini-B has the sequences of N- and C-terminal segments of SP-B. Mini-B might be an even better mimic of native SP-B.

Most SP-C analogues are designed based on its sequence and structure. These analogs have modified SP-C sequence. For example, leucine-rich SP-C derivatives have a poly-valine sequence replaced with leucines or alanines to help form α-helical conformation and to minimize aggregation. Another proposed
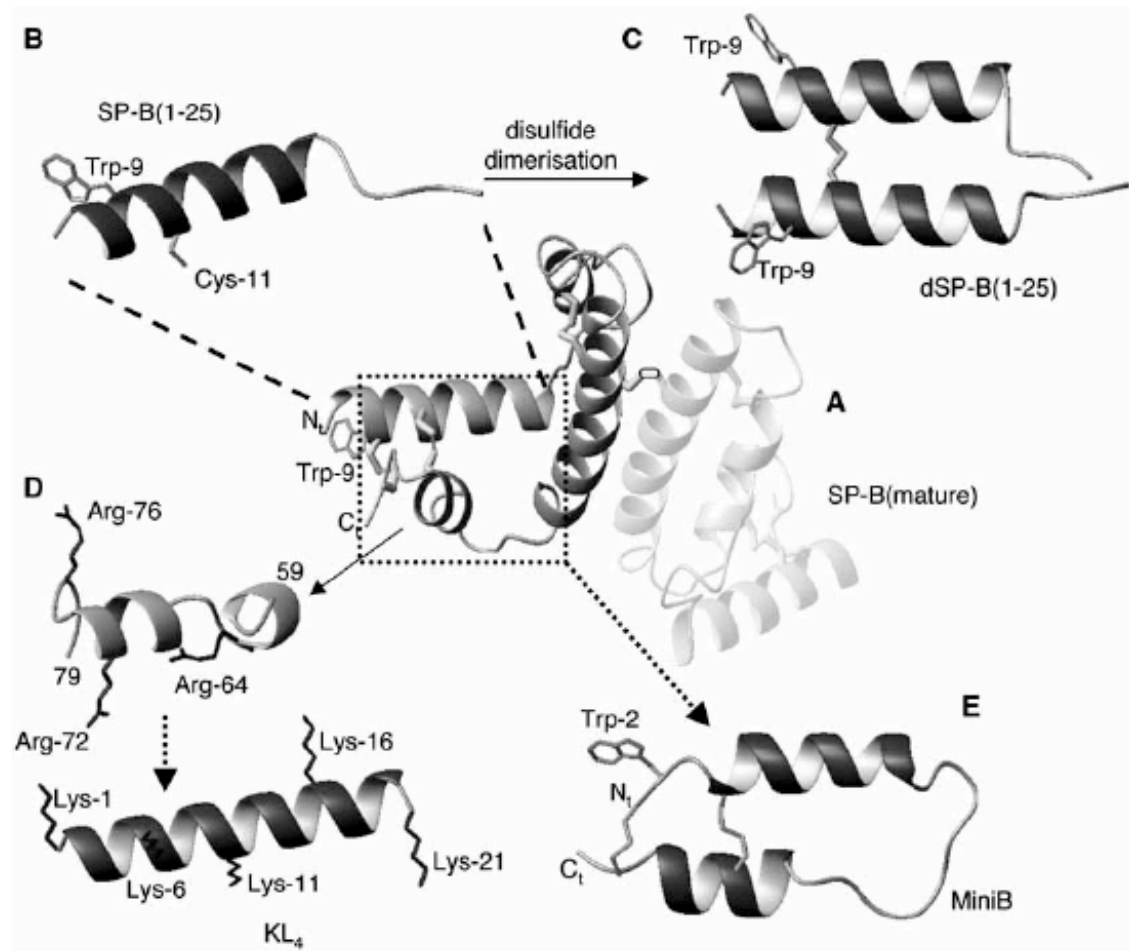
Figure 1-9. Analogs of SP-B (*29*). (A) Model of the SP-B dimer; (B) model of the SP-B 1-25 peptide; (C) Model of SP-B 1-25 disulfide-dimer; (D) Model of KL$_4$ designed from the C-terminal region of SP-B; (E) Model of mini-B motif, derived from the N- and C-terminus of SP-B.

SP-C analogue has the palmitoylation removed from its structure.

These protein analogs with specific sequences are quite expensive to synthesize in large quantities. Protein production through recombinant technology is currently under investigation. There are challenges with this approach; the SP-B proteins are often not properly folded and the disulfides are not correctly formed (*31*), and the recombinant SP-C has to have certain amino acid replaced (*32*) to form its helical structure.

Another class of promising surfactant associated protein analogs is termed "peptoid". Peptoids are a family of oligomers based on a polyglycine backbone, on which the side chains are attached to the amide nitrogen instead of α-carbon (*33*). The structure of a pentapeptoid with five chiral side chains was determined by NMR (*34*). This molecule forms right-handed helix with cis-amide bonds in methanol. The periodicity of the helix is three residues per turn, with a pitch of ~6 Å. When substituted with α-chiral, sterically bulky side chains, these N-substituted polyglycines are able to adopt extraordinarily stable helical secondary structures. This tendency makes them suitable candidates as biomimetics of proteins that rely on helical structures for proper function.

Peptoids are relatively easy to synthesize with high efficiency. They are stable under thermal stress, and resistant to protease degradation. Three peptoids were designed as analogs of SP-B fragment SP-B 1-25 (*35*). These peptoids were able to mimic and even improve the biophysical function of SP-B 1-25 and KL$_4$. Studies of peptoid mimics of SP-C showed that extreme

hydrophobicity and highly helical structure are more important for replicating the surface activity of SP-C than the amino acid sequence (*36*). The surface activity of these mimics was tested by different methods including Langmuir-Wilhelmy surface balances, fluorescence microscopy, pulsating bubble surfactometer. The ability to promote DPPC enrichment during exhalation is critical to proper function of lungs. Whether peptoid mimics of SP-C can form mulitlayers at high surface pressure (low surface tension) should be investigated and compared to native SP-C as well. We tested the morphology and composition of multilayers from the peptoid containing surfactant model by AFM and IR spectroscopy in the current study.

1.2 Techniques for lung surfactant studies

1.2.1 Techniques to study surface activity

There is currently no simple assay to access the functionality of lung surfactant. Several techniques have been developed to elucidate and evaluate the properties and functions of lung surfactant, especially the surfactant associated proteins. These techniques have been reviewed recently (*13*).

1.2.1.1 Langmuir-Wilhelmy surface balance (LWSB)

Langmuir-Wilhelmy balance was introduced for the study of surfactant (*37*). The instrument setup is shown in Figure 1-10. A film of interest is formed at the

Figure 1-10. Instrumental setup of Langmuir-Wilhelmy balance

surface of subphase through adsorption from subphase or spreading from organic solvents. A movable barrier is used to change the surface area of the resultant surfactant film. The surface pressure, which is defined as the surface tension difference between that of clean subphase and of film covered subphase, is measured by a small plate (or piece of filter paper) attached to an electro balance.

LWSB is used to acquire the isotherms of surfactants at air/water interfaces. The isotherms, plotted as surface pressure changes of a surfactant monolayer *vs.* molecular area changes, monitor the surface thermodynamics of surfactants. At the air/water interface, surfactant molecules undergo a two-dimensional phase transition when compressed. Figure 1-11 shows a generalized isotherm of a fatty acid, adapted from Kaganer et al. (*38*). When surface density of the molecule is very low, the monolayer is described as in a two-dimensional gas phase. With decreasing area per molecule, the monolayer proceeds into liquid expanded (LE) phase. In this phase, the molecules are still disordered as in gas phase. Further compression of the monolayer lead to a transition from LE to a liquid condensed (LC) phase, with (usually) a plateau indicating a first-order transition. The monolayer is less compressible in the condensed state than in the liquid expanded state. Upon further compression, the film compressibility decreases further and the monolayer proceeds to a solid phase. Molecules are packed with high conformational orders both in LC and solid phases. The acyl chain orientations, however, are different in the two cases. In LC phase, the acyl chains
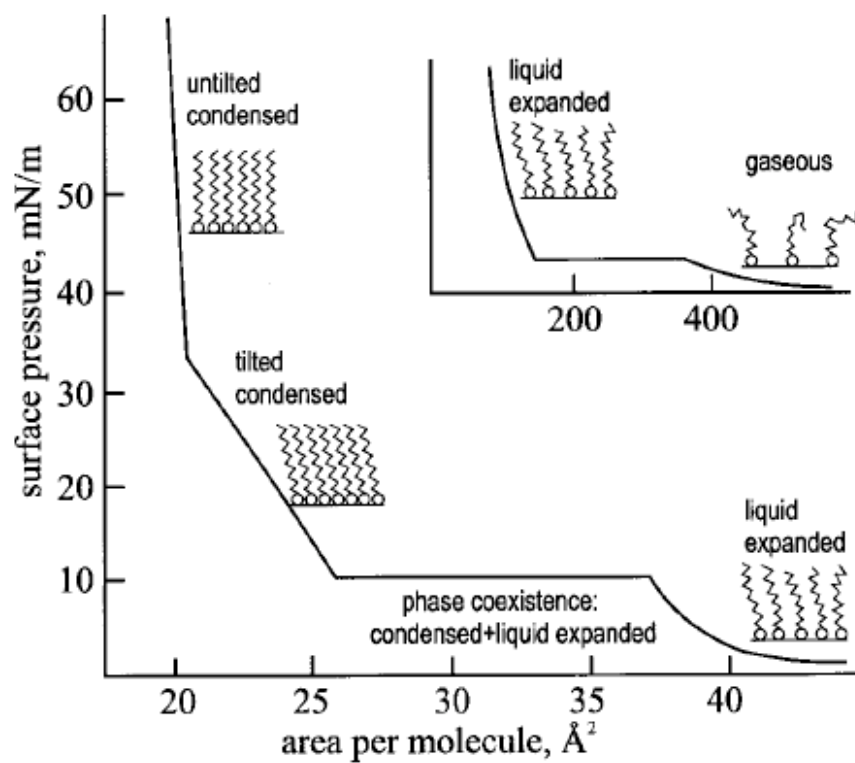
Figure 1-11. Schematic isotherm of lipids (*38*).

of molecules are tilted relative to the water surface while they are perpendicular to the water surface in solid phase. If the monolayer is compressed even further, the film will eventually collapse.

The phase transitions of surfactant at the two-dimensional air/water interface are related to the cross-sectional area ratio of hydrophilic head group and hydrophobic chain region. The isotherms of surfactant are molecule-specific and temperature-dependent.

There are limitations with LWSB studies. The surface area is controlled by barrier movements and cannot be cycled very rapidly to simulate the breathing cycles in lungs. Large subphase volumes are required and are thus less suitable for studies of the adsorbed surfactant film due to the limited supply of lung surfactant.

Despite its limitations, LWSB measurements offer great controllability of experimental variables. The constituents, temperature, and pH of the subphase can be easily controlled. A buffer with a composition similar to that of the fluid lining of the lungs can be used to simulate the alveolar environments. The composition of a surface surfactant layer can be precisely controlled by spreading the film from an organic solution. The instrument also allows for the compression of monolayers under constant speed, to a target surface pressure, and allows the monolayer film to be held at constant surface pressure while other parameters are adjusted. LWSB can be easily coupled with other techniques to obtain molecular information of the system studied. It can be used to transfer

surfactant films to solid substrates for study by fluorescence microscopy, infrared spectroscopy, Raman, AFM, etc. LWSB can also be directly combined with IR, X-ray reflectivity, or fluorescence instrument and study the film in aqueous monolayers under controlled conditions of surface pressure.

1.2.1.2 Pulsating bubble surfactometer (PBS)

Pulsating bubble surfactometry was first described by Enhorning in 1977 (*39*). It is used to monitor the dynamic surface tension of fluid. Figure 1-12 shows the schematic setup of pulsating bubble surfactometer. It consists of a small temperature-controlled sample chamber, connected to the atmosphere by a small capillary, a pulsator unit and a pressure-recording device. The sample chamber is filled with the liquid to be tested. An air bubble is attached to the capillary and this bubble is pulsated by varying the pressure in the sample chamber. A precision pressure transducer is used to record the pressure across the interface when the bubble is of maximal and minimal size. The size of the bubble is checked through a microscope. Assuming a spherical surface for the air bubble, the surface tension can be calculated from Laplace formula, $\Delta P = 2\gamma/r$, where ΔP (the pressure gradient across the surface of the bubble) and r (the radius of the air bubble) are measured.
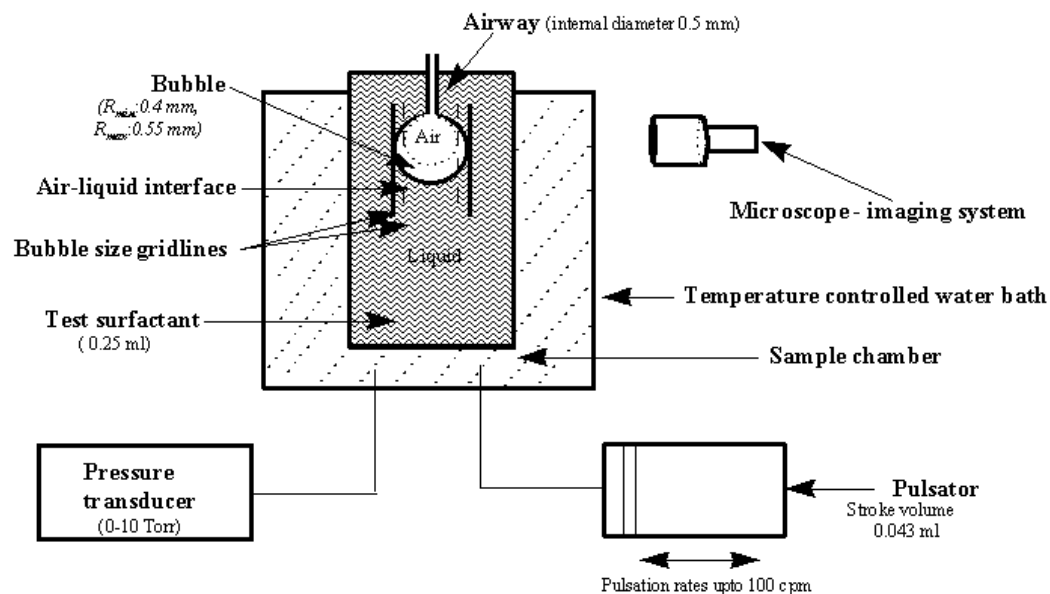
Figure 1-12. Schematic instrumental setup of PBS (*40*)
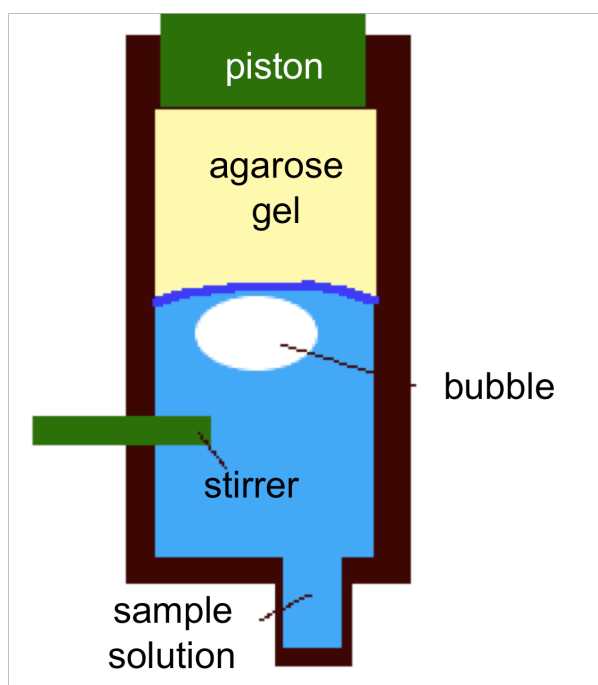
Figure 1-13. Schematic instrumental setup of CBS

1.2.1.3 Captive bubble surfactometer (CBS)

The captive bubble surfactometer (CBS) is an improvement on the PBS. The tested liquid leaks through the capillary in PBS and the air bubble shape deviates from a sphere at low surface tension, which renders the Laplace formula unsuitable. In CBS, the bubble is not open to the exterior and no leakage happens. As shown in Figure 1-13, the captive bubble is floated against a 1% agarose gel and the chamber is sealed and pressurized. Pressure changes are used to change the air volume thereby decreasing the surface area of the sessile bubble and lowering the surface tension. The events of the bubble are observed by a video camera and surface tension at the bubble surface is calculated from its shape.

PBS and CBS are dynamically rapid techniques that resemble natural breathing frequencies. The maximum and minimum surface tensions during cycling are considered to be representative of the adsorption capabilities of the sample and the enrichment in DPPC of the monolayer, respectively. However, the composition of the surfactant system recruited to the air/water interface is not known from PBS and CBS and no other techniques can be coupled with PBS and CBS.

1.2.2 Infrared spectroscopy

The surface activity studies of lung surfactant by LWSB, PBS, and CBS provide surface tension-area characteristics of different surfactant preparations.

However, molecular level information is needed to understand the mechanism of the formation of monolayer and the surface attached reservoir by lung surfactant, and to investigate the pathogen recognition pattern of lung surfactant-associated proteins. Infrared spectroscopy (IR) is the appropriate technique for such investigation. IR monitors molecular vibrations that produce dipole moment oscillations. The observed frequencies depend on molecular conformation, configuration and local environment. Information on lipid acyl chain conformation, head group structure and interaction with ions, protein secondary structure, and the orientation of ordered regions of protein and lipids can be extracted from their IR spectra (*41*).

Lung surfactant models studied by IR spectroscopy can be divided into two categories, the vesicle model and the monolayer model. Information that can be acquired by IR from these models is discussed in the following.

1.2.2.1 Transmission IR of bulk phase surfactant

The bulk phase IR measurement utilizes lipid or lipid/protein vesicles as samples and the spectra are taken in the transmission mode, usually at a series of temperatures. The thermodynamic behavior of lipid vesicles is monitored by their IR spectra. The lipid phase transition from gel to liquid crystalline phase, acyl chain packing (*42*), the hydration state of head groups, the quantification of disorder (*43*), and the effect of lipid/protein interaction on lipid phase behavior can be probed by characterizing the appropriate spectral parameters.

Figure 1-14 is adapted and modified from Snyder et al. (*44*), it shows the IR spectra of a distearoylphosphatidylcholine (DSPC) at both low and high temperatures. The vibrational modes of the lipid acyl chains are marked on the spectra. These include the asymmetric and symmetric methylene C-H stretching, methylene scissoring, and methylene wagging, which are used to monitor chain packing and conformation.

Polymethylene C-H stretching frequencies increase with increasing conformational disorder and can be used to monitor the lipid phase transition and to estimate lipid bilayer conformational disorder (*45*). The frequencies of asymmetric and symmetric C-H stretching bands for ordered chains near room temperature are near 2920 and 2850 cm^{-1}, respectively. Deuteration of CH_2 groups shifts these frequencies to 2090 and 2200 cm^{-1}, respectively. Deuteration can be used to monitor the behavior of single components of lipid mixtures by IR spectroscopy.

The methylene scissoring band is most often used to monitor solid-solid phase changes in the crystalline phase. Its position is sensitive to interchain interactions and chain packing (*44, 46*). The scissoring band has two components for orthorhombic-subcell chain packing, a high-frequency component at ~1472 cm^{-1} and a low-frequency component at 1462 cm^{-1}. With increasing temperature, the two components shift towards each other. The scissoring mode remains a single peak at ~1467 cm^{-1} for hexagonal phases, or ~1471 cm^{-1} for triclinic phases, or ~1465 cm^{-1} for disordered phases (*41*). Thus,
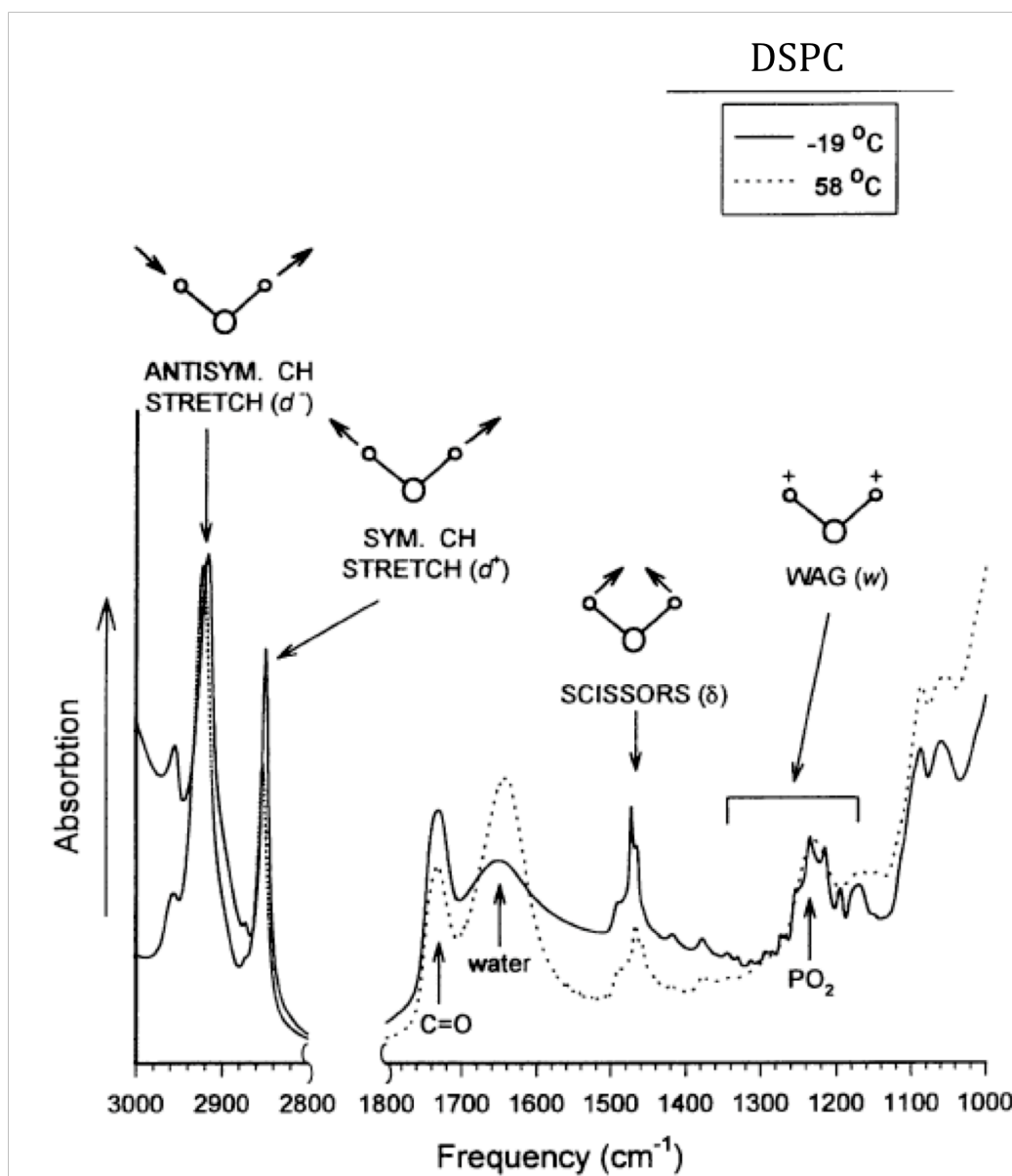
Figure 1-14. IR spectra of fully hydrated DSPC in the gel phase at -19 °C (solid line) and in the liquid-crystalline phase at 58 °C (doted line). IR bands used to monitor the phase behavior are marked on the spectra: methylene asymmetric and symmetric C-H stretching, scissoring, and wagging modes.

chain packing can be determined from the positions and components of the scissoring band.

Methylene wagging modes appear between 1170 and 1380 cm^{-1} as a progression. These modes are delocalized, involving essentially all the acyl-chain methylenes in a concerted motion. The intensities of the methylene wagging mode are dependent on chain packing so that phase transitions are manifest as inflections in intensity *vs.* temperature plots. As temperature increases, the intensities of the bands decrease monotonically, going to zero at the phase transition temperature.

Besides the vibrational modes arising from acyl chains, bands from headgroup region of lipids and proteins are also observed in IR spectra and are informative. The carbonyl band (~1730 cm^{-1}) is sensitive to the hydration state of carbonyl. The phosphate asymmetric and symmetric stretching mode at ~1235 and 1090 cm^{-1}, respectively are also affected by the hydration and ion binding to the phosphate. For protein modes, the most useful for structural studies are the amide I and amide II. The amide I mode arises predominantly from C=O stretching of the amide group in the region of 1600-1700 cm^{-1} and is sensitive to the protein secondary structure. The amide II band arises mainly from a mixture of C-N stretching and N-H in-plane bending. It can be used to monitor the extent of H-D exchange.

1.2.2.2 Infrared Reflection-Absorption Spectrometry (IRRAS) of

surfactant monolayers at the air/water interface

As mentioned earlier, lung surfactant forms monolayers at the alveolar air/water interfaces in lung. It is beneficial to study lung surfactant *in situ* as aqueous monolayers by IR spectroscopy. The air/water interface permits control of many experimental parameters, including temperature, pH, subphase composition, and surface pressure, etc. In the mid-1980s, Dluhy and coworkers demonstrated the feasibility of taking IR spectra from amphiphile monolayers at the air/water interface (*47*). With improvements in technique, IRRAS is now widely used in the studies of lipid monolayers and lipid/protein interactions.

The apparatus requirements for IRRAS instrumentation and the theoretical background for calculating and simulating IRRAS spectra were reviewed by Mendelsohn (*41*) and will not be repeated here. The basic idea of the IRRAS experiment is straightforward. When IR radiation illuminates an aqueous film, a small fraction of the incident light is reflected by water. The reflected intensity depends on the experimental geometry, the optical constants of the film and subphase, and the orientation of the transition moments. The sample vibrational modes appear in the spectrum of reflected light. IRRAS data are reported as plots of reflectance-absorbance (RA) *vs.* wavenumber. RA is defined as -$\log(R/R_0)$, where R and R_0 represent the reflectivity of the film-covered and clean water surface, respectively. As shown in Figure 1-15, the IRRAS peaks may be positive or negative depending on the state of polarization of the incident
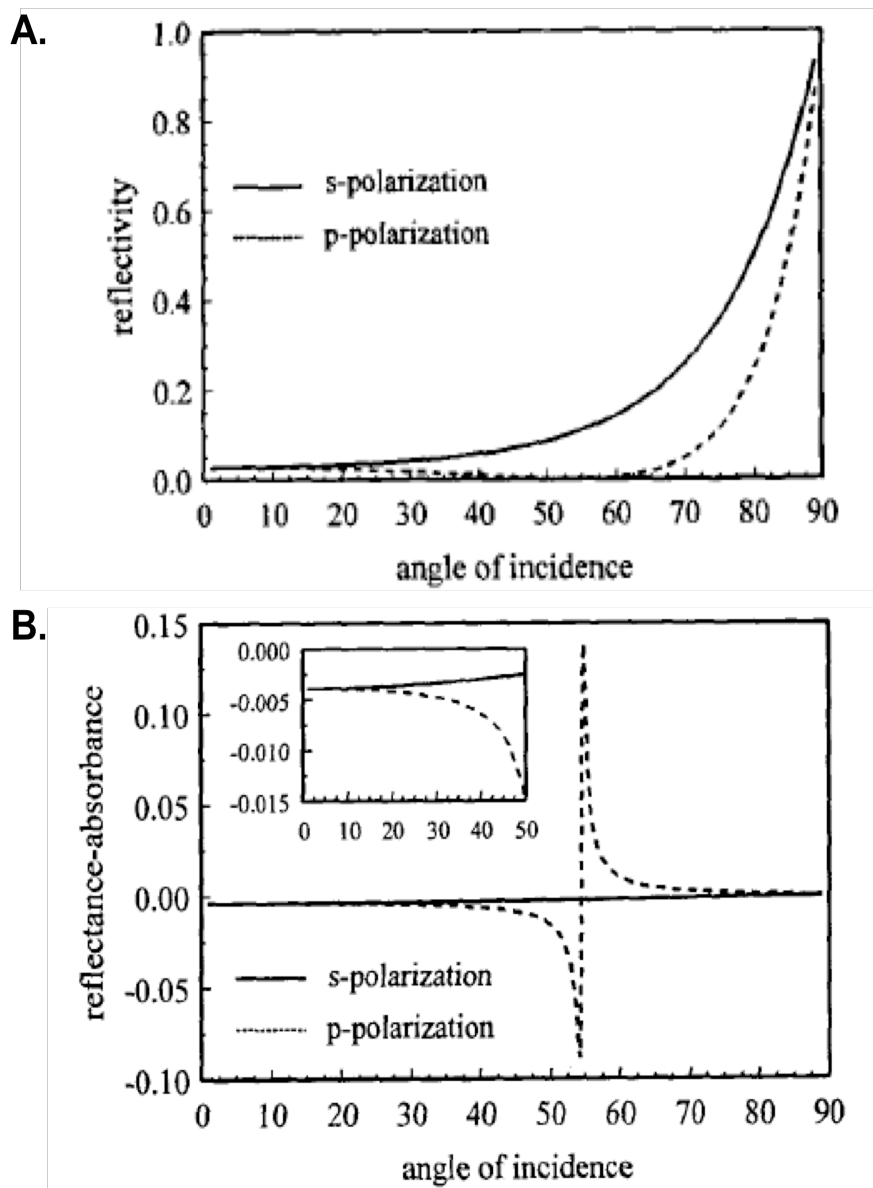
Figure 1-15. (A) Reflectivity and (B) reflectance-absorbance *vs.* angle of incidence for s- and p-polarized radiation, respectively, for an asymmetric methylene stretching vibration at 2917 cm^{-1}(*41*). The thickness of the film is 2.17 nm (the molecules are untilted), and its optical constants are n=1.5 and k$_{max}$=0.4.

light, the angle of incidence, and the direction of the change in the dipole moment during the normal mode.

As in the case of bulk phase IR spectra, vibrational modes from lipid acyl chains, headgroups and proteins are observed in IRRAS spectra. Common IR spectra-structure correlations are shown in Table 1-1 (modified from Mendelsohn et al. *(41))*.

Asymmetric and symmetric methylene C-H stretching modes are the strongest modes observed by IRRAS. The frequencies of these bands are used to track two-dimensional phase transitions of monolayers upon surface pressure changes. Methylene C-H scissoring modes are also detectable in IRRAS. Similar to the bulk phase IR, this mode is sensitive to the lipid packing. Methylene wagging modes are not detected in IRRAS. Carbonyl and phosphate stretching vibrations both appear in IRRAS spectra and provide information about ion binding and hydration. The amide I mode is the most important mode for studies of protein conformation at the air/water interface. Its peak positions are very sensitive to protein secondary structure. The correlations of amide I frequencies to protein secondary structure are given in Table 1-2.

1.2.2.3 IR imaging of transferred surfactant film

Lung surfactant monolayers can be transferred to a solid substrate by Langmuir-Blodgett film transfer techniques. The IR spectra of monolayer can then be acquired from such transferred films. As discussed in the experimental

Table 1-1. Vibrational modes observable in IRRAS spectra

Mode	Wavenumber (cm^{-1})	Structural information
CH$_2$ asymmetric stretch	2916-2924	Lipid acyl chain conformational
CH$_2$ symmetric stretch	2848-2854	order
CD$_2$ asymmetric stretch	2195-2200	Deuterated lipid acyl chain
CD$_2$ symmetric stretch	2090-2100	conformational order
CH$_2$ scissoring	1462, 1474	Orthorhombic phase doublet
	1468	Hexagonal or triclinic phase
CD$_2$ scissoring	1086, 1094	Orthorhombic phase doublet
	1089	Hexagonal or triclinic phase
PO$_2^-$ asymmetric stretch	1220-1250	Ion binding and hydration state
PO$_2^-$ symmetric stretch	1090	Ion binding and hydration state
C=O stretch of fatty acids	1690-1740	Protonation state
C=O stretch of esters	1710-1740	Hydration and hydrogen bonding
Amide I (mostly C=O stretch)	1610-1690	Characteristic of protein secondary structure;
Amide II (N-H in-plane bend and C-N stretch)	1520-1560	Primarily used to monitor H → D exchange

Table 1-2. Correlation of amide I frequency with protein secondary structure

Protein Secondary Structure	Amide I frequency (cm^{-1})
α-helix	~1655 cm^{-1} for unhydrated helix ~20 cm^{-1} lower in frequency if hydrated
β-sheet	1625-1635 cm^{-1}
antiparallel β-sheet	1675-1695 cm^{-1}
random coil	1640-1650 cm^{-1}
aggregated strands	1610-1628 cm^{-1}

chapter, a novel LB transfer-based technique termed COVASP was used for the very first time to produce films with surface pressure gradient in the current study. IR imaging was used to take IR spectra from the COVASP films.

IR imaging is able to acquire a series of IR spectra with ~10 μm spatial resolution. Combined with the COVASP film transfer technique, IR imaging offers a convenient way to take spectra of monolayers at different surface pressures in a time-efficient manner. Since the COVASP film only has a surface pressure gradient in one direction, multiple spectra can be taken and averaged in the other direction, which improves the signal/noise ratio of the resultant spectra. Vibrational modes observed in IR imaging are similar to those in bulk phase IR or IRRAS as summarized in Table 1-1. When spectra are acquired in transmission mode in IR imaging, Beer's law applies and the spectra can be used for quantitative study.

1.2.3 Other techniques

Besides the surface activity measurements and IR spectroscopy discussed above, a broad range of techniques offer insight into lung surfactant study. Epifluorescence microscopy is used to study monolayer domain formation. X-ray reflection and diffraction offers information on molecular orientation and subcell structures. Brewster angle microscopy visualizes the domain structure in monolayers at the air/water interfaces. Viscosity measurements also help

differentiate between fluid and solid phases. We also utilized the high resolution

AFM to study multilayer formation in lung surfactant model in the current study.

Chapter Two: Materials and Methods

2.1 Materials

1,2-dipalmitoyl-sn-glycero-3-phosphocholine (DPPC), 1,2-dipalmitoyl-d_{62}-sn-glycero-3-phosphocholine (DPPC-d_{62}), 1,2-dipalmitoyl-sn-glycero-3-phospho-rac-(1-glycerol)] (sodium salt) (DPPG), 1,2-dipalmitoyl-d_{62}-sn-glycero-3-[phospho-rac-(1-glycerol)] (sodium salt) (DPPG-d_{62}), and cholesterol were purchased from Avanti Polar Lipids (Alabaster, AL) and used without further purification. Chloroform, methanol, ethylenediamine tetraacetic acid, disodium salt dihydrate (EDTA), calcium chloride dihydrate (CaCl$_2$•2H$_2$O) and HPLC-grade water were purchased from Fisher Scientific (Pittsburgh, PA). Lipid A, diphosphoryl from Salmonella enterica serotype Minnesota Re 595 (Re mutant), Lipopolysaccharides (rough strains) from *Salmonella enterica* serotype minnesota R7 (Rd mutant), Tris(hydroxymethyl)aminomethane hydrochloride (Trizma hydrochloride), Tris(hydroxymethyl)aminomethane (Trizma base), and sodium chloride were purchased from Sigma-Aldrich (St. Louis, MO). D$_2$O with 99.9% isotopic enrichment was purchased from Cambridge Isotope Laboratories (Andover, MA).

Highly purified porcine pulmonary surfactant protein SP-C was the generous gift of Ms. June Stewart and Professor Kevin Keough (Memorial University, St. John's Newfoundland, Canada). The peptide mimics of SP-C, the poly-N-

substituted glycines or "peptoids" were kindly provided by Dr. Annelise E. Barron (Stanford University, Stanford, CA). Full length porcine pulmonary surfactant protein SP-A was gift of Ms. June Stewart, and genetically engineered truncated Neck-CRD SP-A including N187S/PL SP-A, D215A/PL SP-A were kindly provided by Dr. Francis X. McCormack (University of Cincinnati, Cincinnati, OH). N187S/PL SP-A and D215A/PL SP-A were received in 5mM Tris buffer at pH 7.4.

2.2 Methods

2.2.1 Sample preparation

DPPC, DPPC-d_{62}, DPPG-d_{62} and cholesterol were dissolved in chloroform, while DPPG, lipid A, R7 LPS and SP-C solutions were prepared in chloroform/methanol (19:1, 9:1, 9:1, and 2:1 v/v, respectively). Phospholipid and SP-C solutions were prepared at ~1 mg/mL and lipid A and R7 LPS solutions had concentrations of ~0.5-1 mg/mL. R7 LPS solution was slightly heated to 45 °C to facilitate dissolution. Peptoid solutions were prepared in methanol at a concentration of ~2.5 mg/ml. The phospholipid/cholesterol/peptide mixture solutions consisted of DPPC/DPPG at a 4/1 molar ratio with 7 mol % cholesterol and 4 mol % SP-C. The deuterium labels were switched between the DPPC and DPPG as needed, although most of the reported measurements had the PC chains perdeuterated. For the peptoid study, the standard lipid film used consisted of DPPC-d_{62} /DPPG at a 4/1 molar ratio with 7 mol % cholesterol and

various mole % levels (generally 4 or 10 mol %) of peptoid or 4 mole % SP-C as desired.

2.2.2 π-A isotherm acquisition

A model 611D standard LB trough (Nima Technology, Coventry, UK) equipped with a PS4 surface pressure sensor and a D1L-75 linear dipper was used to acquire π-A isotherms, monitor the dipper position as described below and transfer the Langmuir film onto the substrate. The subphase containing 5 mM Trizma HCl and Trizma base, 150 mM NaCl and 0.02 mM EDTA at pH ~7.00 in HPLC-grade water was used to float the DPPC/DPPG/Cholesterol/SP-C film. A buffer consisting of 5 mM Trizma HCl and Trizma base and 150 mM NaCl at pH ~7.00 in HPLC-grade water was used for peptoid experiments. The temperature of the subphase was controlled at 20.0 (±0.5) ^{o}C. Typically, 25-50 μL of the lipid, lipid/protein, or lipid/peptoid solution was spread onto the subphase surface, and 30 minutes were allowed for solvent evaporation and film stabilization. Isotherms were then recorded as the film was compressed or expanded with a barrier speed of 15 cm^2/min.

2.2.3 Langmuir-Blogett film transfer

Freshly cleaved mica sheets were used to transfer lipid/peptoid films under constant surface pressures and for the subsequent AFM imaging. The mica sheets were partially immersed underneath the subphase before film spreading.

When the films were compressed to the desired surface pressures, the compression was switched to a constant surface pressure mode, which kept the film surface pressure constant by barrier movements. ~2-5 minutes after achieving the desired pressure, film transfer was initiated by lifting the mica sheets up at a speed of 1mm/min. The transferred film was allowed to air dry and then used for AFM imaging.

2.2.4 COVASP film transfer

A 25 mm diameter circular CaF_2 window used as the substrate was clamped onto the "dipper" accessory of the trough (total surface area ~600 cm^2) and partially immersed in the subphase prior to spreading the film. Typically, 50μL of a ~1 mg/mL solution was spread onto the clean subphase surface, and 30 min was allowed for solvent evaporation and film relaxation/equilibration. The film was then compressed at a rate of area change of 15 cm^2/min. When the desired starting surface pressure was achieved, the substrate was lifted at a rate of substrate movement of 1 mm/min while the barrier continued moving at a constant rate. The π-A isotherm and the dipper position were recorded simultaneously during the transfer. The compression was continued until the end of the plateau region when the surface pressure started to increase at an altered rate. The direction of barrier travel was then switched to expand the film at the same rate (15 cm^2 /min) to the maximum area desired. At the completion of the transfer, the dipper was raised until the substrate was completely removed from

the solution. The transferred film was typically 20-23 mm long along the substrate diameter. The entire process is schematically depicted in Figure 2-1A.

The clamp position on the substrate was physically marked before the experiment. The length of the transferred film was calculated from the dipper position at the beginning and end of the transfer. The film starting position was known to be at a certain distance away from the clamp position. The meniscus radius was also considered in the calculation. We employed an additional method for correlating sample position with surface pressure. The sample point with the highest IR peak intensities occurred just prior to film expansion, and had the highest surface pressure. From this point the surface pressures of all the sampling points were obtained. These two methods were in good accord. A schematic representation of the surface pressure during the transfer and IR sampling process for a typical experiment with four-component surfactant system is given in Figure 2-1B. The points along the curve depict the position/pressure values at which IR spectra were typically acquired during a cycle. As shown in the figure, transfer was initiated at a relative sample position on the crystal defined as "0" mm and at a typical surface pressure of 25 mN/m. The compression process was continued and revealed a monotonic increase in pressure to a value of 54 mN/m at a sample position of ~6.6 mm. The horizontal region of the isotherm displays nearly constant surface pressure until a position of ~13 mm, at which point expansion was initiated and followed the position-pressure trajectory marked on the figure. The transfer was terminated at a pressure of ~23 mN/m.
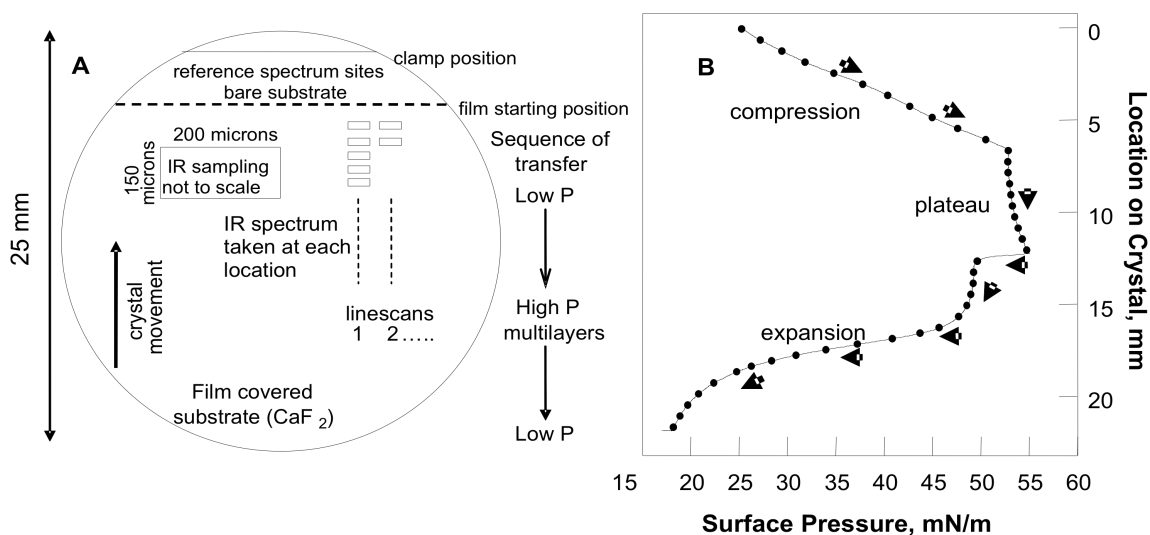
Figure 2-1. (A) Schematic of the COVASP transfer. A CaF$_2$ crystal substrate clamped to the "dipper" was partially immersed in the subphase prior to spreading the film. The substrate was lifted at a constant rate as the surface area changed during film compression and expansion. IR spectra were acquired with an aperture size of 200×150 µm (with the latter parallel to the film transfer direction) and 35 IR spectra were typically acquired for one linescan along the transfer direction. 5 or 10 linescans were averaged for each sample. (B) Correlation between the transferred sample position and surface pressure. Film location on the crystal as a function of surface pressure (—) was calculated from the dipper position *vs.* surface pressure curve, which was recorded during the film transfer. IR spectra were acquired every 600 µm (●) along the film transfer direction. The arrows indicate the temporal sequence of events.

2.2.5 Atomic force microscopy

Lipid/peptoid LB films were transferred onto freshly cleaved mica substrates at specified constant pressures and imaged with a multimode AFM (Nanoscope III A, Digital Instruments, Santa Barbara, CA, USA). Tapping mode topographic images were acquired in air using a phosphorus (n) doped silicon cantilever/tip assembly (Model: MPP-12100, Veeco) with a resonance frequency of approximately 127-170 kHz, a spring constant of approximately 5 N/m, and a tip radius of less than 10 nm. The applied frequency was set on the lower side of the resonance frequency and scan rate was ~1.0 Hz.

2.2.6 IR imaging

IR spectra of the transferred film at different surface pressures were collected with the single point detector in the Perkin-Elmer "Spotlight" system (PerkinElmer Life and Analytical Sciences, Inc., Waltham, MA) at particular positions along a line on the substrate. Samples were positioned on a high-precision computer-controlled motorized sample stage. The stage was enclosed in a home-built chamber and purged with dry air and N_2 to control the relative humidity levels to 11% or lower. Spectra were acquired with an aperture size of 200x150 μm (the latter parallel to the transfer direction) every 300 or 600 μm along lines parallel to the transfer direction. 128 scans with 2 cm^{-1} resolution were co-added for each spectrum and background spectra were acquired from a clean spot on the crystal every 2 sample points. Approximately 35 spectra were usually taken for each line

scan, requiring a collection time of ~2 hours. Five or ten line scans were averaged for each sample.

2.2.7 IRRAS

The IRRAS instrument setup is shown in Figure 2-2. Spectra were acquired with a Bruker Instruments Equinox 55 spectrometer equipped with an external variable angle reflectance accessory, the XA511. The accessory is coupled to a custom-designed Langmuir trough (maximum surface area of 96 cm^2) constructed by Nima Technology Ltd. (Coventry, England) with a model PS4 surface pressure sensor. The trough was designed to permit the injection of aqueous solutions into the subphase without disturbing a preexisting monolayer. The trough has two independently controlled barriers and a center divider, the top of which lies just beneath the water surface. Injections are made when the back barrier is positioned over the divider which leaves a small gap of ~0.25 mm. This retards the rate of solute diffusion to the background side while maintaining an equal subphase height on either side of the barrier for acquisition of high-quality IRRAS spectra.

The IR beam is directed through the external port in the spectrometer and is reflected by three mirrors in a rigid mount prior to being focused on the water surface. Computer-driven stepper motors rotate the mirrors to obtain the desired

IRRAS INSTRUMENT

back barrier

divider

front barrier

Wilhelmy plate

reference surface

film covered surface

injection port

LANGMUIR TROUGH
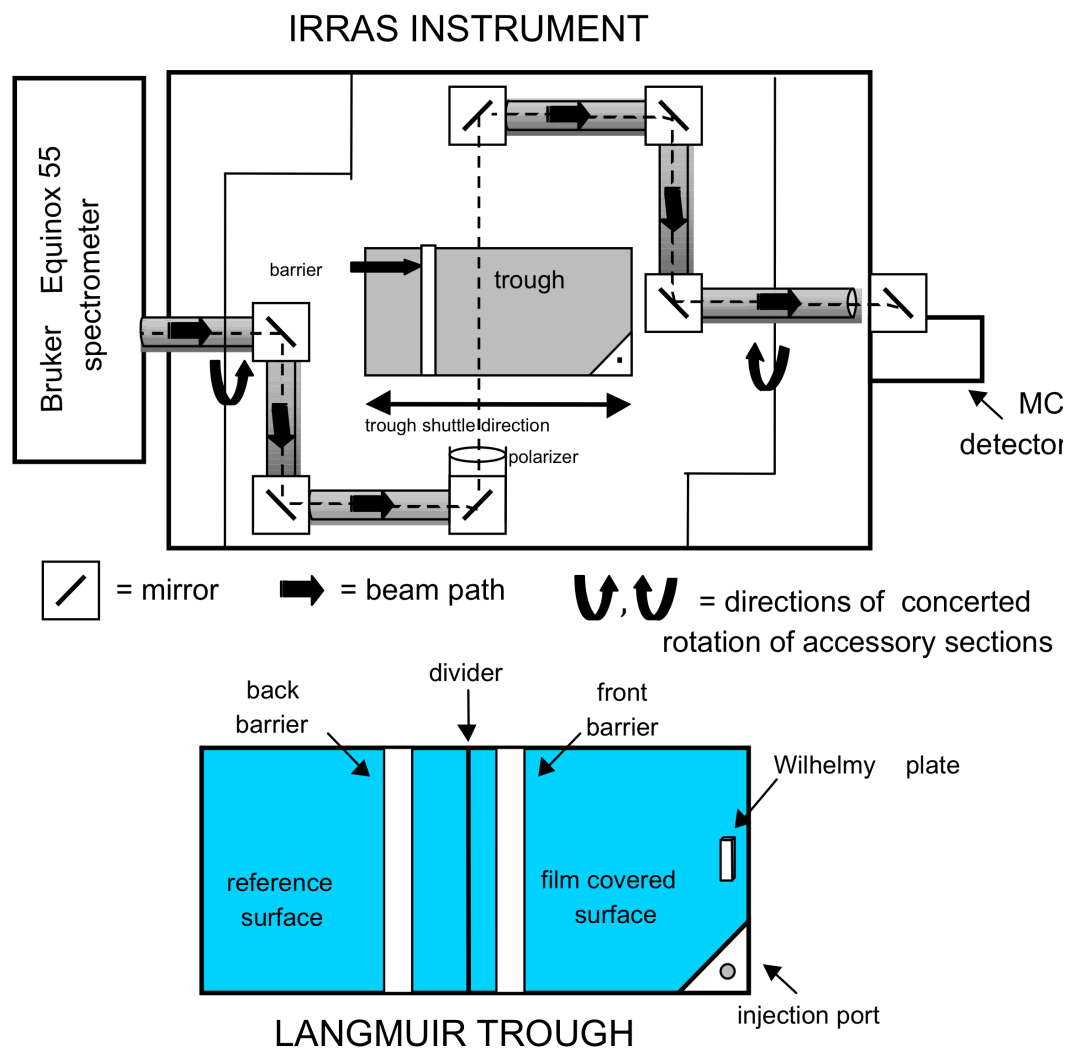
Figure 2-2. Instrumentation setup of IRRAS.

angle of incidence. A wire grid polarizer is mounted in the optical path directly before the beam impinges on the water surface. The reflected light is collected at the same angle as the angle of incidence, follows an equivalent mirror path, and is directed onto a narrow band mercury/cadmium/telluride (MCT) detector. The entire experimental setup is enclosed and purged to keep the relative humidity levels both low and as constant as feasible.

Interferograms were collected with the use of a sample shuttle program to compensate for the residual water vapor rotation-vibration bands in the amide I region. For each spectrum, a total of 1024 scans were acquired at ~4 cm^{-1} resolution, in 4 blocks of 256 scans each, co-added, apodized with a Blackman-Harris-3-term function, and fast Fourier transformed with one level of zero-filling to produce spectral data encoded at ~2 cm^{-1} intervals. IRRAS spectra are reported as -log (R/R$_o$) where R is the intensity of light reflected from the film-covered surface and R$_o$ is the intensity of light reflected from the background surface.

IRRAS experiments were conducted as follows. Aliquots of ~10-25 μL of lipid solution were spread dropwise on a H_2O- orD_2O-based subphase (same composition as described above) and 30 minutes were allowed for equilibration. The initial surface pressure for all experiments was 0 mN/m. Spectra were collected during intermittent compression while π-A isotherms were recorded. A barrier speed of 1cm^2/min was used. The barrier was stopped at particular surface pressure values and a relaxation period of 5 minutes was allowed before spectral acquisition. Unless otherwise noted, spectra were collected using s-

polarized light at a 50° angle of incidence. For studies of SP-A or truncated SP-A adsorption, when the desired surface pressure (10 or 25 mN/m) was reached, 100-200 μL of protein solution containing 60 μg of protein was injected beneath the preformed lipid monolayer with the back barrier positioned over the divider. When the surface pressure had stabilized (30-45 min), spectra of the lipid/protein film were acquired either during further intermittent compression or at a series of time delays after protein injection using s-polarized radiation at incidence angle of 50°. Within the IRRAS spectral acquisition time, there was no indication of protein diffusion to the reference side of the trough.

2.3 Data analysis

2.3.1 IR and IRRAS spectroscopy

Spectra were initially examined and averaged with Grams/32 (Galactic Industries Corp., Salem, NH). IR frequencies were calculated with a center-of-gravity algorithm written by D. Moffatt and generously provided by the National Research Council of Canada. Peak integrated areas were calculated with the same program. All figures were prepared for presentation with SigmaPlot 2000 (SPSS Inc., Chicago, IL).

2.3.2 AFM

The acquired AFM images were analyzed by Nanoscope Software (Veeco, Plainview, NY). Height differences were obtained from section analysis of the topographic images and were presented by color-coding. The detail height profiles of the surface were analyzed along lines on the sample surface.

Chapter Three: Structural Characterization of the Monolayer-Multilayer Transition in a Pulmonary Surfactant Model

3.1 Introduction

As discussed in the introduction, hydrophobic lung surfactant associated proteins SP-B and SP-C are suggested *(48, 49)* to control the surface properties of surfactant, although the molecular level mechanism of their action is not fully determined.

The rapid adsorption and spreading of those surfactant constituents able to sustain high surface pressures under compressive forces are required for surfactant to stabilize the lung. Two primary attributes of surfactant must be explained within any model of lung function. First, surfactant must form and maintain stable surface films during exhalation-inhalation cycles within the alveolar lining layer. Since DPPC is the major constituent able to form stable monolayers under compressive forces, it was postulated some decades ago that the surface concentration of DPPC must be enhanced at high pressures by exclusion of other surfactant constituents from the monolayer, a process termed "squeeze-out" *(20)*. This laboratory *(50, 51)* and others *(52)* have used a variety of physical techniques to demonstrate the general phenomenon, although quantitative information about the composition and molecular structures of the phases is incomplete.

The second issue that any model of surfactant function must address is the mechanism of re-spreading of the surface film following compression, i.e. expansion *in vitro* or inhalation *in vivo*. A variety of experiments utilizing both intact lung tissue and model films have demonstrated the existence of surfactant-associated multilayers formed at high pressures. In a seminal study, Schurch et al. *(14)* used transmission electron microscopy to probe the ultrastructure of an alveolar surface film from guinea pig lung. Under their experimental conditions, the surface film was partially "multilaminated" with variation in the number of lamellae from two to seven. These lamellae were presumed to act as reservoirs for substances such as the surfactant proteins SP-B and SP-C which enhance the rate at which surfactant lipids spread across the air/water interface. Very recently, neutron reflection studies *(53)* of porcine surfactant have revealed a multilayer structure of lipid-protein bilayers alternating with aqueous layers. In additional prior work (*21, 23, 54-57*), supramolecular organizational changes upon compression were observed in films that mimic the alveolar lining layer.

In vitro studies by the Galla group *(22, 58)* have convincingly demonstrated the role of SP-C in stabilizing the reversible formation of multilayers in three- or four-component systems that include *(58)* DPPC and DPPG. The role of cholesterol has also been probed *(59, 60)*. Elevated levels of cholesterol were shown to disrupt the assembly of an efficient film. As a result of all the above investigations, the phenomenon of multilayer formation is now accepted in most models of surfactant function.

Few techniques can provide direct molecular structure information from models for the thin films comprising the pulmonary lining layer. IRRAS is a useful means for studying lipid and protein films from monolayers in situ at the air/water interface *(41)*. This laboratory applied *(23)* IRRAS in conjunction with atomic force microscopy and pressure-area isotherms to investigate both molecular and supramolecular aspects of the monolayer-multilayer transition in a four-component model (DPPC/DPPG/cholesterol/SP-C) for the lining layer. Polarized IRRAS measurements indicated that the SP-C helix tilt angle changed from ~80° to the surface normal in monolayers to a transbilayer orientation in multilayers. These results suggest that the projected area occupied by SP-C in the film plays an important role in achieving reversible multilayer formation during cycling.

To overcome technical difficulties in measuring relative concentrations of constituents under conditions of both compression and expansion, we recently presented *(61)* a new method for the analysis of surface films. The approach is termed COVASP, an acronym for "continuously varying surface pressures". As the name implies, surface films are transferred to substrates chosen for specific physical measurements while the surface pressure is continuously changing. The entire pressure-area phase diagram is thus available on the substrate. The substrates chosen for initial transfer were appropriate either for IR spectroscopy (CaF$_2$ crystals) or fluorescence microscopy (glass) measurements. In the COVASP film, the transferred monolayer resides on an IR window and may be examined by transmission spectroscopy at relative leisure, since, as shown below, the phase and domain properties are preserved on the substrate for at

least a week. Initial IR measurements of chain conformational order for transferred DPPC monolayers indicated that the molecules retained at least in part, their surface-pressure-dependent chain-conformational order characteristic upon transfer to the CaF_2 substrate.

Several aspects of the monolayer ↔ multilayer transition are probed in the current work. First, the chemical composition of the multilayer *vs.* the monolayer phase, e.g., relative amounts of lipid and protein ratios in the two states, and the preference of particular lipids for one phase or another, are underdetermined although the development of spatially resolved time-of-flight secondary ion mass spectrometry (TOF-SIMS) has demonstrated (*56, 62*) the ability to examine the composition of the surface layer in films transferred from the collapse region. Second, no data are currently available to monitor structural alterations in the lipid and protein components upon multilayer formation. Finally, the nature of the above parameters during the re-expansion part of the cycle has not been studied to any substantial extent.

In the current study, we utilize COVASP-IR and π-A isotherms to monitor the composition and molecular structure of the components of multilayer phases as well as to demonstrate the feasibility of this experiment for studying the expansion process in the aforementioned four-component surface film mimic of pulmonary surfactant (DPPC-d_{62}/DPPG (4:1)/cholesterol (7 mol %)/SP-C (4 mol %)). Limitations and possible extensions of the COVASP method are discussed.

3.2 Results

3.2.1 Film stability on a CaF$_2$ window.

The temporal persistence of chain conformational order following the transfer process is demonstrated in Figure 3-1 for a COVASP film of pure DPPC. The spectral parameter used for this purpose is the CH$_2$ asymmetric stretching mode of DPPC (ν_{asym}CH$_2$) near 2920 cm^{-1}. As is well known, this frequency directly tracks chain conformational order, and is shown as a function of pressure for three increasing times following transfer. In each case, the decrease observed in ν_{asym}CH$_2$ is characteristic of the LE $\rightarrow$ LC transition between ~5 and 6 mN/m and reveals chain conformation ordering upon compression. It is clear that the transition as monitored by this parameter mostly persists following transfer for a time period of at least seven days on the film-containing substrate, although some progressive increased chain ordering at all pressures was observed with time. Thus the conformational order and phase transition characteristics are preserved to a significant extent on the substrate. However, it is reemphasized that the substrate does not "lock" the conformation of the transferred molecules. Thus, for the experiments reported below, IR spectra of COVASP films were routinely acquired on the day of film transfer. As a further indication of transferred film stability, observations of DPPC domains on glass with epifluorescence microscopy revealed that the domain formation observed following film transfer *(61)* persisted for several weeks with COVASP transferred films (Prof. J. Perez-Gil, personal communication). Thus both molecular and supramolecular
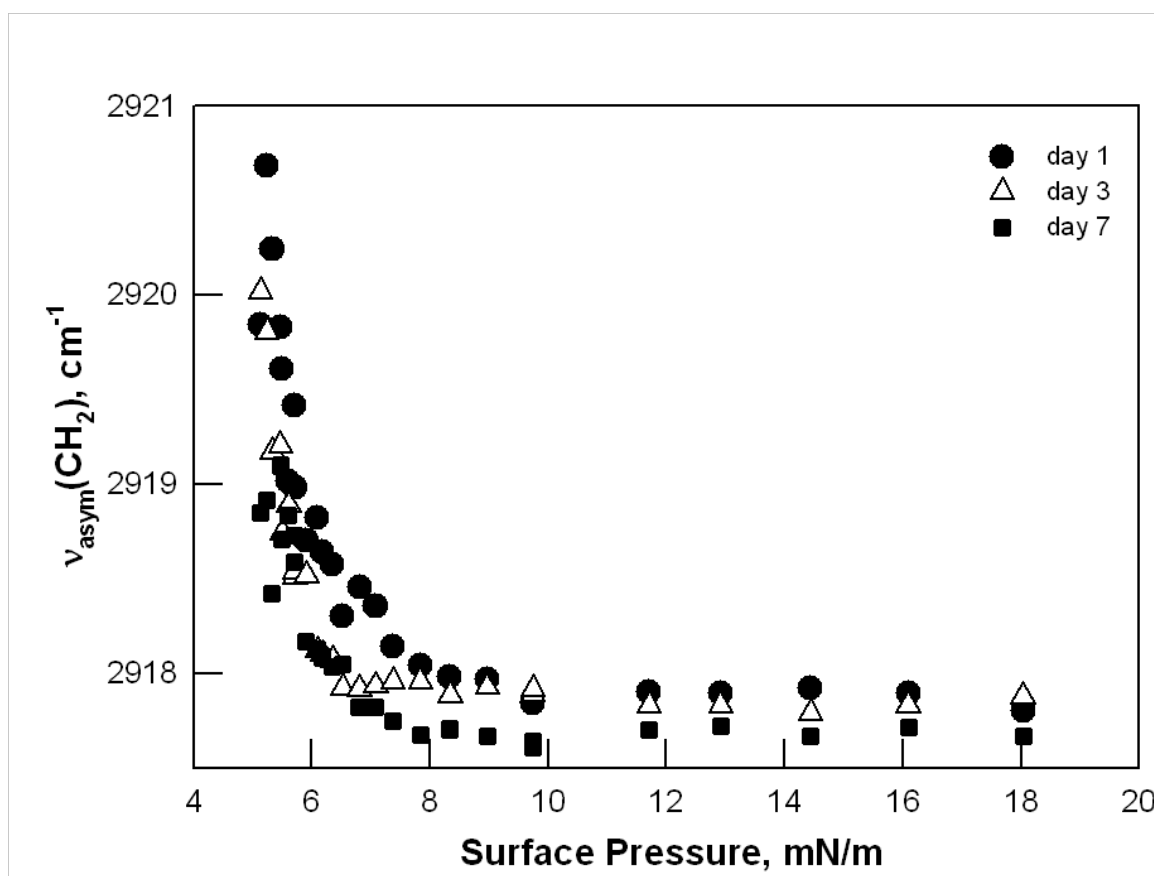
Figure 3-1. Surface pressure dependence of the asymmetric CH_2 stretching frequency of DPPC on the day of film transfer (●), 2 days after film transfer (△) and 6 days after film transfer (■). Results for a single film are shown. Similar data were acquired for several films of DPPC and DPPC-d_{62}.

properties of the samples are transferred and preserved during the COVASP transfer. Film ordering, the formation of defects, and the kinetics of reorganization in LB films have been discussed by Takamoto et al. (*63*), who investigated the effects of pH on the cadmium arachidate films.

3.2.2 Pressure-area isotherms

The four-component system, DPPC-d_{62}/DPPG (4:1)/cholesterol (7 mol %)/SP-C (4 mol %) undergoes a reversible monolayer ↔ multilayer transition at a surface pressure of ~53 mN/m. π -A isotherms for this system (without transfer of material) in the presence of SP-C are shown in Figure 3-2A. The plateau at ~53 mN/m is indicative of multilayer formation. The transition is essentially completely reversible as demonstrated by the retracing of the isotherm during successive compression-expansion cycles. The vital role of SP-C for the reversibility of the process is demonstrated through the isotherm acquired in the absence of the peptide (inset to Figure 3-2A). This monolayer is unstable at high pressures; the isotherm reveals film collapse and/or leakage. The exact shape at high pressures is neither reproducible nor reversible.

π -A isotherms for the four-component system (in the presence of transfer) with the deuterium labels exchanged (e.g., DPPC/DPPG-d_{62} (4:1)/cholesterol (7 mol %)/SP-C (4 mol %) *vs.* DPPC-d_{62} /DPPG (4:1)/cholesterol (7 mol %)/SP-C (4 mol %)) are compared in Figure 3-2B. Switching the deuterium label positions produce small changes in the isotherm, which is not considered significant at this
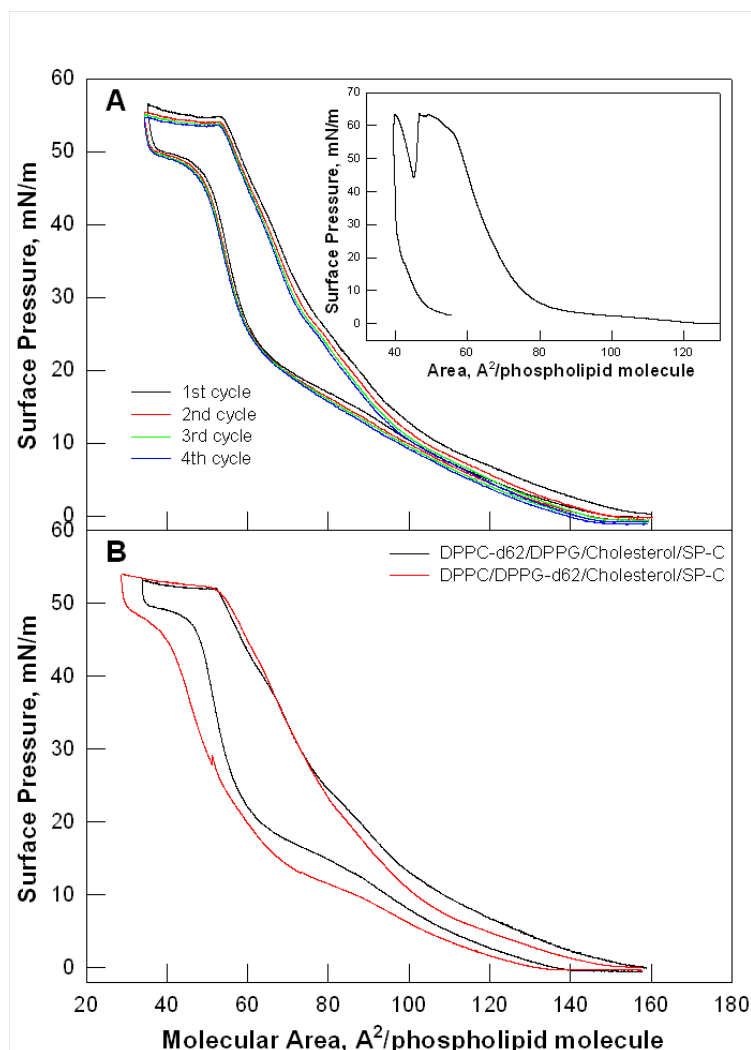
Figure 3-2. (A) π-A isotherms of the four-component system without film transfer (DPPC-d_{62}/DPPG 4:1 mol ratio; cholesterol 7 mol %; SP-C 4 mol %) showing four cycles of compression/expansion (1st cycle, black; 2nd cycle, red; 3rd cycle, green; 4th cycle, blue). Inset: π-A isotherm for the three-component system (DPPC-d_{62}/DPPG 4:1 mol ratio; cholesterol 7 mol %). (B) π-A isotherms for the four-component system with film transfer (DPPC /DPPG 4:1 mol ratio; cholesterol 7 mol %; SP-C 4 mol %) with PC acyl chains perdeuterated (black line) and with PG acyl chains perdeuterated (red line).

point. IR spectra acquired following transfer with the DPPG labeled occasionally produced data sets with better signal/noise or signal/water vapor ratios in spectral regions containing the SP-C amide I mode.

3.2.3 COVASP-IR measurements

3.2.3.1 Control system: DPPC-d_{62}/DPPG/cholesterol

The three-component film DPPC-d_{62}/DPPG/cholesterol was compressed until a surface pressure of 48 mN/m, i.e., before the collapse point, and then reexpanded as shown in Figure 3-3A. The COVASP transfer sequence which occurred simultaneously with the compression is presented as an inset to the π-A isotherm in Figure 3-3A. The shift in the isotherm between the first and second compression reflects a slight loss of material due to transfer to the CaF_2 window.

The C-H and C-D stretching regions from typical COVASP-IR spectral data for the control system are overlaid in Figure 3-3B. The use of DPPC-d_{62} permits the separate monitoring of both the DPPC and DPPG constituents of the film through the CD_2 and CH_2 stretching frequencies, respectively, the most prominent of which are identified on the figure.

The surface-pressure induced variation in the CH_2 and CD_2 stretching modes between 10 and 48 mN was tracked during the compression-expansion cycle. The intensities and frequencies of the asymmetric CH_2 stretching modes of the DPPG are shown in parts A and B, respectively, of Figure 3-4, while equivalent parameters for the asymmetric CD_2 stretching modes of DPPC-d_{62} are shown in
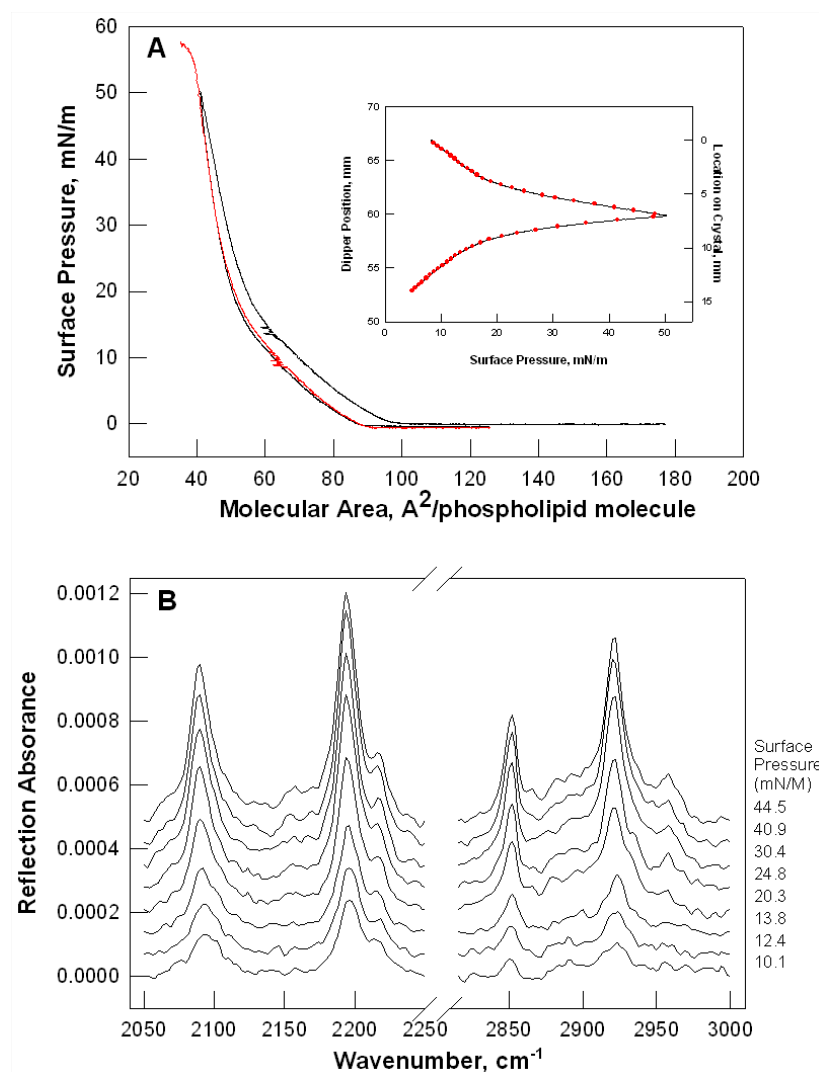
Figure 3-3. (A) π-A isotherm for the three-component system (DPPC-d_{62}/DPPG 4:1 mol ratio; cholesterol, 7 mol %) with COVASP film transfer during the 1st cycle (black line). A second compression was conducted following film transfer (red line). Inset: COVASP film transfer process. Both the film location on the crystal (black line, left axis), and the IR beam sample positions (red spherical spot, right axis) are shown. (B) Overlaid CH_2 and CD_2 stretching regions for the three-component system. Spectra were acquired at different surface pressures (as indicated) during compression.
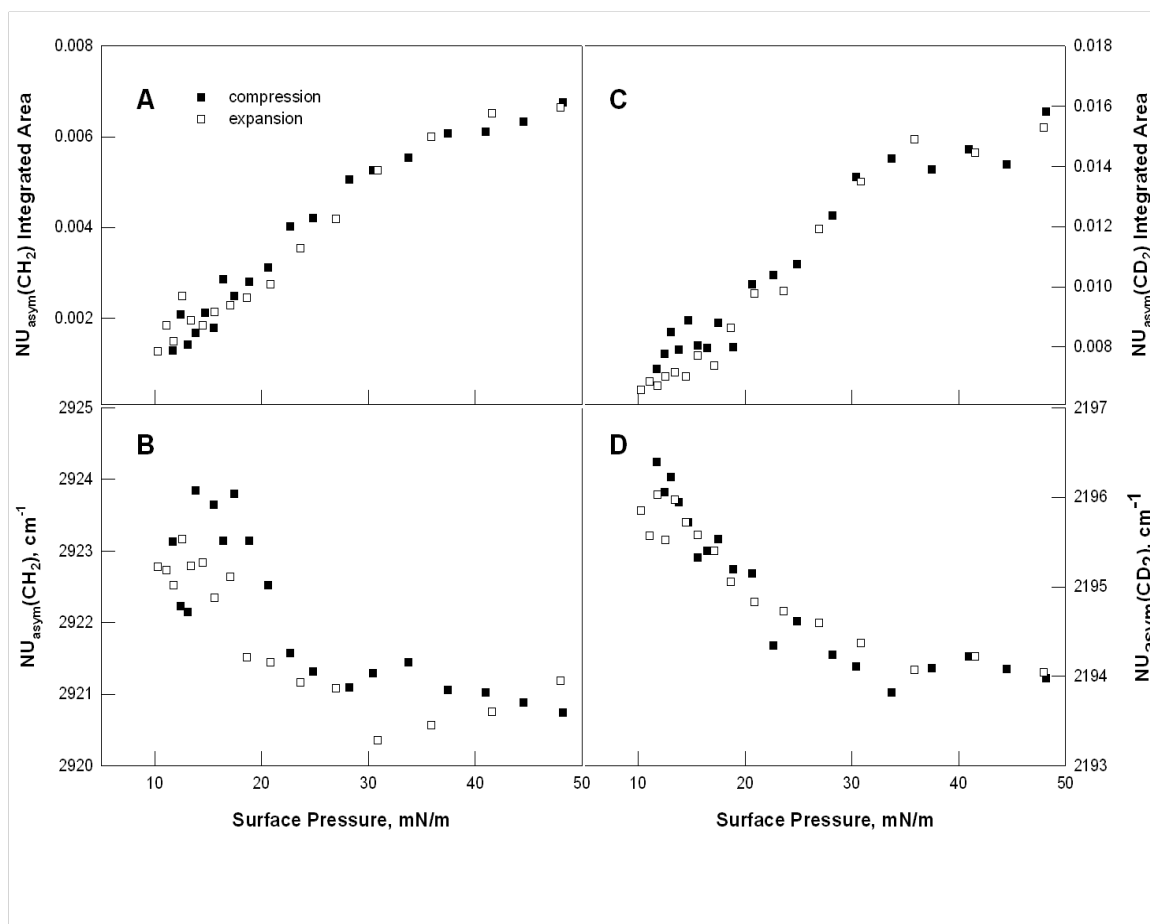
Figure 3-4. (A) Surface pressure dependence of the integrated area of the asymmetric CD_2 stretching of the three-component system (DPPC-d_{62}/DPPG 4:1 mol ratio; cholesterol 7 mol %). (B) Surface pressure dependence of the asymmetric CD_2 stretching frequency. (C) Surface pressure dependence of the integrated area of the asymmetric CH_2 stretching mode. (D) Surface pressure dependence of the asymmetric CH_2 stretching frequency of the same system. Spectra were acquired both during film compression (■) and expansion (□).

parts C and D, respectively, of Figure 3-4. The CD_2 stretching frequencies in Figure 3-4D show an essentially monotonic decrease between 10 and ~30 mN/m due to chain ordering as the pressure is increased, while the integrated intensities (Figure 3-4C) show an increase over the same pressure range due to an increased density of molecules in the beam during the compression. Both parameters exhibit essentially horizontal regions at higher pressures, indicating the well-packed nature of the chains during the putative LC→S transition. No significant hysteresis is observed upon expansion; the curves for both parameters retrace themselves. Similar results are shown for the CH_2 stretching modes of DPPG, although the scatter in the frequency plots at low pressures (Figure 3-4B) is increased, presumably because of the lower concentration of DPPG and somewhat worse instrument response in the C-H stretching compared to the C-D stretching region.

3.2.3.2 DPPC-d_{62}/DPPG/cholesterol/SP-C

COVASP-IR spectra for the four-component system as a function of surface pressure are depicted in Figure 3-5. The high spectral quality is evident; modes relevant for the current study are labeled. The transfer plot is that given in Figure 2-1B, while the isotherm is that shown in Figure 3-2B. Several aspects of the COVASP data will be considered.

The surface pressure-dependent intensities of the CH_2 asymmetric stretching modes, the CD_2 asymmetric stretching modes, the lipid C=O stretching modes

(~1735 cm^{-1}), and the protein amide I modes (~1655 cm^{-1}) during the compression-expansion cycle for the four-component system are presented in parts A-D, respectively, of Figure 3-6. The data are plotted for surface pressures greater than ~25 mN/m, of most interest in the current work. Each of the intensities shows a marked increase during the compression part of the cycle with a discontinuity at a surface pressure of ~53 mN/m, which corresponds closely to the onset of multilayer formation as observed in the isotherm, both with and without transfer (Figure 3-2B). During the expansion part of the cycle, the peak intensities diminish to approximately their initial values following some observable hysteresis that corresponds to a surface pressure lag of ~6 mN/m under the current conditions of film transfer. The hysteresis seems characteristic of multilayer formation, since little or none is observed for the three-component system (Figure 3-3).

3.2.4 Quantitative anlysis of the average extent of multilayer formation.

An important feature of COVASP-IR is the availability of quantitative or semi-quantitative information concerning the relative concentrations of various components of the multilayer along the phase diagram. Since the spectra are acquired in the transmission mode, Beer's law will apply to the intensities as a function of surface pressure, assuming no major orientation changes in the oscillating dipoles. The latter is unlikely for the phospholipids, since the acyl chain frequencies are consistent with highly ordered chains at the high surface pressures of interest here. Our previous study (*61*) also showed that the acyl
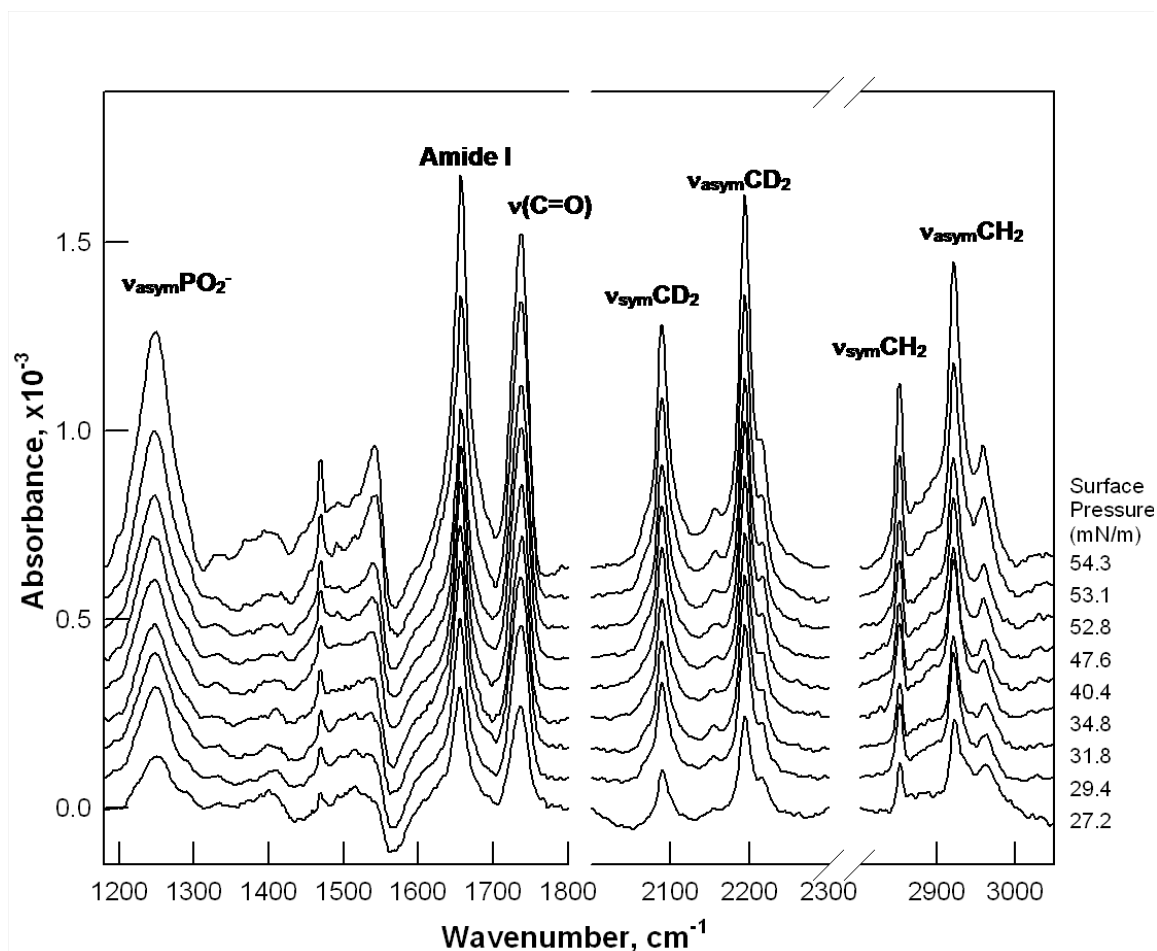
Figure 3-5. IR spectra for the four-component system (DPPC-d_{62}/DPPG, 4:1 mol

ratio; cholesterol, 7 mol %; SP-C, 4 mol %) overlaid at different surface

pressures, as shown, during compression.
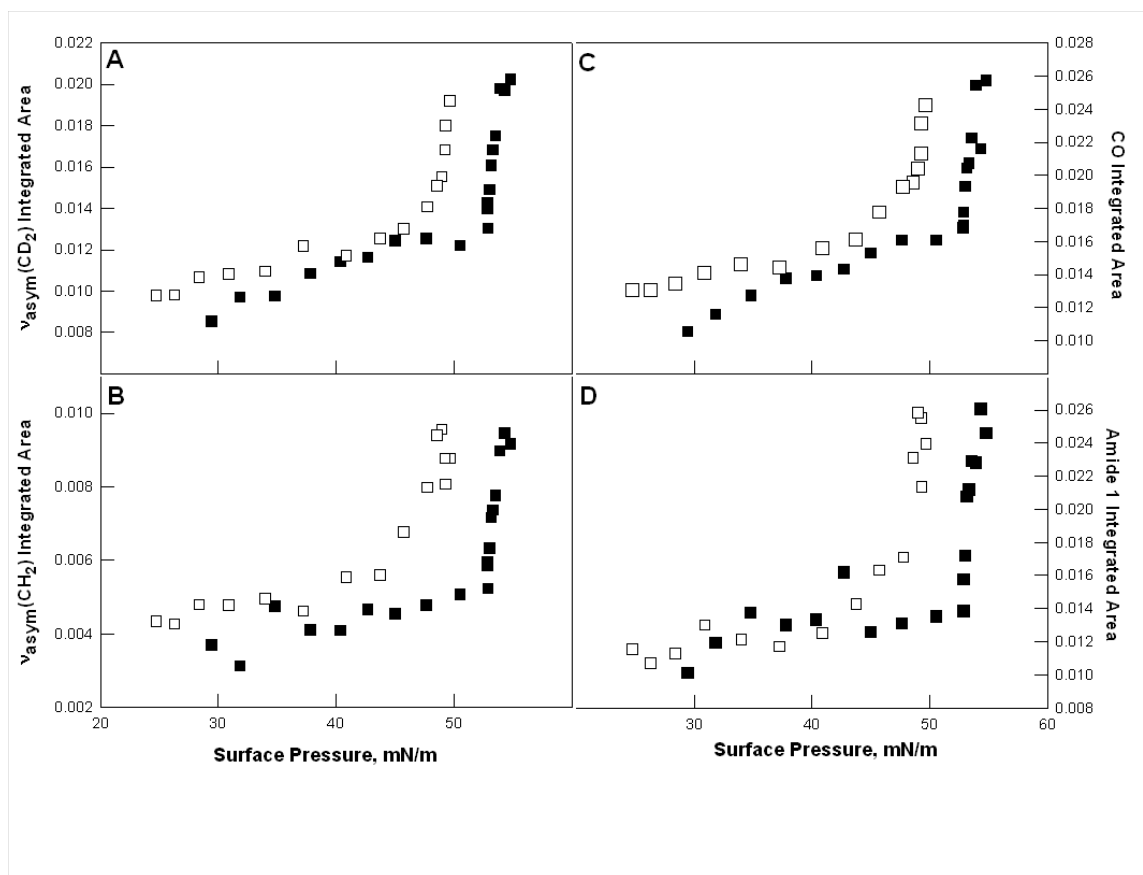
Figure 3-6. Surface pressure dependence of the integrated area of the characteristic peaks from the four-component system (DPPC-d_{62}/DPPG, 4:1 mol ratio; cholesterol, 7 mol %; SP-C, 4 mol %) for: (A) The asymmetric CD_2 stretching mode (~2195 cm^{-1}), (B) The asymmetric CH_2 stretching mode (~2918 cm^{-1}), (C) The ester C=O stretching mode (~1735 cm^{-1}), and (D) The amide I mode (~1655 cm^{-1}). Points collected during both film compression (■) and expansion (□) are shown.

chains are nearly perpendicular to the aqueous surface at pressures of 25, 40 and 55 mN/m.

The COVASP experiment measures structural properties averaged over all the molecules in the IR beam. The relative changes in the concentrations of the DPPC-d_{62} and DPPG, as calculated from the CD_2 (for DPPC-d_{62}) and CH_2 (for DPPG) asymmetric stretching intensities and from the amide I (for SP-C), are depicted in Figure 3-7. The data for two independent data sets (one in the inset) are plotted as a percentage increase in the peak area arising from a particular component as the pressure is increased beyond the onset of multilayer formation. This effectively eliminates the contribution to the band intensity of the particular component from the residual monolayer (assuming, as above, no orientation changes). Thus, if one of the components were completely excluded from the multilayer, the ordinate values would be approximately constant for that component, across the entire surface pressure range.

The level of SP-C in the multilayers increases monotonically and to about 90% as the surface pressure increases across the plateau and reflects dramatic concentration increases occurring over slight increases in surface pressure (52.0 to 52.8 mN/m for the data shown in the main body of the figure); the changes approximately parallel those for the DPPG component. This clearly reveals the strong preference for both SP-C and DPPG to reside in the multilayer rather than the monolayer environment under conditions of this transfer experiment. In contrast, the DPPC-d_{62} component, although evidently present in multilayers, is enriched by only ~60% over the same range of surface pressure change. Similar
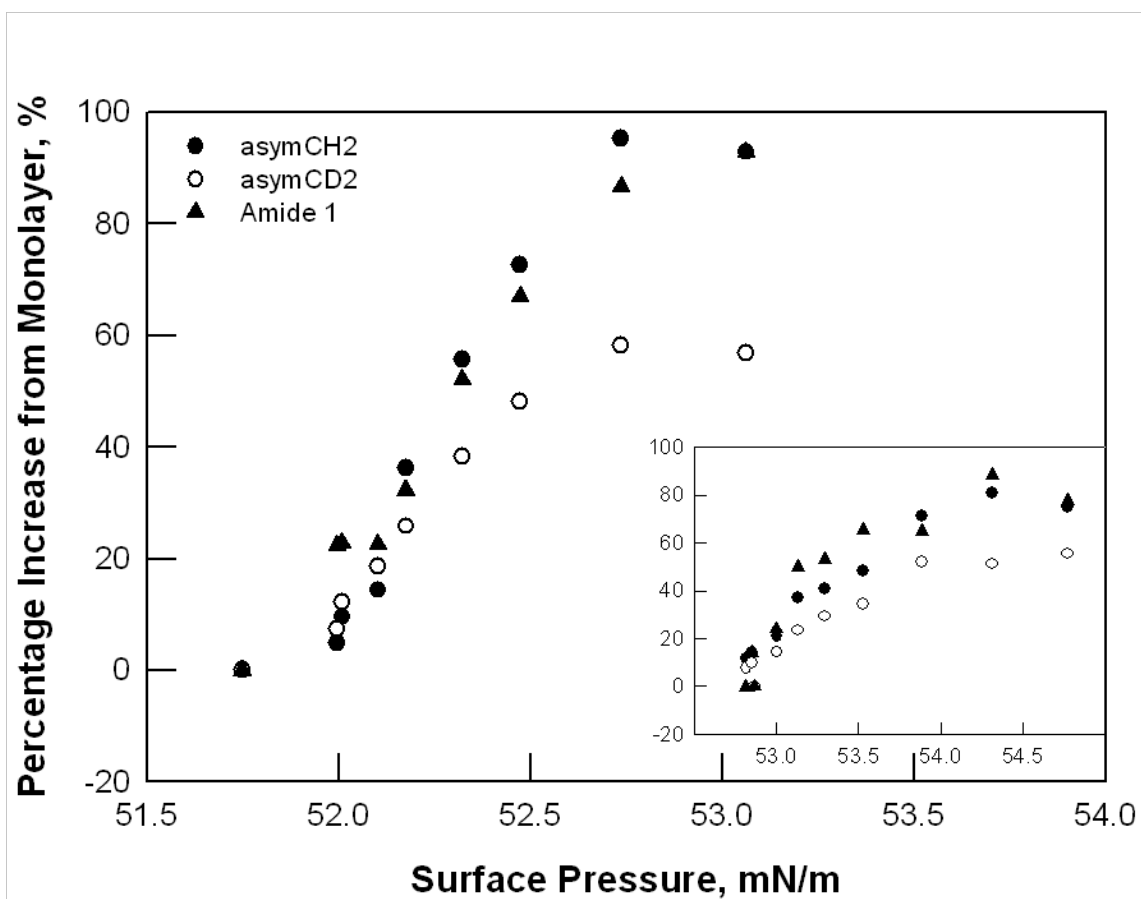
Figure 3-7. Peak intensity percentage increase in multilayers relative to the monolayer, from two experiments for the four-component system (DPPC-d_{62}/DPPG, 4:1 mol ratio; cholesterol, 7 mol %; SP-C 4 mol %) for the CH$_2$ asymmetric stretching mode (●), the asymmetric CD$_2$ stretching (○), and the

amide I mode (▲). The inset shows a replicate measurement which exhibits the same trends, but with the increases occurring at a slightly higher surface pressure.

Changes, occurring at a slightly higher surface pressures, are noted in the data shown in the figure inset.

3.2.4 Molecular structural information

As shown in Figure 3-8, some information about the molecular structure changes in the multilayers may be gleaned from the surface pressure dependence of particular vibrational modes. The DPPC component shows (Figure 3-8A) a small ~(0.2 cm^{-1}) decrease in $\nu_{asym}CD_2$ upon multilayer formation indicative of slightly increased conformational chain order of this component in the multilayers. Although close to the limit of experimental uncertainty (estimated at 0.05-0.1 cm^{-1}) of the measurement, the reversibility of the process as shown in the figure lends confidence to the suggested interpretation. In particular, the conformational order change for DPPC-d_{62} reversed itself upon expansion, following a hysteresis of ~5 mN/m. Changes in the minority component DPPG (not shown) were too close to the uncertainty in the measurement (~0.05 cm^{-1}) to lead to definite conclusions about conformational order changes.

A potentially useful spectral marker for the state of polar head groups in both lipids is available from the phosphate asymmetric stretching mode ($\nu_{asym}PO_2^-$) near 1245 cm^{-1}. This frequency is sensitive to the phosphate hydration state. In Figure 3-8B, an increase of ~2 cm^{-1} is noted in this mode during the compression, suggestive of head group dehydration in the multilayers relative to the monolayer. The scatter in the data is a result of the weakness of

the signal. As noted by Cameron et al.(*64*), in a paper not often cited, the precision of the frequency measurement using the center-of-gravity algorithm is strongly dependent on the signal/noise ratio.

Finally, the surface pressure dependence of the amide I mode is shown in Figure 3-8C. A frequency increase of ~0.9 cm^{-1} is observed upon compression following the onset of multilayer formation. The process is not significantly reversible during reexpansion. The origin of the observed frequency shift is unclear. We suggest (but cannot prove) that sequestration of the protein into a more hydrophobic environment (multilayers) may cause exclusion of water bound to peptide bond C=O, resulting in an amide I frequency increase due to restoration of C=O electron density induced by H-bond breakage or weakening. Alternatively, an early study by Rothschild and Clark (*65*) suggested that an anomalously high IR amide I frequency of bacteriorhodopsin in purple membrane fragments might result from an increased H-bond distance *within* a distorted α-helix. We cannot choose between these possible mechanisms for the origin of the observed frequency increase in the current experiments.
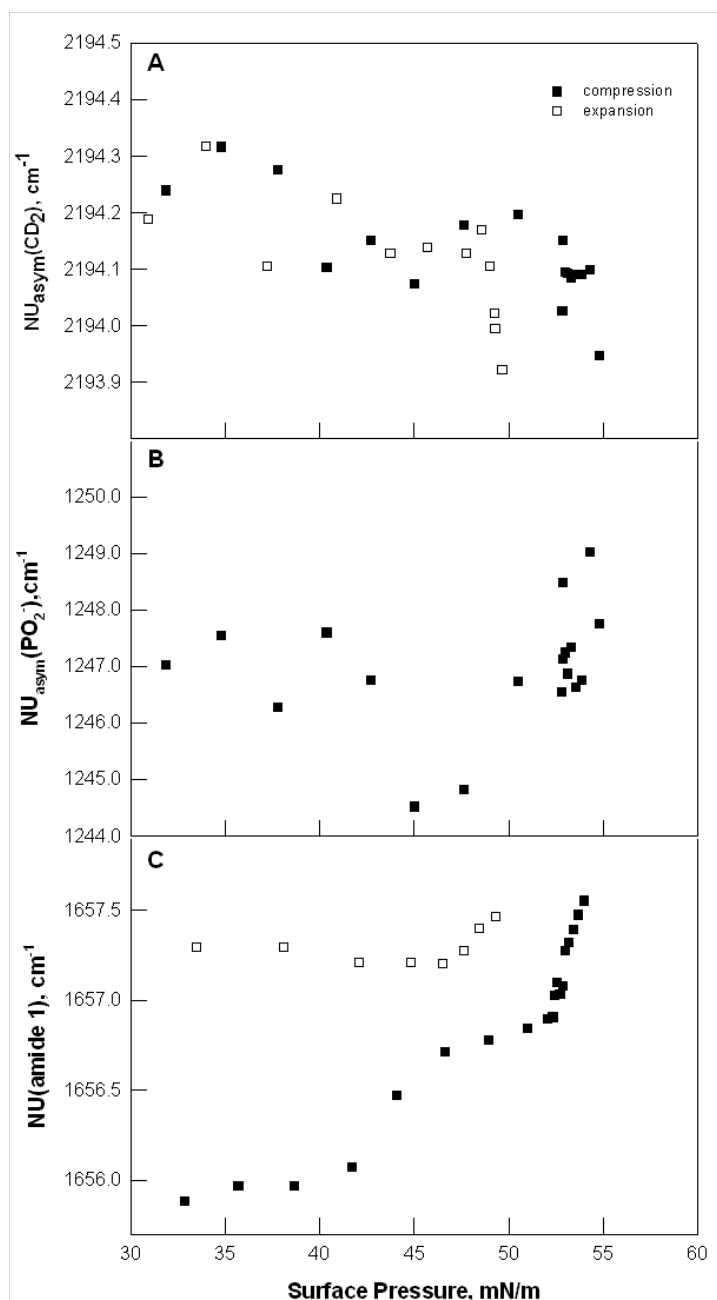
Figure 3-8. Surface pressure dependence of the peak frequency.

(A) The asymmetric CD_2 stretching mode;

(B) The phosphate asymmetric stretching mode, for the four-component system (DPPC-d_{62}/DPPG 4:1 mol ratio; cholesterol 7 mol %; SP-C 4 mol %);

(C) The amide I C=O stretching, for the four-component system (DPPC /DPPG-d_{62} 4:1 mol ratio; cholesterol 7 mol %; SP-C 4 mol %).

Points collected during both film compression (■) and film expansion (□) are shown.

3.3 Discussion

3.3.1 Advantages and drawbacks of the COVASP-IR approach

The COVASP-IR approach provides several advantages for the examination of multilayer films and especially for characterization of the monolayer-multilayer transition. Considering the weakness of the spectral features, IR spectra at high signal/noise ratios (150:1 for a 0.001AU peak height) may be acquired. Thus, characterization of both concentration (Figure 3-7) and structural (Figure 3-8) changes that occur during the monolayer-multilayer transition is feasible. For quantitative analysis of concentration changes, it is assumed that the intensities obey Beer's law, providing there are no large changes in transition dipole moment directions (unlikely at high pressures) as the surface pressure is altered. Thus relative concentration changes may be estimated. In addition, perhaps somewhat surprisingly, physical properties of the films such as chain conformational ordering, phase characteristics, etc., are preserved for times of at least one week (see Figure 3-1) in the transferred films, so that aspects of molecular structure of the film may be conveniently probed. Finally, isotopic labels are useful for tracking the concentrations and physical states of particular lipid constituents in the surface film. This traditional advantage of vibrational spectroscopy requires that the isotopically labeled constituent have very similar surface properties to the unlabelled system. Galla and his associates (57) have shown that in the case of DPPC/DPPG-SP-B, exchanging the isotope label

(between PC and PG) induces only small changes in the domain structure/thermodynamics of the surface film and does not significantly alter the formation of multilayers. We suggest that this is also the case for the current experiments incorporating SP-C (Figure 3-2B).

A drawback of the COVASP approach is that the experiment is macroscopic. Thus, enrichment of multilayers in SP-C and DPPG as reported in Figure 3-7 is an average over the monolayer and multilayers sampled within the area of the IR beam. It is noted that the extent and average number of bilayers in the multilayer is also awkward to ascertain from "nanotechniques" such as AFM and TOF-SIMS, since typically these methods do not sample a sufficiently large area to provide a meaningful average. Although such an analysis could be undertaken, it would be quite time-consuming.

Finally, we note that the concentration of 4 mol % SP-C was chosen to provide adequate signal/noise levels from the IR spectrum of that constituent. A concentration closer to a recently reported (*66*) quantitative value (weight ratio of SP-C/phospholipid in bronchial lavage = 1:37.6 or ~0.6 mole % SP-C) suggested to exist *in vivo* might reveal additional effects, such as complete exclusion of this component from the monolayer. Such a situation might be observed through a greater frequency shift in the amide I mode in the multilayer than currently observed in Figure 3-8C.

3.3.2 Connection to the role of SP-C in squeeze-out and multilayer formation.

The "squeeze-out" hypothesis was originally invoked (*20*) to provide a mechanism whereby the surface film at high pressures was enriched in DPPC, the only component thought capable of sustaining a film at high pressure. At that time, it was improbable that organized multilayers were seriously considered as a repository for the excluded material. As noted in the Introduction, the relatively recent observation of multilayers (over the last decade) by several groups in both *ex vivo* lung preparations and *in vitro* engenders confidence as to their relevance for the breathing mechanism. Thus the composition and molecular structure of the multilayers is an issue of central importance, and COVASP is used here to provide some molecular structure information along with relative concentration information.

The COVASP data qualitatively (Figure 3-6) reveal that the three components with identifiable IR signatures (DPPC-d_{62}, DPPG, and SP-C) all exist within the multilayer phase. This is best noted by discontinuities in the absorbance *vs.* pressure plots for functional groups from each species which occur at surface pressures of ~53 mN/m, precisely at the onset of multilayer formation. A possible confounding factor in the quantitative analysis is that alterations in the transition moment direction for a given normal mode could induce discontinuities in the plots independent of concentration changes (i.e., the extinction coefficients could be altered). However, similar shapes are observed

for the surface pressure-induced intensity (Figure 3-6) or frequency (Figure 3-8) changes of modes arising from both lipid constituents (e.g., the phosphate or C=O stretches) compared with modes arising from either the DPPC-d_{62} or DPPG constituents (e.g., the CD or CH stretching vibrations). It is unlikely that all these modes would change their transition moment directions in the same way so as to produce increased COVASP intensities without concentration increases.

In contrast, SP-C orientation is known (*23*) to be altered in going from monolayers to multilayers; this effect could indeed alter the relative concentration measurement. Since the SP-C helix is oriented preferentially perpendicular to the bilayer plane and more parallel to the monolayer plane, its amide I transition moment in bilayers is preferentially parallel to the normal to the plane (z-direction). Its IR spectral signature (per protein molecule) will thus be *reduced* in the bilayer compared with the monolayer, since the C=O bond direction of monolayer-bound SP-C is preferentially perpendicular to the normal to the plane (x, y direction). Thus the current estimate in Figure 3-7 of the relative amount of SP-C in bilayers is an *underestimate* of the true value. By simple geometric manipulation of the crystal geometry in the IR beam along the lines described some time ago by Nabedryk and Breton (*65, 66*), it will be feasible to undo the cylindrical (x, y) symmetry of the current experimental geometry and carry out polarized IR measurements to render the quantitative analysis of the SP-C distribution between monolayers and multilayers more precise. That is, we will be able to monitor the relative proportions of the SP-C transition moment in the "z" *vs.* the "x, y" directions.

The COVASP-IR method cannot distinguish complete from partial transfer of material from monolayers to multilayers. Without a spatially resolved measurement (not feasible with current technology) the most we can deduce from increased intensities in the plateau region is the average increase in the relative concentration of each constituent in the sampled area. The plots in Figure 3-7 are constructed by initially subtracting the contribution from a particular constituent in the monolayer phase. Although we can safely conclude from the intensities of the pressure-absorbance plots for various modes that DPPC, DPPG and SP-C must all be present in the multilayer structure, we cannot conclude that there is *no* DPPG or SP-C in the residual monolayer structure at high pressure. We also can clearly conclude (Figure 3-7) there is relative enrichment of both SP-C and DPPG compared to the DPPC in the bilayer phase. These results even in semi-quantitative form are difficult to achieve with IRRAS, due to film relaxation during data collection in that experiment.

It is of interest to compare our current results with those obtained from the microscopic measurements of the Münster group (*58*). They attached a fluorescent dye to SP-C in a DPPC-DPPG (4:1) mixture and tracked its lateral distribution in LB films transferred at 30 mN/m and at the midpoint of the plateau in the monolayer/multilayer isotherm. Scanning near-field optical microscopy allowed for simultaneous fluorescence and optical imaging measurements to be made. At high pressures, the formation of multilamellar fluorescent structures from protein aggregates was observed. These were surrounded by a monolayer

of reduced fluorescence, suggesting that SP-C is depleted in the monolayers, hence enriched in the multilayers. The fluorescence intensity was proportional to the height of the multilayer stacks. To explain this result, it was suggested that a fixed number of lipid molecules accompanied each SP-C molecule during the transfer.

The above observations mesh well with our current COVASP and previous IRRAS studies of SP-C orientation in monolayer and multilayer phases. The COVASP-IR measurements show a strong preference of the protein for the multilayer phase, consistent with fluorescence data. As noted above, our prior IRRAS measurements indicated that the SP-C helix tilt changed from a monolayer orientation nearly parallel to the monolayer plane to an orientation perpendicular to the bilayer (or multilayer) at high surface pressures. This change in tilt angle maximizes hydrophobic interaction of the SP-C with the lipid acyl chains in both lipid monolayer and multilayer states, and provides a molecular rationale for the suggestion by the Galla group of a reasonably well-defined lipid-protein complex. The current data also suggest that the SP-C exhibits a preference interacting with DPPG over DPPC, a result presumably based in electrostatics since SP-C carries three positive charges located near the N-terminus. Morrow et al. have suggested from NMR studies of SP-C/PG interaction (*67*) that the charges on SP-C are located near the bilayer surface, which would obviously facilitate their interactions with the PG negative head group charge.

A different view of monolayer collapse has been propounded by the Oregon group(*68-70*). In recent studies, they indicate that phospholipid films can achieve high surface pressures without the presence of gel phase lipid and without individual components necessarily being "squeezed-out" from the film. In additional studies (*71*), they employed a variety of techniques to investigate the collapse of calf lung surfactant extract (CLSE) as well as DPPC/ dehydrocholesterol from the interface. CLSE contains all of the hydrophobic constituents of endogenous surfactant. The formation of bilayer disks residing above the monolayer was observed. Their model suggested that components of surfactant films must collapse collectively rather than being squeezed out individually. Our qualitative data are partially consistent with their mechanism since we observe that DPPC, DPPG and SP-C all transfer to the multilayer state, albeit to different extents. It would be interesting to further test some of the ideas expounded above with lipids possessing expanded isotherms. However, we have been unable to acquire reproducible COVASP-IR data from films in which one of the components is in the liquid-expanded phase (e.g., POPG or POPC).

It is certainly possible that CLSE and the four-component system used here (as well as the surfactant film!) may collapse by entirely different mechanisms. As noted by Schief et al. (*71*), model films of surfactant and its components may collapse by a variety of mechanisms, including buckling into extended folds toward the aqueous phase, three-dimensional crystal formation, and nanoscale budding, in addition to multilayer formation.

Several extensions of the COVASP approach appear feasible. It will be possible to create a more complex surfactant mimic with an experimental sequence in which each single lipid component is deuterated in succession, to search for conformational alterations or exclusion from the monolayer, of that particular species. The COVASP approach may also permit evaluation of some aspects of the expansion process. This is a technically awkward experiment, since the expansion events are probably far removed from equilibrium; thus experiments will have to be performed as a function of expansion rate. Along these lines, significant differences are already noted between the expansion of monolayers (DPPC/DPPG/ cholesterol) from ~50 mN/m (Figure 3-4), which exhibits little or no hysteresis compared with the expansion from the plateau region of the four-component system (Figure 3-6), in which substantial hysteresis is observed for the intensity parameters.

Chapter Four: Evaluation of Peptoids as the Biomimetics of Lung Surfactant Protein SP-C by COVASP and AFM

4.1 Introduction

Pulmonary surfactant functions to facilitate the work of breathing and to prevent alveolar collapse. The physical basis of surfactant action is of substantial interest. Many studies in this area are targeted toward providing a rational basis for the design and testing of putative therapeutic agents for pathological states of the pulmonary system such as the neonatal and adult versions of respiratory distress syndrome (RDS).

A variety of synthetic mimetics for both SP-C and SP-B have been developed (*72-74*). There are important advantages for the use of synthetic mimics rather than animal-derived preparations for *in vivo* therapy, including improved batch-to batch consistency, elimination of biological contamination, and reduction in the substantial purification steps required in preparation of animal-based material. The Barron group has undertaken a biomimetic approach for synthesis of SP-C analogues which effectively bypasses the difficulties noted above with use of the natural material. The approach involves the use of poly-N-substituted glycines or "peptoids" as mimics (*36, 75*). This class of molecules, one of which is used in the current study (see Figure 4-1), has a backbone structure in common with peptides. Unlike native proteins, the side chains are appended to the amide
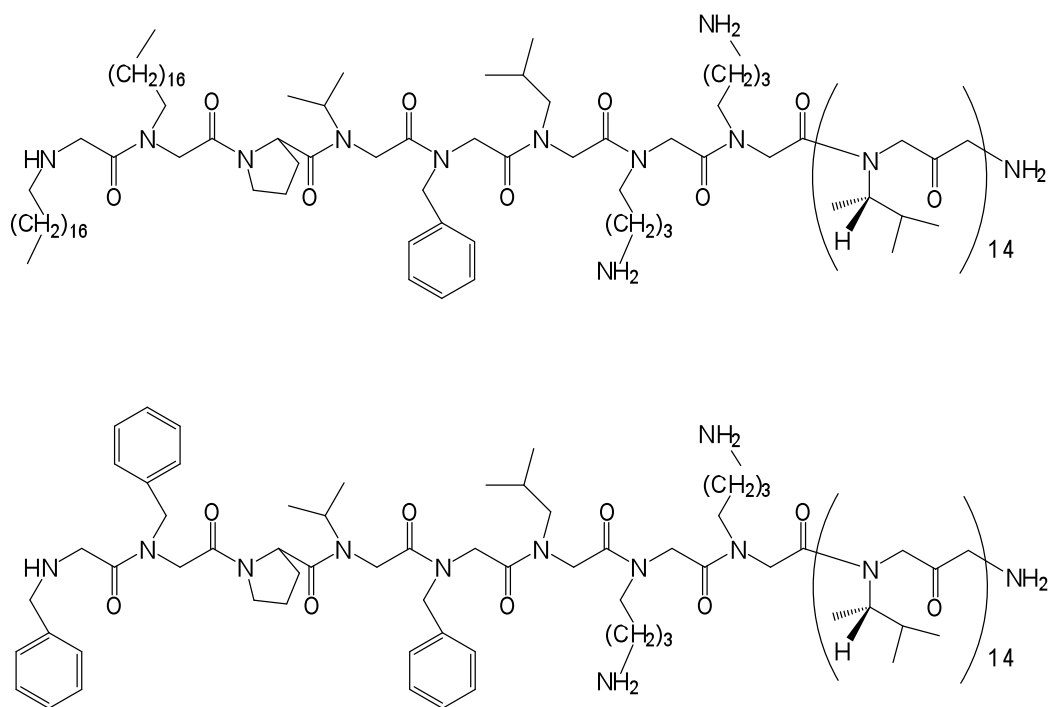
Figure 4-1. Peptoid structures of the diN-palmitoylated (top) and the non-palmitoylated (bottom) forms of the peptoid mimetic of SP-C.

nitrogen rather than to the α-carbon atoms. Several structural features of this peptoid class render it an attractive candidate for an SP-C mimic. First, N-substitution renders these molecules strongly resistant to protease activity. Second, the polyproline type I helices adopted by analogous peptoids with sterically bulky side chains are stable and the aggregation of peptoids is minimized (*76, 77*). Third, these peptoids are relatively easy to synthesize, utilizing methods with coupling efficiencies comparable to solid phase peptide synthesis.

Prior to *in vivo* testing, it is reasonable to investigate whether a putative therapeutic agent mimics the biophysical action of the native material in surface films at the air/water interface. The basic actions of lung surfactant at the air/water interface are reasonably well established. At the relatively low pressures of inhalation *in vivo,* the surface-active film consists mostly of a monolayer; while at the highest surface pressures of exhalation, the film develops multilayer structures attached to the monolayer surface. The seminal observations of multilayers in lung tissues were made by Schurch et al. (*14*), who used TEM to view the ultrastructure of the alveolar surface film from guinea pig lung. Multilamellar regions consisting of two to seven layers were clearly evident. *In vitro* studies from the Haagsman/Batenburg (*21*)*,* Galla (*78*)*,* and Zasadzinski (*79*) laboratories along with our prior studies (*23*), have demonstrated the role of SP-C, including the essential effects of S-palmitoylation, on multilayer formation. These structures presumably provide a reservoir for recruitment of material into the surface film during reexpansion following compression.

Thus, two generic attributes would seem to constitute the minimal biophysical requirements of a potential therapeutic agent for RDS. First, when mixed with surfactant lipids, the material should form stable surface films over the physiologically relevant surface pressure range during repetitive compression-expansion cycles at the air/water interface. This propensity may be readily evaluated with standard techniques, i.e., with π-A isotherms or with pulsating bubble surfactometry. Second, more difficult to quantitatively evaluate either *in vivo* or *in vitro*, is the extent of formation of surfactant-associated multilayers at high surface pressures.

Direct visualization of multilayers *in vitro* requires an imaging technique with high spatial resolution. Atomic force microscopy (AFM) has proven useful for the study of surfactant films. Both the Utrecht and Munster groups have examined the topography of SP-B and SP-C-containing films and observed the formation of multilayer structures (*21, 78*). While AFM is the most powerful approach currently available for qualitative observation of multilayers, it is limited in two ways. The method is unable to provide direct molecular structure information about the film constituents. Second, the superb spatial resolution of the technique precludes the examination of surface areas of macroscopic dimensions. Thus, it is difficult with nanotechnology-based methods to measure properties such as the "average" number of layers that form in the film.

To quantitatively characterize film components in both the monolayer and multilayer states requires methods that directly monitor molecular structure. Toward this end, we have developed and applied IR reflection-absorption

spectroscopy (IRRAS) to determine protein secondary structure and lipid chain conformational order (*80, 81*). In addition, we have used polarized IRRAS measurements to monitor the orientation of ordered regions of protein secondary structure and of the lipid chains in monolayer films *in situ* at the air/water interface (*82-84*). A drawback of IRRAS at the high surface pressures required for multilayer formation is that quantitative evaluation of spectral parameters is difficult, since these pressures require that the films be studied under conditions of continuous compression. This constraint provides only a limited time window for IRRAS data acquisition and renders quantitative analysis difficult.

To overcome this difficulty, our laboratory recently developed an approach in which Langmuir films are transferred to solid IR-transmitting crystals such as CaF_2 under conditions of continuously varying surface pressure (COVASP) (*61*). Following transfer, the films on the substrate are examined with conventional (transmission) IR spectroscopy to monitor the properties of film constituents as a function of surface transfer pressure under more favorable conditions than with IRRAS. As an initial demonstration of the utility of COVASP, the monolayer → multilayer transition known to occur in the four-component model DPPC/DPPG/cholesterol/SP-C was examined (*85*). IR parameters from both the lipid and protein constituents of the transferred film all indicated that the monolayer-multilayer transition persisted during the transfer process and could be detected readily. A major advantage of COVASP is the expectation that Beer's Law is obeyed so that the extent of multilayer formation may be determined.

The current work utilizes biophysical methods to determine whether the synthetic peptoid exhibits the two relevant biophysical characteristics discussed above. Toward this end, three complementary techniques are used to evaluate the effect of the peptoid on surface films of DPPC/DPPG/cholesterol, as follows: Surface properties are monitored from π-A isotherms, AFM is used to visualize the formation of multilayers at high surface pressures, and COVASP is used to characterize the molecular composition and the average extent of multilayer formation.

4.2 Results

4.2.1 π-A isotherms

π-A isotherms are shown in Figures 4-2A-D for the standard lipid system with (i) 4 mole % native porcine SP-C (Figure 4-2A), (ii) with 4 and 10 mol % of N-palmitoylated peptoid (Figures 4-2B and C, respectively), and (iii) with 10% non-palmitoylated peptoid (Figure 4-2D). Each set of isotherms in Figures 4-2A-C was reproduced at least three times with independent fresh samples, while the isotherm of the four-component system in Figure 4-2D was inherently non-reproducible. In Figure 4-2A, four cycles of the standard system with SP-C are plotted. The film undergoes a reversible transition characterized by a horizontal plateau upon compression at ~53 mN/m. In the experiment shown, the horizontal plateau has been shown to result from multilayer formation. COVASP film transfer was carried out during the first cycle while the next three cycles were

Figure 4-2. π-A isotherms for the standard lipid system, DPPC-d_{62}/DPPG (4/1 mol ratio) with 7 mol % cholesterol on 5 mM Tris buffer with 150 mM NaCl with various protein or peptoid constituents.

(A) Standard system with 4 mol % SP-C. Four cycles are shown. Films were transferred to CaF$_2$ crystals during the first cycle.
(B) Standard system with 4 mol % N-palmitoylated peptoid. Five cycles are shown. Films were transferred to CaF$_2$ crystals during the first cycle.
(C) Standard system with 10 mol % N-palmitoylated peptoid. Five cycles are shown. Films were transferred to CaF$_2$ crystals during the first cycle.
(D) Standard system with 10 mol % non-palmitoylated peptoid. Two cycles for separate samples are shown.

performed to test for reversibility of the isotherm. Virtually complete reversibility is indicated by the nearly accurate retracing of the isotherm. The essential role of SP-C in conferring film stability during successive compression/expansion cycles is revealed through isotherms (shown in Figure 3-2), which demonstrate irreversible film collapse/leakage in isotherms lacking the protein.

In Figure 4-2B, isotherms of the standard lipid film with 4% N-palmitoylated peptoid do not exhibit a plateau region, although they demonstrate reversibility upon cycling with a kink at ~44 mN/m. Increasing the N-palmitoylated peptide concentration to 10% causes significant changes in the isotherms. As shown in Figure 4-2C, isotherms for a single film taken through a series of compression-expansion cycles (with COVASP transfer during the first cycle) depict nearly horizontal plateaus beginning near 42 mN/m suggestive of multilayer formation. Slight irreversible loss of material into the subphase is noted during successive cycles.

The startling role of peptoid N-palmitoylation in the formation of multilayers is revealed in Figure 4-2D. Films with 10% depalmitoylated peptoid showed no horizontal plateau and an isotherm unable to manifest significant cycling. In addition, isotherms generated from independent aliquots of the same material deviates from one another (isotherms not shown).

4.2.2 AFM studies of peptoid-containing film

The molecular interpretation that horizontal or near horizontal regions in the π-A isotherms in Figures 4-2A and C arise from multilayer formation is not unique. Such features may also be associated for example, with LE-LC phase transitions or exclusion of particular components from the film, rather than with multilayer formation. To test for the occurrence of multilayer structures, film topography was investigated with AFM for the standard film incorporating 10 mol% palmitoylated peptoid and transferred to freshly cleaved mica at surface pressures of 10, 30, 42, and 43 mN/m along the isotherm. Representative AFM topography for 10 x 10 μm^2 areas at these transfer pressures is shown in Figures 4-3A-D. In each case, the variations in height are depicted underneath each image for the lines drawn. The vertical scale in the lower plot ranges from +/- 5 nm for the films transferred at 10, 30 and 42 mN/m, to +/- 10 nm for the film transferred at 43mN/m. The latter was required to accommodate larger height differences in this image.

For the film transferred at 10 mN/m (Figure 4-3A), a basic roughness level of 0.3-0.4 nm is evident in the surface while a rare 1.6 nm protrusion is depicted. Monolayer heights are expected in the 1.5-2 nm range (perhaps diminished slightly by tip action) so that this image provides a useful baseline for expected height variation above the mica surface in the presence of monolayers. No multilayer structures are evident. Images (Figure 4-3B) were also acquired for a film transferred at 30 mN/m, well below the plateau for this isotherm (42-44
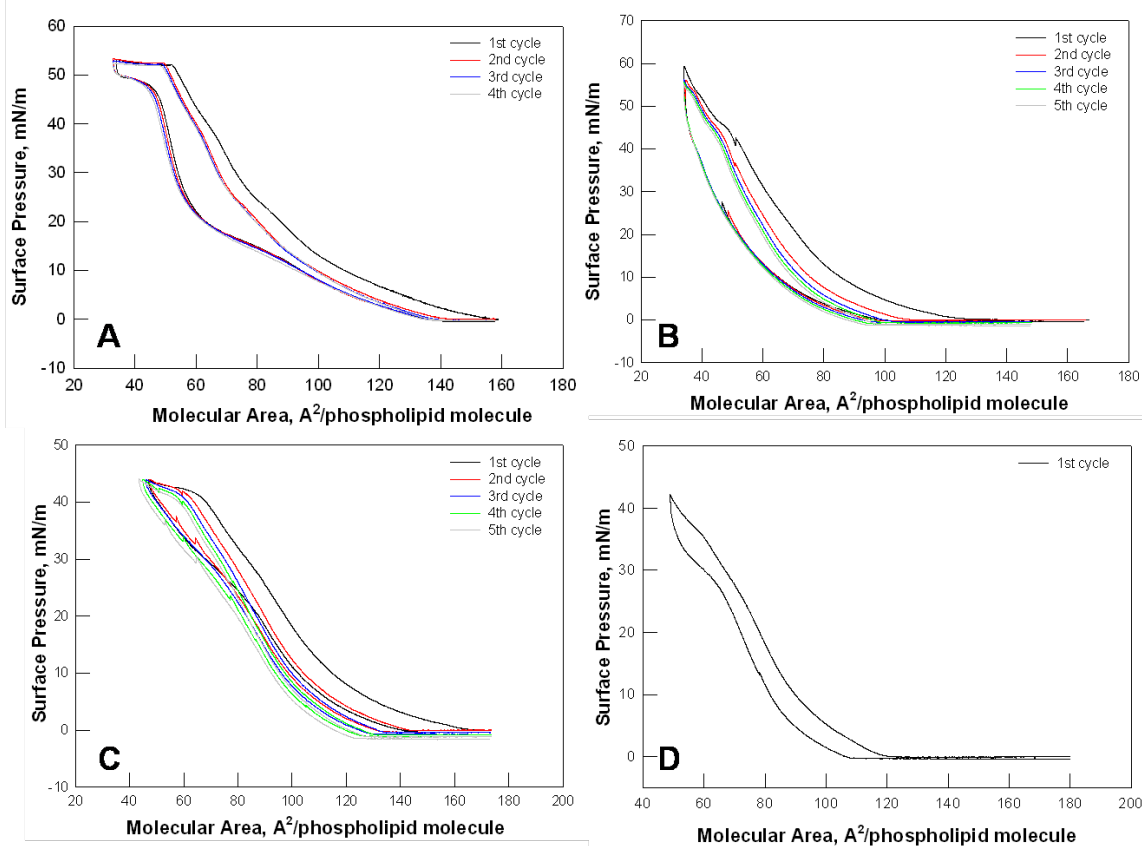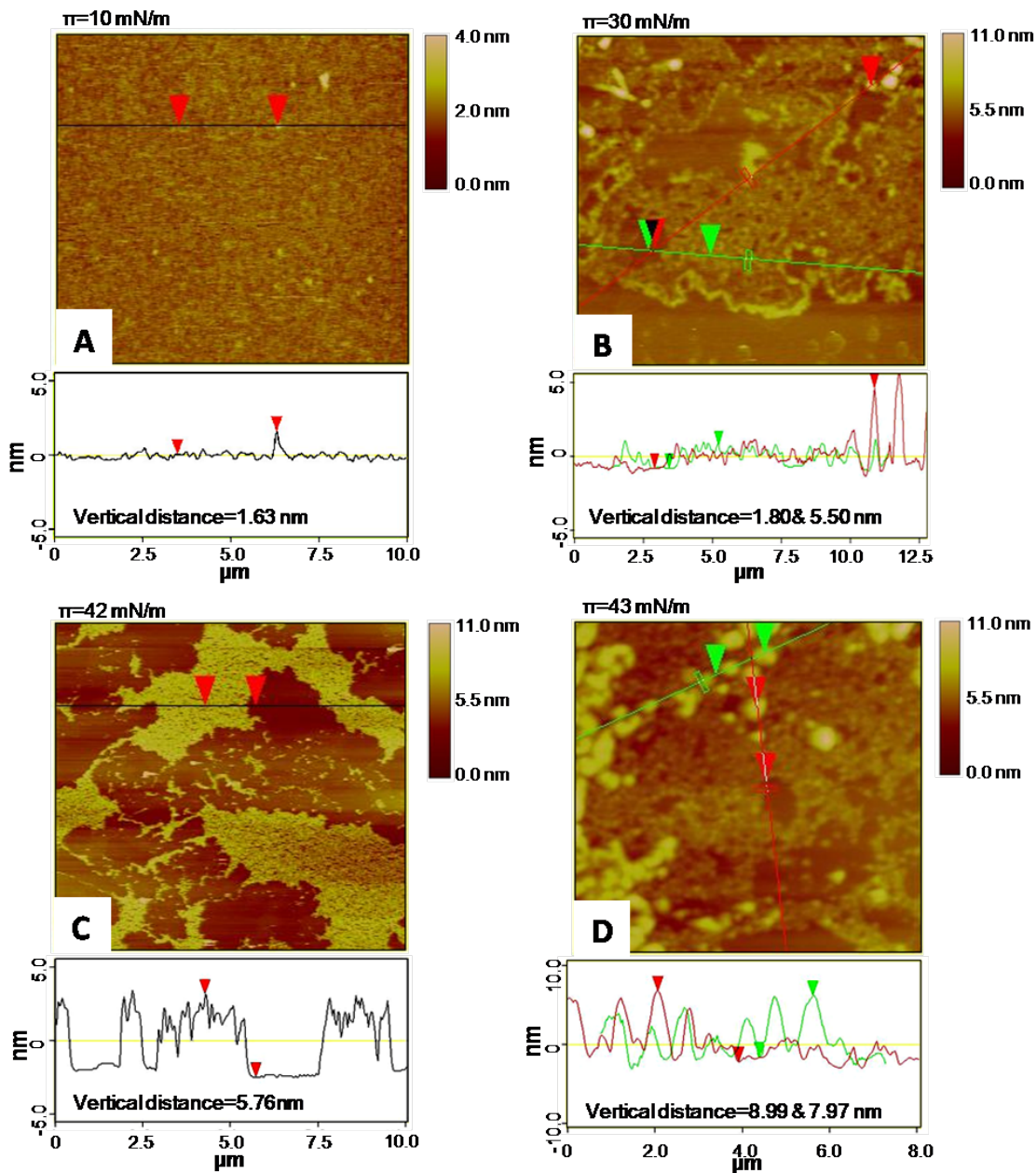
Figure 4-3. AFM images for the standard lipid system, DPPC-d_{62}/DPPG (4/1 mol ratio) with 7 mol % cholesterol on 5 mM Tris buffer with 150 mM NaCl and 10 mol % N-palmitoylated peptoid for films transferred to mica at (A) 10 mN/M, (B) 30 mN/m, (C) 42 mN/m, (D) 43 mN/m. The vertical scale in A-C is +/-5 nm and in D is +/-10nm, to accommodate larger height differences in this instance.

mN/m). In this instance, a greater number of 1.5-2 nm protrusions are observed compared to the 10mN/m image (Figure 4-3A), consistent with a greater extent of monolayer coverage. Occasional higher protrusions were observed in the 5-6 nm range, which may suggest the presence of nucleation sites for multilayer formation.

The plateau region in the isotherm for this film spans a rather limited range of surface pressures, namely from ~41-44 mN/m with variations in the onset pressure of ~1 mN/m. A small surface pressure change from 42→43 mN/m produces significant changes in the nature of the multilayers formed, as discussed below. The AFM image from a film transferred at 42 mN/m (Figure 4-3C) reveals the formation of large domains with heights generally corresponding to 5-6 nm. Assuming a bilayer thickness of ~4 nm, the observed heights of ~5-6 nm depicted along the line shown may represent single bilayers on the mica surface with monolayers lying above them. Finally, the film transferred at 43 mN/m reveals (Figure 4-3D) the presence of additional layers, the ~8 nm heights perhaps arising from 2 bilayers, with a single monolayer above. The AFM images generally confirm the interpretation that the plateau in π-A isotherm arises from the formation of 1 or 2 bilayers. In addition, there is no evidence for protrusions containing > 4-5 bilayers.

4.2.3 COVASP IR

The heterogeneity of the AFM films, the lack of molecular structure information about the multilayer constituents and the necessarily limited surface areas sampled by AFM, make it difficult to determine either the representative chemical composition of the multilayer or the average number of bilayers or multilayers formed in the horizontal region of isotherm. The COVASP experiment developed in our previous publications (*61, 85*) was designed to overcome these issues. The transfer of films under conditions of continuously varying surface pressures onto an IR-transparent (hydrophilic) CaF_2 substrate permits acquisition of high quality IR spectra from regions of film isotherms corresponding to known transfer pressures. Typical COVASP spectra for the standard film with 10% N-palmitoylated peptide at a range of surface pressures encompassing the monolayer and multilayer regions of the phase diagram are shown in Figure 4-4. Considering the paucity of material in the monolayer, IR spectral quality is quite high (data have not been smoothed nor have signal/noise ratios been otherwise enhanced). Various vibrations arising from the DPPC-d_{62}, DPPG, and peptoid components of the sample are labelled on the figure. Vibrations from the cholesterol component cannot be observed under current conditions.

Three spectral regions are of interest for possible quantitative measurement of the relative concentrations of the DPPC-d_{62}, DPPG, and peptoid components of the film. The 1600-1800 cm^{-1} region contains the lipid C=O stretching modes near 1730 cm^{-1} arising from both the DPPC-d_{62} and DPPG components, along
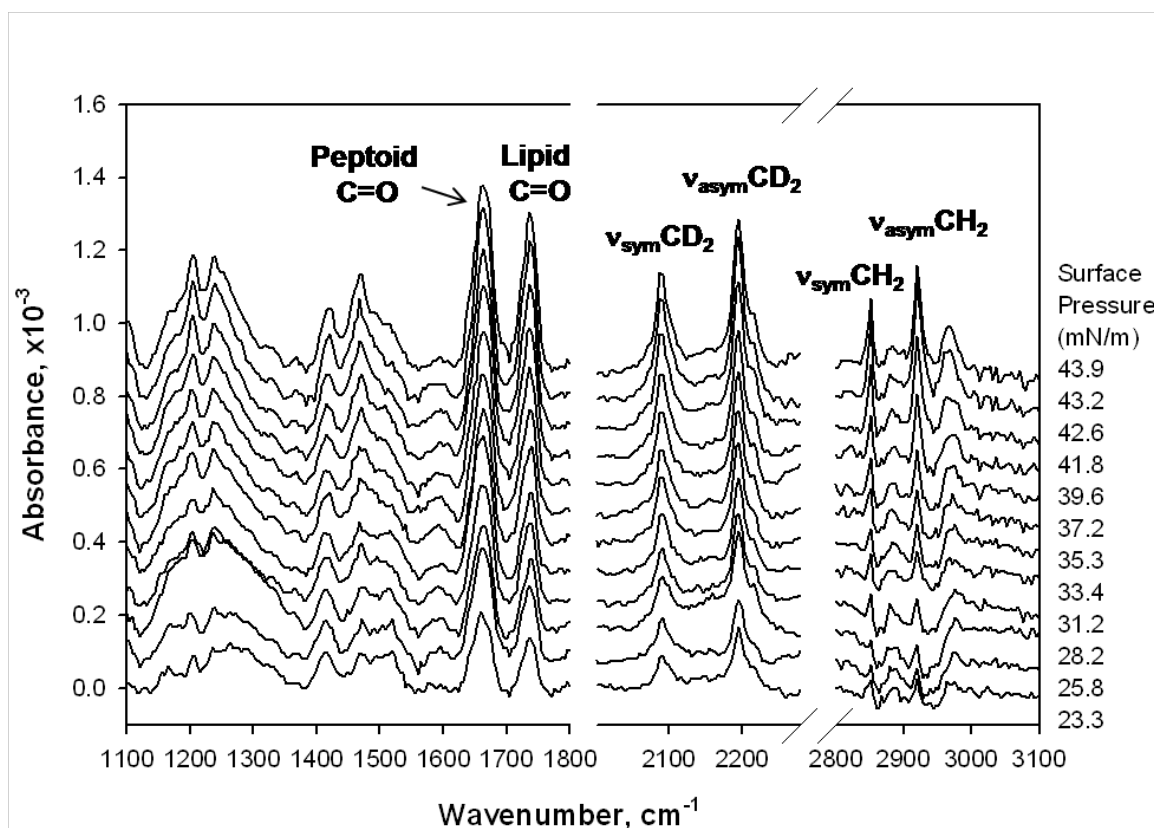
Figure 4-4. Overlaid COVASP-IR spectra for the standard four-component system, DPPC-d_{62}/DPPG (4/1 mol ratio) with 7 mol % cholesterol and 10 mol % N-palmitoylated peptoid, transferred from 5 mM Tris buffer with 150 mM NaCl . Spectra were acquired at different surface pressures (as indicated) during compression. Some relevant assignments are given for some of the spectral features.

with the peptoid C=O mode (similar to the peptide bond amide I mode in proteins) at 1650 cm^{-1}. The CD$_2$ (2000-2300 cm^{-1}) and CH$_2$ (2800-3050) stretching regions arise from the DPPC-d_{62} and DPPG film components, respectively. Some relevant spectral features are marked on the traces (Figure 4-4).

Typical surface pressure-dependent intensity variations of spectral parameters corresponding to these constituents are shown in Figures 4-5A-C. Figure 4-5A depicts the surface pressure-dependent integrated peak areas for the peptoid C=O stretching mode for two independent experiments covering a slightly different range of surface pressures in standard films with 10 mol% peptoid. Figures 4-5B and C depict variation for the DPPG CH$_2$ stretching and DPPC-d_{62} CD$_2$ stretching modes, respectively. For each parameter, substantial increases in peak intensity are observed in the transferred film beginning at a surface pressure of ~41 mN/m that coincides with the onset of multilayer formation in the isotherms (Figure 4-2).   This observation indicates the preservation of at least some film properties on the CaF$_2$ substrate, as has been observed previously for SP-C-containing films (*85*).

Additional control experiments are shown in Figures 4-6A-C. In Figures 4-6A and B, the integrated intensity of the DPPG CH$_2$ stretching vibration and the DPPC-d_{62} CD$_2$ stretching vibrations are plotted for films with 10% peptoid, 4% peptoid, and 10% non-palmitoylated peptoid in each case. Multilayer formation, as characterized by a sharp increase in the measured spectral parameter, is observed only for the film containing 10% N-palmitoylated peptoid. Further
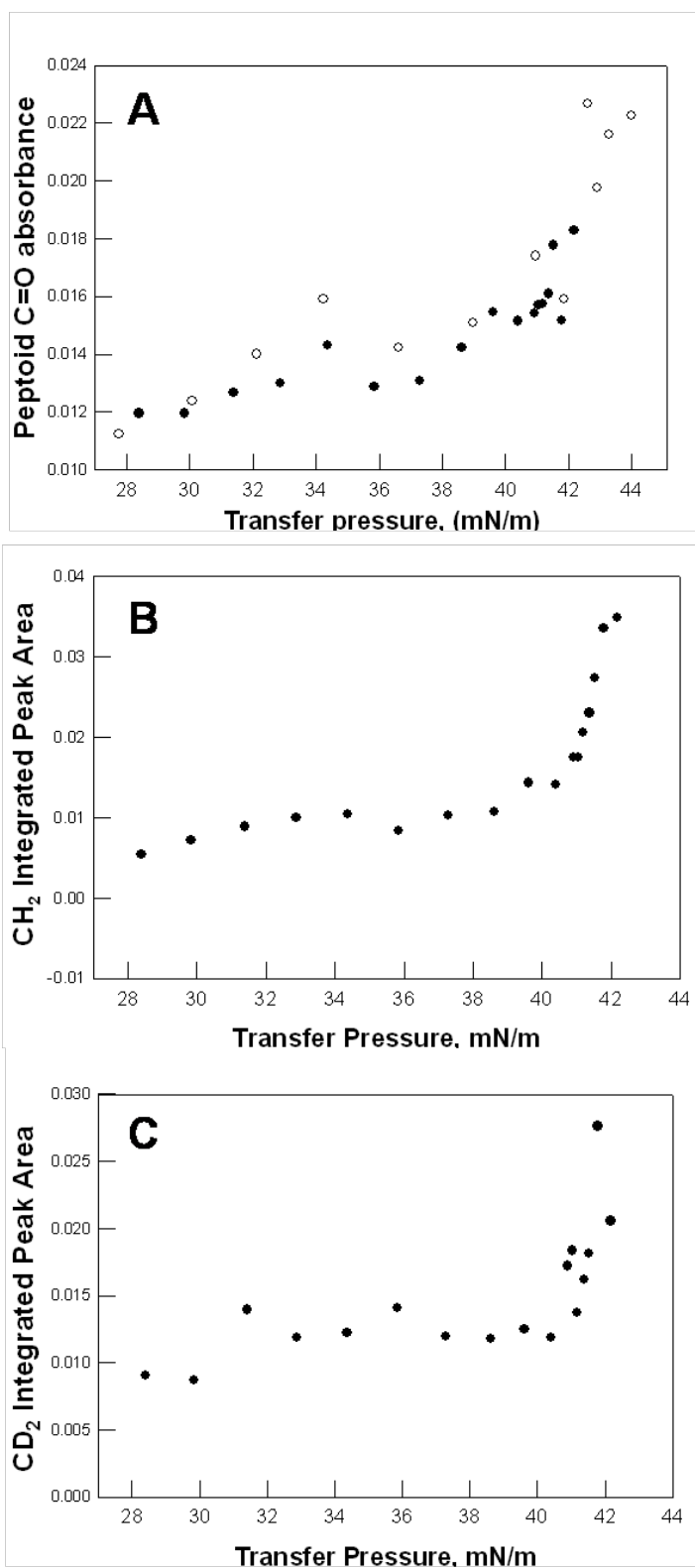
Figure 4-5. Surface transfer pressure dependence of the integrated area for the standard four-component system (DPPC-d_{62}/DPPG (4/1 mol) with 7 mol % cholesterol and 10 mol % N-palmitoylated peptoid), on 5 mM Tris buffer with 150 mM NaCl.

(A) The integrated band area of the peptoid C=O stretching mode centered at ~1650 cm^{-1} (two independent runs encompassing slightly different surface pressure ranges are overlaid);

(B) The area under the entire CH$_2$ stretching region from the DPPG component;

(C) The area under the entire CD$_2$ stretching region from the DPPC-d_{62} component.

evidence for the essential role of peptoid palmitoylation in multilayer formation is shown in Figure 4-6C in which COVASP intensities are plotted for the peptoid C=O stretching intensity in films with 10% peptoid, 4% peptoid, and 10% non-palmitoylated peptoid. The latter two films show little change in peptoid C=O intensity as π is increased. In general, the peptoid absorbance in the non-palmitoylated case is ~1/3 of that for the 10%-palmitoylated peptoid in the pressure region 32-40 mN/m. The reduced intensity is consistent with the incorporation of reduced levels of non-palmitoylated molecule into the film.

The pressure dependence of the DPPG CH_2 and DPPC-d62 CD_2 stretching intensities for films containing palmitoylated and non-palmitoylated peptoids have been presented in Figures 4-6A and B. In each case, over the pressure range corresponding to the monolayer regime in the film with the palmitoylated peptoid, the integrated methylene (CH_2 or CD_2) stretching intensities are substantially increased in the film prepared with the non-palmitoylated material. This observation is consistent with Figure 4-6C, in which the peptoid C=O intensity is decreased in this film, and hence provides useful supporting evidence for reduced levels of modified peptoid in the film. Thus, exclusion of the non-palmitoylated peptoid permits greater levels of lipid to be incorporated into the film and hence, increased methylene intensities. It is noted that the CH_2 stretching intensities for the sample transferred with 4% palmitoylated peptoid resemble those for the sample with 10% non-palmitoylated material, suggesting similar (low) levels of peptoid incorporation in each case (and insufficient for extensive multilayer formation).
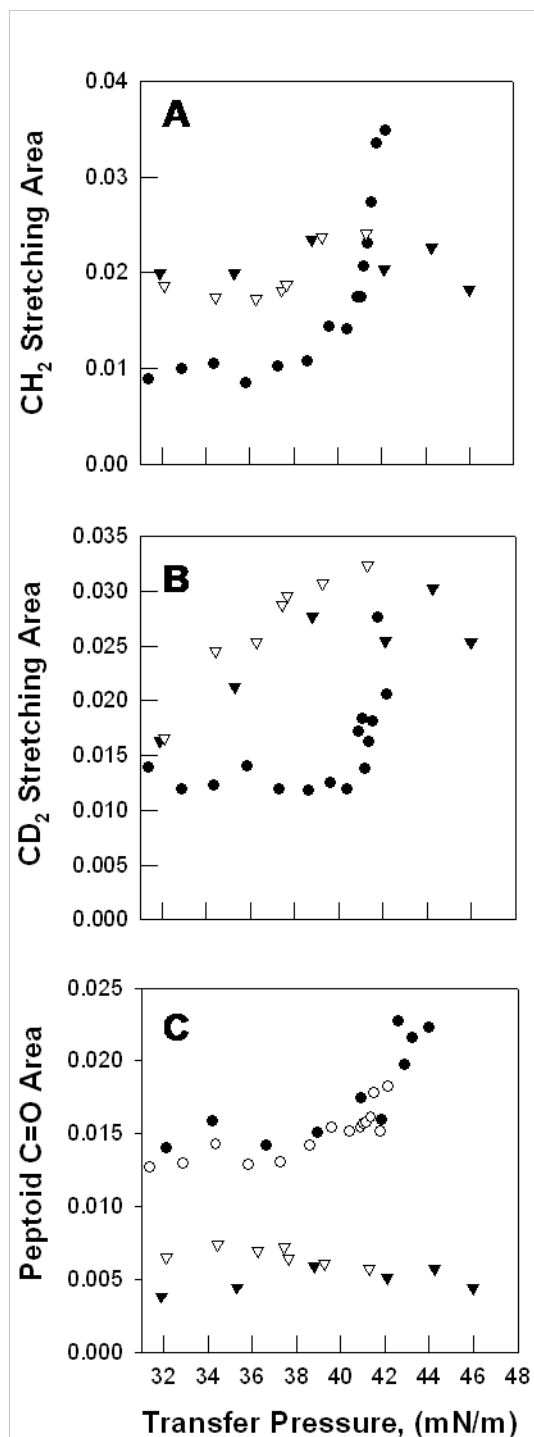
Figure 4-6. Comparison of integrated areas for three spectral parameters from a sample with controls, as follows:

(A) The CH_2 stretching band area from the DPPG component of the standard sample with 10 mol % N-palmitoylated peptoid ($\bullet$), the standard sample with 10 mol % non-palmitoylated peptoid (∇) and for the standard sample with 4 mol % N-palmitoylated peptoid ($\blacktriangledown$);

(B) The CD_2 stretching band area from the DPPC-d_{62} component of the standard sample with 10 mol % N-palmitoylated peptoid ($\bullet$), for the standard sample with 10 mol % non-palmitoylated peptoid (∇), and for the standard sample with 4 mol% N-palmitoylated peptoid ($\blacktriangledown$).

(C) Peptoid C=O stretch (1650 cm^{-1}) area of a standard sample with 10 mol % N-palmitoylated peptoid ($\bullet$), a repeat of the standard sample with 10 mol % N-palmitoylated peptoid ($\circ$), for the standard sample with 10 mol % non-palmitoylated peptoid (∇) and for the standard sample with 4 mol % N-palmitoylated peptoid ($\blacktriangledown$).

4.2.4 Determination of DPPG and DPPC relative concentrations in multilayers.

As noted above, the COVASP experiment monitors film structural properties averaged over all the molecules sampled by the IR beam. Assuming the applicability of Beer's Law for the IR transmission experiment, relative changes in the concentrations of the DPPC-d_{62}, DPPG, and peptoid, may be calculated from the CD_2 and CH_2 stretching intensities, respectively, as follows:

The data in Figure 4-6 reveals the highest surface pressure at which the film consists purely of monolayers to be ~40-41 mN/m. Thus, the IR band intensity measurement at this pressure provides the equivalent of an extinction coefficient for a particular component in the monolayer state. This value was subtracted from intensities in spectra acquired within the plateau to determine the extent of multilayer formation at higher pressures along the isotherms. The "excess intensity" determined in this fashion due to bilayer and multilayer formation was divided by the pure monolayer intensity to determine the "excess number of monolayers" for a particular component in the plateau region of the film as a function of surface pressure, with an inherent assumption about lipid chain tilt as discussed below. This procedure, the results of which are shown in Figure 4-7, effectively eliminates the contribution to the band intensity of the particular component from the original monolayer. As shown in the figure, our approach clearly reveals the significant preference for DPPG over DPPC in the bilayer or multilayer environment. At pressures well into the plateau (>41.6 mN/m), we
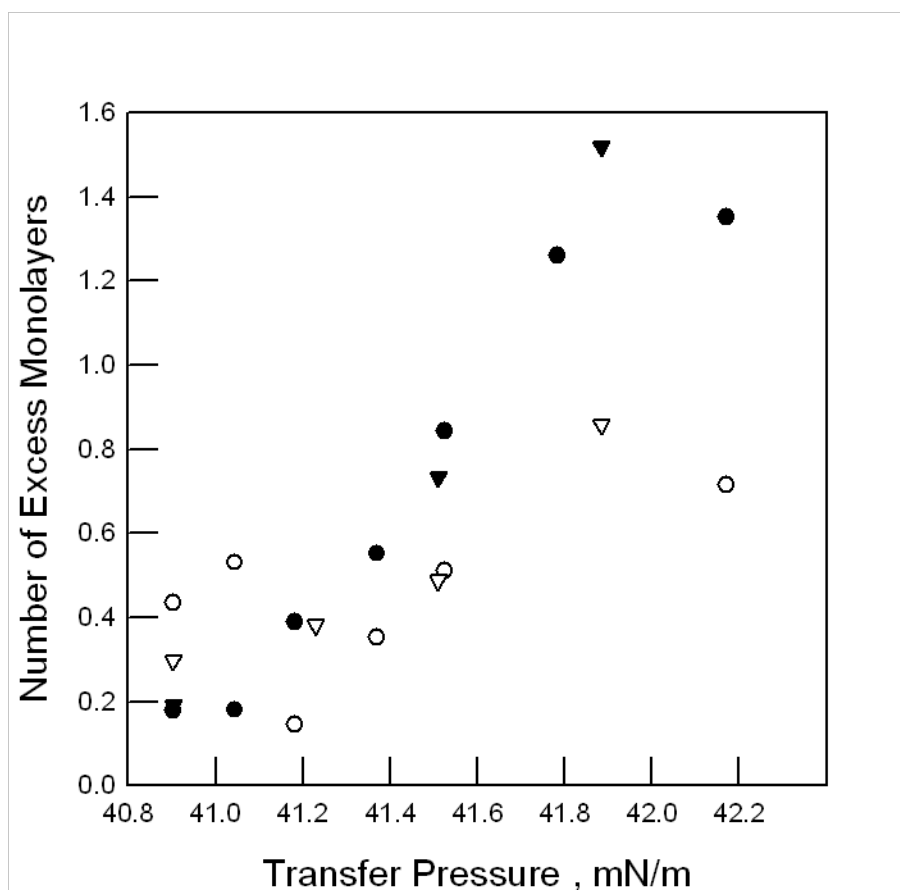
Figure 4-7. Number of excess monolayers for DPPC-d_{62} defined and computed as discussed in the text, for two independent samples of DPPC-d_{62}/DPPG (4/1 mol ratio) with 7 mol % cholesterol and 10 mol % N-palmitoylated peptide on 5 mM Tris buffer with 150 mM NaCl (∇, $\bigcirc$) as well as the number of excess monolayers for DPPG in the same two samples ($\blacktriangledown$, $\bullet$). The horizontal axis for the sample whose data points are given by empty and filled circles has been lowered by ~1.4 mN/m to compensate for slighted altered onset pressures for the plateau in the two experiments.

observe a 1.5 to 2-fold increase in the average number of excess DPPG monolayers compared with DPPC-d_{62}. Similar results were noted for SP-C in our prior study.

4.3 Discussion

A general goal of lung surfactant research is to develop clinically useful exogenous agents for therapeutic intervention in both neonatal and adult RDS. Toward this end, synthetic peptides with patterns of structure or charge found in human SP-B or SP-C appear to mimic some of the functional properties of the native proteins and thus may offer a useful basis for the design of agents for therapeutic intervention. For example, Cochrane et al. (*86*) suggested that the simple peptide KLLLLKLLLLKLLLLKLLLLK mimics aspects of the positive charge and hydrophobic residue distribution in the C-terminal region of SP-B. This molecule, used in the synthetic surfactant, Surfaxin (Discovery Laboratories, Philadelphia), shows similar efficacy as animal derived surfactants in phase 3 clinical trials (*87*).

In terms of biophysically based evaluation of potential therapeutic agents, synthetic analogues of SP-C, such as CPVHLKRLLLLLLLLLLLLLLLL, showed a high level of surface activity (*88, 89*). This and related molecules improved PV characteristics in premature rabbits. As a final example, Zasadzinski and associates synthesized SP-B$_{1-25}$ as well as an analogue of SP-C in which the palmitoylated cysteines are replaced by phe residues (*79*). It was suggested that

$SP-B_{1-25}$, when used to supplement a clinically used replacement surfactant, appeared to induce a reversible peptide folding transition that permitted all surfactant components to be retained at the interface during respreading. Thus the aforementioned (for a recent review of synthetic surfactant preparations, see Mingarro et al. (29)) studies tend to suggest that synthetic surfactants are close to being widely accepted for therapeutic intervention. In addition, a judicious selection of biophysical measurements may provide a role in demonstrating the possible utility and mode of action of these agents.

As noted in the Introduction, there are important advantages for the possible clinical use of the current class of synthetic peptoid mimetics of SP-C as therapeutic agents. N-substitution renders these molecules strongly resistant to protease activity. In addition, the polyproline type I helices adopted by these peptoids are stable and minimize aggregation. Finally, these peptoids are relatively easy to synthesize efficiently.

There were two major motivations for the current study. The first was to determine whether the synthetic peptoid displays properties during compression-expansion cycling similar to native SP-C. The techniques chosen, namely π –A isotherms, AFM, and COVASP, focus on the two main attributes required of a surfactant material, namely the ability to cycle in reversible fashion and the ability to form multilayers as reservoirs at high compression. In addition, COVASP permits an evaluation of the extent of multilayer formation and of the partitioning preferences of particular film components at macroscopic (0.1 – 1 mm) distance scales, information inaccessible with AFM.

The current results show that the peptoid mimics some but not all of the properties of the SP-C containing films (*85*). Thus, the molecule depicts reversible cycling through several compression-expansion cycles with a near horizontal plateau (Figure 4-2), while the identification of the formation of multilayers in this region of the isotherm is clearly seen in the AFM images in Figure 4-3. As observed for SP-C, the COVASP data (Figure 4-6) reveal a significant preference for the partitioning of DPPG into the multilayers. In addition, as shown in Figures 4-2 and 4-6, deletion of the palmitoyl chains eliminates the ability of the peptoid to form multilayers, and the IR intensities in Figure 4-6 suggest that the level of peptoid incorporated into the monolayer film is drastically reduced.

Some differences between the action of SP-C and peptoid on the standard film are also observed. First, a concentration of 10% peptoid is required for multilayer formation as deduced both from the isotherms (Figure 4-2) and from the COVASP data (Figure 4-6), as compared to 4% for native SP-C. Second, the surface pressure at which peptoid-induced multilayer formation commences is reduced by about 10 mN/m compared with the standard lipid film containing SP-C. This suggests a degree of film destabilization (inability to achieve as high a surface pressure) at the higher level of peptoid required possibly due to differences in the hydrophobic interaction between the lipids/SP-C or lipids/peptoid.

The second motivation for the current work was to demonstrate the utility of the COVASP experiment. Our initial measurements showed that transferred films

were stable on the CaF_2 window for at least a couple of days and demonstrated the feasibility of studying the monolayer→multilayer transition in surfactant films with this technique (*61, 85*). The current experiments show the advantages of integrating COVASP with more commonly used biophysical approaches. The combined π-A isotherm, AFM and COVASP data demonstrate the complementary nature of the techniques, produce consistent results, and provide information about film properties at quite different distance scales. The COVASP results, in addition to confirming the existence of multilayers, reveal that all three-components with identifiable IR signatures (DPPC-d_{62}, DPPG, and peptoid) exist within the multilayers. This is evident from discontinuities in the IR intensity *vs.* surface transfer pressure plots for each species (Figure 4-5) occurring at pressures of ~41 mN/m, precisely at the onset of multilayer formation.

The calculation of the extent of additional monolayers (to form multilayers) in the plateau region requires application of Beer's Law. A possible confounding factor in its application is the occurrence of changes in the orientation of the transition moment direction for a given normal mode relative to the film plane between monolayers and multilayers. Such an occurrence would produce altered apparent extinction coefficients for these two states. This is not a problem for the DPPG and DPPC components in the current instance. The transition moments of the methylene stretching modes used to determine the relative participation of DPPC-d_{62} and DPPG in multilayers are perpendicular to the chain direction, which is fortuitous in the current experiment. Simple geometric considerations show that a change in chain tilt from a maximum of 20° to 0° from

the surface normal (between monolayers and multilayers, for example), would change the intensities of the methylene stretching modes (in a transmission experiment) by less than 10%, a factor probably within current experimental uncertainties. Thus for the phospholipid components of the film, COVASP provides unique macroscopic information about the average composition of the multilayers.

In contrast, quantitative analysis of the relative peptoid or SP-C concentrations through measurements of the C=O stretch is precluded by the following consideration. For SP-C, we determined that the protein helix orientation relative to the film normal is altered from 70-80° in monolayers to ~25° in multilayers (*23, 82*). Thus the amide I transition moment direction in bilayers is directed preferentially more parallel to the normal to the plane (z direction) than in monolayers. The amide I IR absorbance (per protein molecule) is therefore reduced in bilayers compared with monolayers, in a transmission IR experiment. This in turn will confound the attempted measurements of relative concentrations in the two physical states using the amide I intensity.

For the peptoid, unlike the SP-C, there currently is no information about either the transition moment direction of the C=O stretching mode in the presumed peptoid polyproline I geometry relative to the molecular structure or of the direction of the molecule itself relative to the film plane in either the monolayer or multilayer states of the film. Thus, reliable quantitative analysis cannot yet be performed for the peptoid.

Chapter Five: Innate Immune Response of Lung surfactant Protein SP-A

5.1 Introduction

SP-A is one of four pulmonary surfactant-associated proteins. Its structure and function was reviewed in the introduction to the thesis. SP-A belongs to the structurally homologous family of innate immune defense proteins known as collectins (*90*). SP-A, the other hydrophilic lung surfactant protein SP-D, and the serum mannose-binding protein (MBP) are the three collectins found in humans. SP-A serves important roles in innate host defense by binding, opsonizing and permeabilizing microorganisms (*91-94*). SP-A binds to a diverse pool of ligands, including monosaccharides, sugars associated with glycoproteins and glycolipids, phospholipids, lipopolysachharides (LPS) found in Gram-negative bacterial cell walls, and peptide ligands (*95*). It also detects intruding microorganisms through pathogen-associated molecular pattern recognition (*94*).

Great effort was devoted to understand the role of SP-A in pulmonary host defense function and to elucidate the mechanism of its interaction with ligands. Its function was recently reviewed (*94-97*). SP-A -/- gene knockout mice showed altered surfactant function and structure and were more susceptible to microbial infections (*98, 99*). SP-A was shown to bind to various ligands *in vivo* and caused phospholipid aggregation by self-association (*100*). Researchers also worked on

correlating SP-A structure with its function. The function of each domain of SP-A was studied (*101-104*). Mutagenesis was utilized to evaluate the importance of conserved amino acids (*105-108*). The structure of SP-A could be viewed as the starting point for evaluation of SP-A/ligand interactions. SP-A conformation in solution is affected by cations (*19, 109, 110*). Single particle electron crystallography and molecular modeling were used to determine the 3-D structure of collagen-deleted recombinant SP-A in the presence of a lipid monolayer. The results showed that SP-A interacts with the monolayer through its globular domain (*111*). The crystal structure of the trimeric carbohydrate recognition domain and neck domain (NCRD) of SP-A provided high resolution atomic level information on SP-A structure (*8*). Two metal binding sites were detected. The SP-A trimer showed structural differences from SP-D and MBP, which provided SP-A with a more extensive hydrophobic surface capable of binding lipophilic membrane components.

The literature to date has made use of variety of methods to study SP-A function. Gene-modified mice were used to study the effects of SP-A deficiency (*98, 99*); binding assays and fluorescence were used to identify SP-A ligands (*18, 112, 113*); DSC, turbidity and light scattering helped to evaluate SP-A binding (*100*). These techniques have greatly advanced our understanding of SP-A structure-function relationships. However, to investigate the mechanism of SP-A/ligand interactions, molecular level information is required. The size and complexity of the reactants and association products of SP-A limit the applicability of high-resolution crystallography and NMR approaches (*114*).

Infrared and Raman spectroscopy can provide molecular level structural information. IRRAS technology developed in our lab and other labs (*81, 82, 115*), takes advantage of the molecular structure information of IR and permits experiments to be carried out at the air/water interface. The technique probes SP-A/ligand interaction under biologically relevant conditions while providing structural information. The technique may be considered as a "vector" that can transfer high resolution X-ray and NMR results to more physiologically relevant physical states.

IRRAS has been used to study the interaction between SP-D/LPS (*116*). A simulation method was combined with IRRAS result to provide information on protein orientation. The current chapter was designed along the same lines to probe the interaction of SP-A and its ligand lipid A, which is a well-conserved domain of LPS. Even though the lack of stability of SP-A NCRD at the air/water interface renders quantitative study of protein orientation rather difficult, qualitative results on this system still proved useful. In this chapter, the effects of Ca^{2+} on SP-A/lipid A interaction are studied, the binding mode of SP-A/lipid A interaction is probed, and mutants of SP-A NCRD are compared. These results are combined with structural information from X-ray crystallography to deepen our understanding of SP-A/ligand interaction.
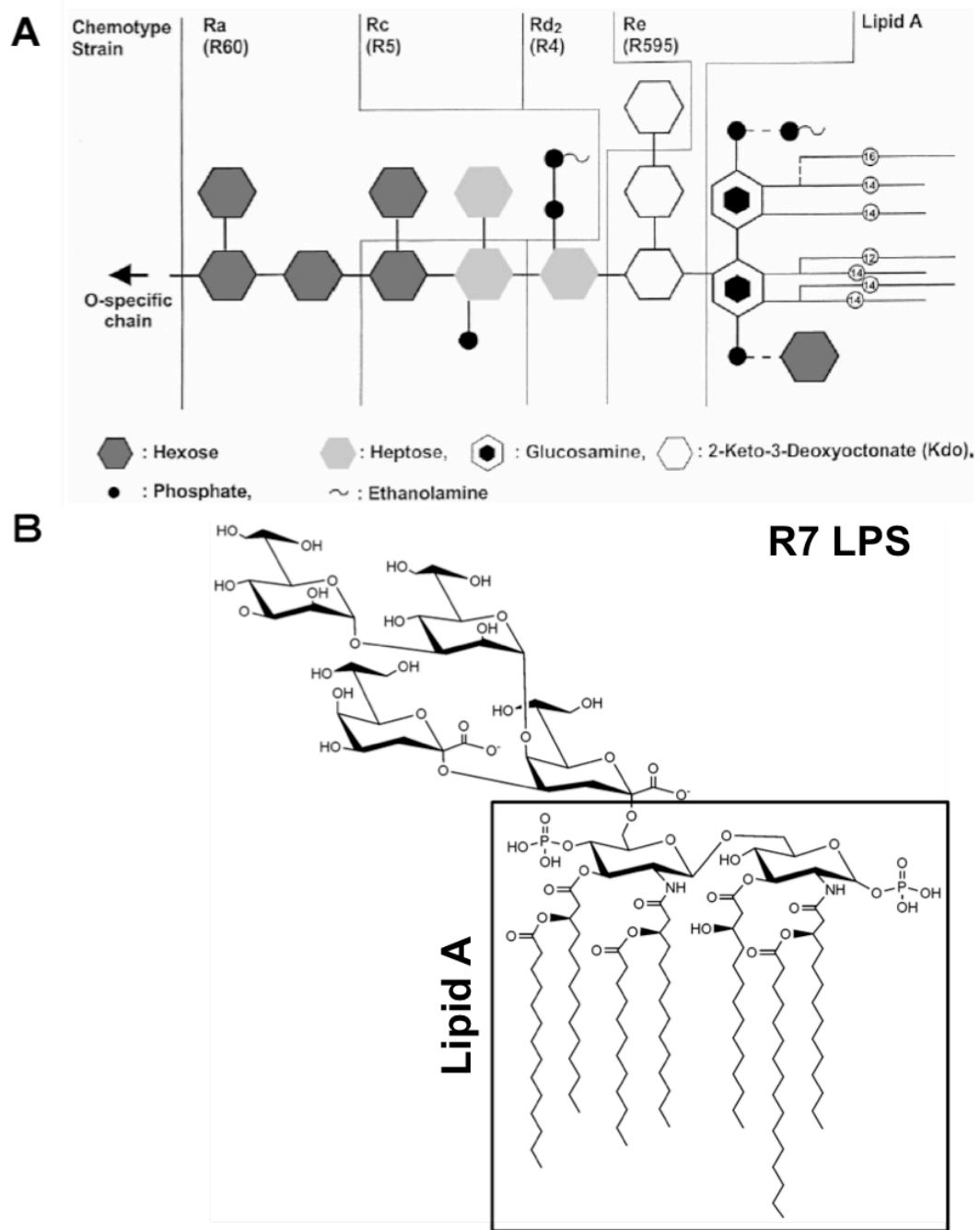
Figure 5-1. (A) Chemotype strains of various rough mutants and smooth form LPS from *Salmonella Minnesota* (*117*); (B) chemical structures of R7 LPS from *Salmonella minnesota* (Rd mutant) and lipid A, diphosphoryl from *Salmonella Minnesota* Re 595 (Re mutant).

5.2 Results

5.2.1 Lipid A monolayers

LPS are the major components of Gram-negative bacteria outer cell membrane. Their structures consist of a core region with varying length of the oligo- or polysaccharide chains depending on the bacterial mutant and a conserved hydrophobic lipid part, which is called lipid A. Schematic structure of different chemotype strains of LPS (rough mutant Re- to Ra- or smooth S- form LPS) is shown in Figure 5-1A. R7 LPS from Rd mutant and lipid A from Re mutant of LPS were used as SP-A ligands in the current study. Their chemical structures are shown in Figure 5-1B.

Initial experiments monitored the behavior of lipid A monolayers at the air/water interface. Isotherms of lipid A monolayers shown in Figure 5-2A are consistent with an expanded film. To check the effect of Ca^{2+} on lipid A monolayers, experiments were carried both in the presence and absence of subphase Ca^{2+}. The acyl chain conformational order as characterized by CH_2 stretching frequencies is displayed in Figures 5-2C and D, which depict surface pressure-induced changes in the asymmetric and symmetric modes, respectively. The CH_2 stretching frequency decreased as the monolayer was compressed to a higher surface pressure in each case, indicating that the acyl chains became more conformationally ordered upon compression. Lipid A monolayer acyl chains were more disordered in the absence of Ca^{2+} at lower
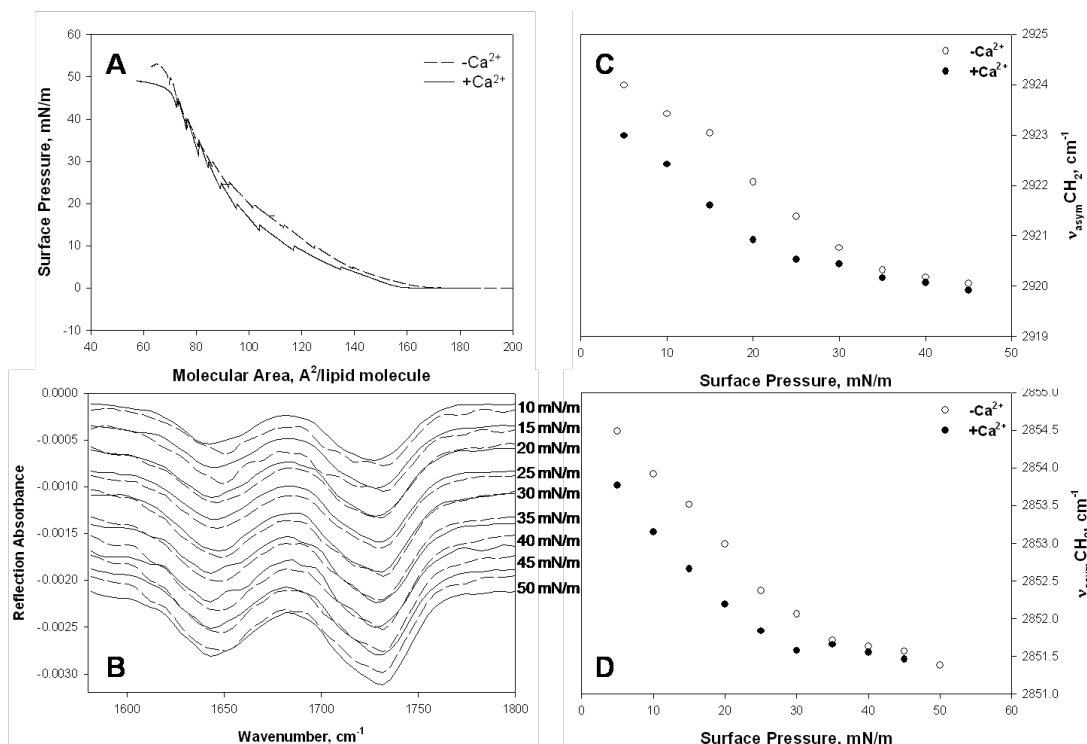
Figure 5-2. (A) π-A isotherms of lipid A and (B) IRRAS spectra showing lipid carbonyl (~1735 cm^{-1}) and lipid amide I (1640 cm^{-1}) of lipid A at various surface pressures on 5mM Tris buffer with 150 mM NaCl and 4mM Ca^{2+} (——) or 0.1 mM EDTA (– –); (C) asymmetric and (D) symmetric CH$_2$ stretching frequency as a function of surface pressures for lipid A monolayers floating on 5mM Tris buffer with 150 mM NaCl and 4mM Ca^{2+} (●) or 0.1 mM EDTA (○).

pressures, but when surface pressure reached 35 mN/m or higher, acyl chain conformations were about the same in both situations. The isotherms of lipid A showed the same trend, more expanded at lower surface pressure in the absence of Ca^{2+}, but coincided at higher surface pressures. Since the headgroup of lipid A has two negative charges, it is speculated that the presence of Ca^{2+} neutralizes the repulsive forces between lipid A headgroups and causes monolayer to pack more closely. However, the evolution of absorption bands at 1080 cm^{-1} and 1274 cm^{-1} with surface pressure from the headgroup phosphate region did not show any Ca^{2+}-dependentdifferences over the entire range of surface pressure (spectra not shown), indicating that Ca^{2+} did not affect the hydration state of the phosphates (*80*).The amide I vibration, sensitive to protein secondary structure (*81*)*,* absorbs between 1600-1700 cm^{-1}. Lipid A showed weak absorption in this region as well. Figure 5-2B shows the 1600-1800 cm^{-1} region of lipid A IRRAS spectra. Lipid A had two peaks in this region, the ester carbonyl stretching at 1730-1735 cm^{-1}, and the amide I carbonyl stretching at 1645-1650 cm^{-1}. These two modes arise from the acyl chain part of the lipid A chemical structure. The intensity of both modes increased as the lipid A film was compressed and the molecular concentration increased. As with the phosphate bands, no obvious difference was caused by the presence of Ca^{2+}.

5.2.2 Interaction of full-length (FL) SP-A with Lipid monolayers

Interaction of SP-A and its ligands were studied in this chapter in biologically relevant monolayers. As a control experiment, SP-A was first injected to clean

air/water surfaces to check its surface activity. Then the protein was injected under preformed ligand monolayers compressed to specific initial surface pressures. The effect of Ca^{2+} on lipid A/SP-A interaction was investigated by floating lipid monolayers on tris buffer subphases that contained either Ca^{2+} or EDTA.

5.2.2.1 Effects of Ca^{2+} on FL SP-A/lipid A interaction

Figure 5-3A shows the surface pressure change *vs.* time curve when SP-A was injected to clean air/water interface and lipid A monolayers either in the presence or absence of subphase Ca^{2+}. SP-A injection induced surface pressure increases in all cases. Although water soluble, SP-A was surface active. When injected to a clean air/water surface, SP-A produced a surface pressure increase of ~2 mN/m. SP-A also adsorbed to lipid A monolayers, due to its surface activity or interaction with lipid A. For the preformed lipid A monolayer which was stabilized at ~10 mN/m, SP-A injection caused a surface pressure increase of ~5 mN/m regardless of the presence of subphase Ca^{2+}. However, the kinetics of SP-A adsorption is different. When Ca^{2+} was present in the subphase, the system achieved its equilibrium surface pressure more quickly.

Figure 5-3B shows the 1600-1800 cm^{-1} spectral region spectra of SP-A and SP-A/lipid A monolayers. Lipid A spectra are also shown for reference. The largest amide I intensity of ~5.6 miliabsorbance arose from SP-A adsorption to a clean air/water interface. Although larger surface pressure increases were

Figure 5-3. (A) Surface pressure increases caused by SP-A injections to clean air/ D_2O interface (black) or lipid A monolayers at 10 mN/m floating on Ca^{2+}-containing buffer (red) or EDTA-containing buffer (blue); (B) IRRAS spectra of SP-A injection to clean air/D_2O interface (black) and lipid A monolayers at 10 mN/m floating on Ca^{2+}-containing buffer (red) or EDTA-containing buffer (blue); IRRAS spectra of lipid A monolayers at 10 mN/m when floating on Ca^{2+}-containing buffer (grey solid line) or EDTA-containing buffer (grey dash line) were also shown for references.

observed with protein injection to lipid A monolayers than to the clean air/water interface, the amide I intensity was smaller with the protein/lipid systems. When measuring the amide I intensity resulted from protein, a 0.4 miliabsorbance from lipid A was subtracted first. An amide I of ~4.2 miliabsorbance was detected for SP-A/lipid A monolayers in the presence of Ca^{2+}. Without Ca^{2+} in the subphase, the amide I was much smaller, ~0.4 miliabsorbance. The discrepancy between IR and surface pressure measurements might originate from the limitation of the techniques. Surface pressure monitors only the surface layer and could not detect proteins adsorbed underneath the lipid layer. IRRAS is believed to be able to detect monolayers in the top 0.5-1 microns of water but its intensity is also sensitive to protein orientation (*41*). These complications will be addressed later.

Figure 5-4 shows the effect of SP-A on the lipid A acyl chain packing, as monitored from the CH_2 symmetric and asymmetric stretching frequencies. Figures 5-4A and B show the results from the EDTA-containing subphase while Figures 5-4C and D were from a Ca^{2+}-containing subphase. Two trials for each experiment from different lipid A batches are shown in the graph. As seen from the plots of lipid A monolayers alone, lipid A itself showed batch-to-batch variation in CH_2 stretching frequencies. If lipid A batch variation is ignored, Figure 5-4 showed that SP-A injection to preformed lipid A monolayers at 10 mN/m caused the surface pressure to increase to 15 mN/m, and acyl chain stretching frequency decreased ~1 cm^{-1} as expected, indicating that SP-A injection caused lipid A acyl chain conformational order to increase regardless of the presence of Ca^{2+}. Upon further compression, lipid A/SP-A monolayers floating on a Ca^{2+}-
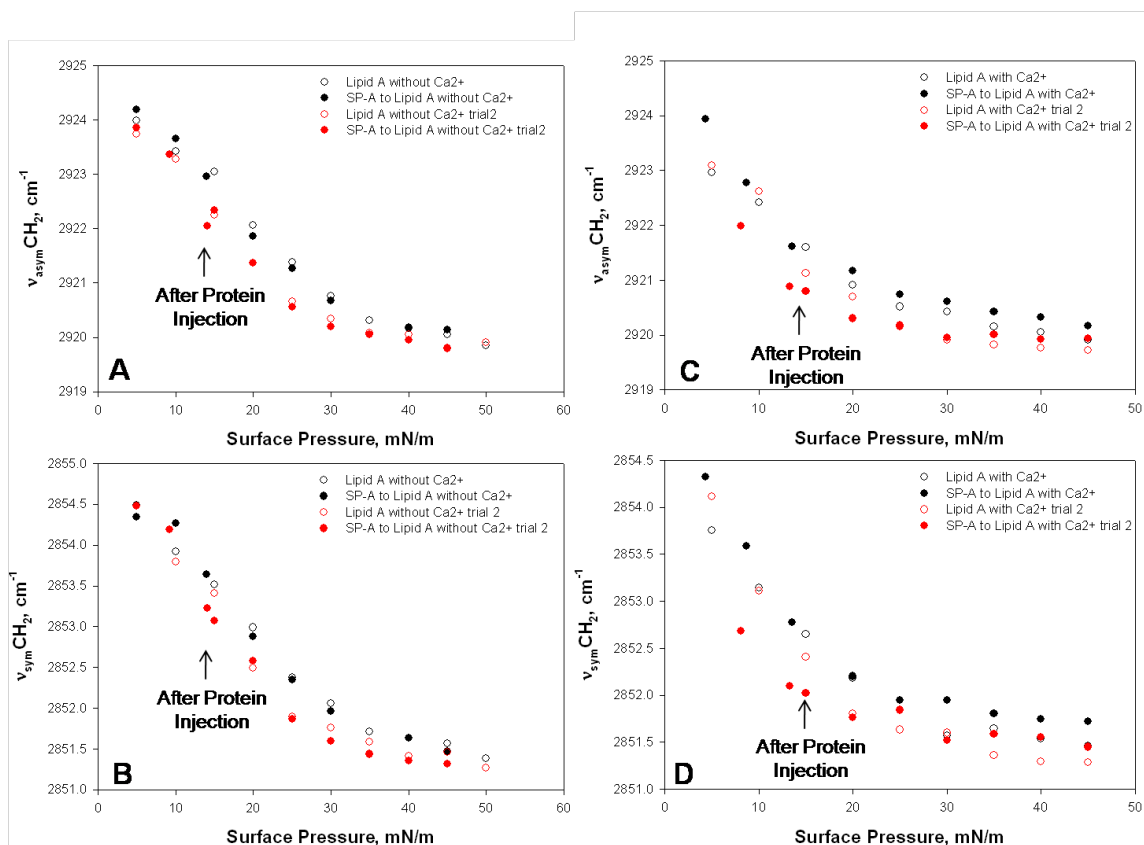
Figure 5-4. Frequency of asymmetric (A & C) and symmetric (B & D) CH$_2$ stretching modes as a function of surface pressure for lipid A monolayers in the absence (open circle) or presence (filled circle) of SP-A injection at 10 mN/m with monolayers formed on Ca^{2+}-containing buffer (A & B) or EDTA-containing buffer (C & D); Results of two trails are shown for each graph, with first trial in black and second trial in red.

containing subphase showed slightly higher CH_2 streching frequency/lower conformational order, compared to the pure lipid A monolayer at each comparable surface pressure. No such effect was observed for SP-A injection to lipid A monolayers on EDTA-containing subphase. Their CH_2 stretching frequency plots overlapped the one of the corresponding lipid A monolayer. These comparisons might indicate that SP-A was able to adsorb to lipid A monolayers independent of Ca^{2+}, but it can only insert into the monolayer deep enough to affect its conformation order in the presence of Ca^{2+}. However, due to batch variation in lipid A monolayer itself, the confidence in such small changes in the CH_2 stretching frequency and hence the interpretation of SP-A insertion is limited.

5.2.2.2 Interaction of FL SP-A with R7

To study a more complex ligand, SP-A was also injected beneath R7 LPS (structure indicated in Figure 5-1). Lipid A and R7 LPS have the same acyl chain compositions but R7 has a larger hydrophilic core region. Figure 5-5A shows the pressure increases caused by protein injection while Figure 5-5B monitors the 1500-1800 cm^{-1} region of the spectra. The plot of surface pressure increases and IR spectra of SP-A injection to water and lipid A with Ca^{2+} present in the subphase are shown for comparison. Spectra of pure R7 LPS are also plotted in Figure 5-5B. SP-A injection to R7 LPS monolayer at 10 mN/m resulted in a surface pressure increase of ~2.5 mN/m and an amide I peak of ~2.6
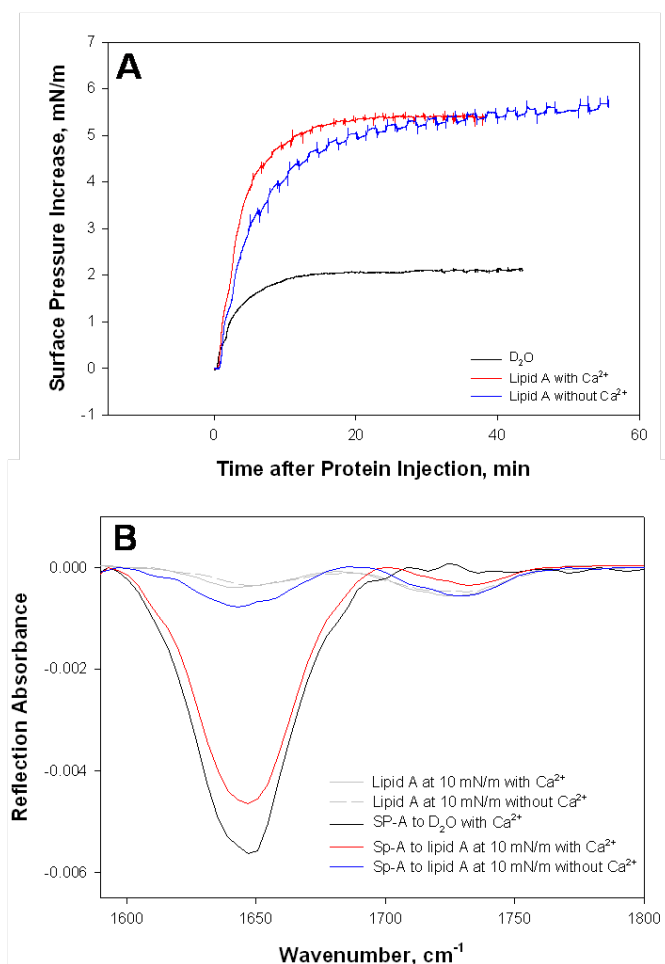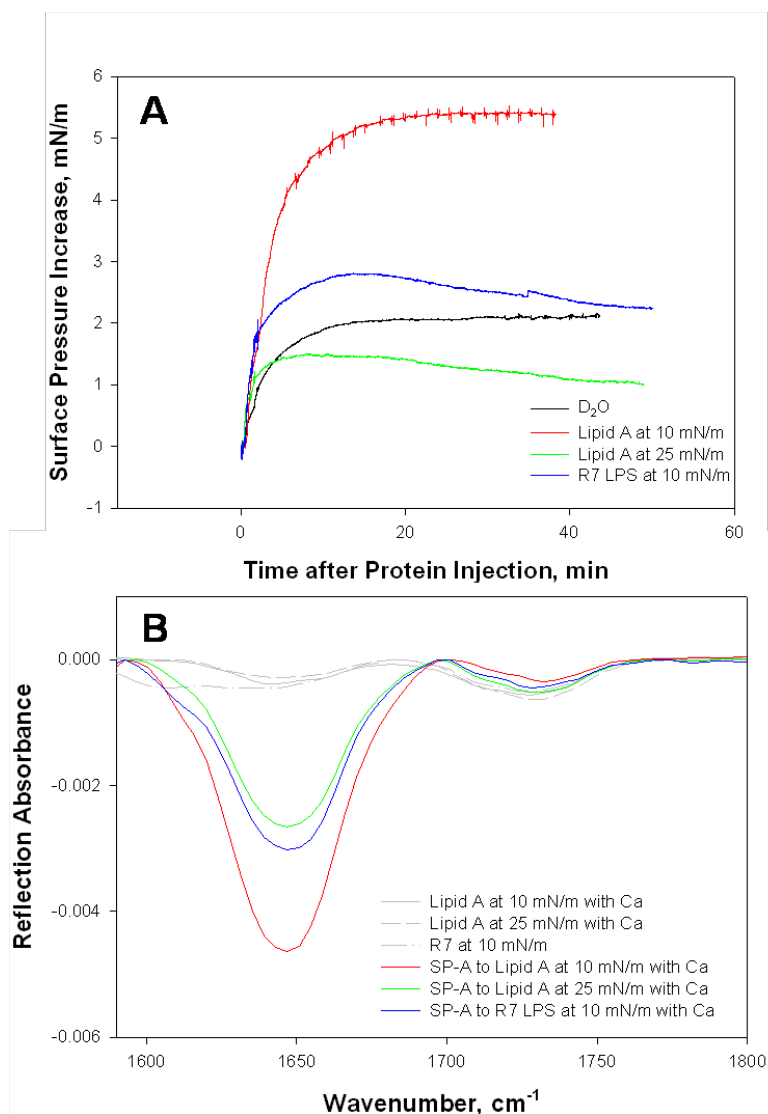
Figure 5-5. (A) Surface pressure increases caused by SP-A injections to clean air/ D$_2$O interface (black), lipid A monolayers at 10 mN/m (red) and 25 mN/m (green), and R7 LPS monolayer at 10 mN/m (blue); (B) IRRAS spectra of SP-A injection to lipid A monolayers at 10 mN/m (red) and 25 mN/m (green), and to R7 LPS monolayer at 10 mN/m (blue); IRRAS spectra of lipid A monolayers at 10 mN/m (grey line) and 25 mN/m (grey dash line) and R7 LPS monolayer at 10 mN/m (grey dash-dot line) were shown for references.

milliabsorbance, both of which were smaller than those for SP-A/lipid A monolayers.

5.2.2.3 FL SP-A/lipid A interaction at different surface pressures

Due to its surface activity, SP-A was detected at the surface when injected into a clean air/water interface. For a lipid A monolayer at 10 mN/m, there is still open

air/water surface available because of the expanded nature of the surface film. SP-A could adsorb onto the available air/water interface without having to interact directly with the lipid monolayer. To evaluate that possibility, SP-A injection was carried out with a lipid A monolayer at the higher surface pressure of 25 mN/m, which is also a biologically relevant surface pressure (*19*). As shown in Figure 5-5, the detected surface pressure increase decreased to ~1 mN/m, and the amide I peak intensity was also lower, ~2.3 milliabsorbance.

Figure 5-6 shows a plot of the ratio of the amide I peak area to lipid A carbonyl peak area when SP-A/ligand films were compressed after initial protein injection onto lipid A or R7 LPS monolayer at different surface pressures. The curves showed that much larger amide I peaks were observed when Ca^{2+} was present in the subphase. When Ca^{2+} was present, different amide I/carbonyl ratios were observed when SP-A was injected onto lipid A or R7. Injection onto a lipid A monolayer at 10 mN/m showed the highest ratio and decreased slightly with increasing pressure. For an R7 monolayer and lipid A monolayer at 25
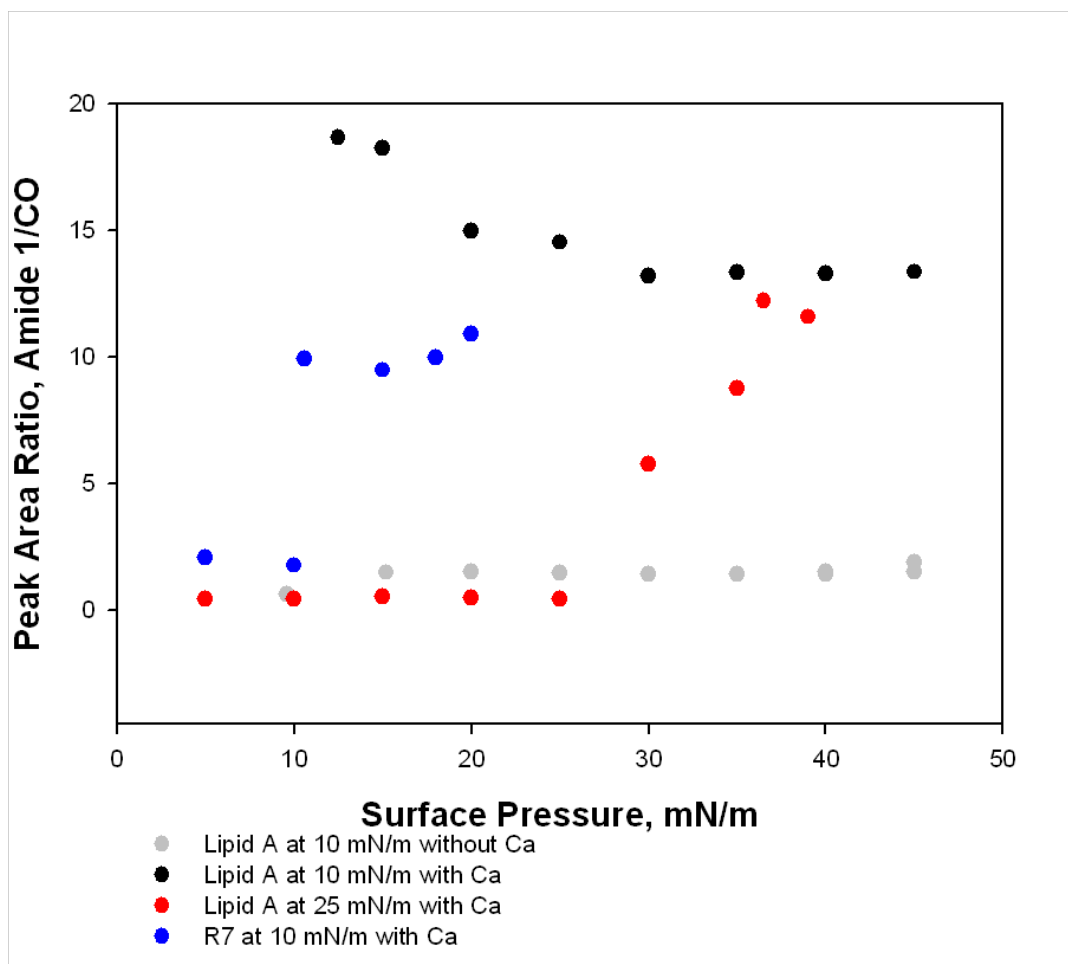
Figure 5-6. Integrated amide I/Carbonyl peak area ratio as a function of surface pressure for SP-A injection to lipid A monolayers at 10 mN/m (black), 25 mN/m (red) and to R7 LPS monolayer at 10 mN/m (blue) on Ca^{2+}-containing buffer; SP-A injection to lipid A monolayer at 10 mN/m on a EDTA-containing buffer (grey) is also shown.

mN/m, the ratios were lower but increased with surface pressure. Interestingly, the ratios all ended at about the same number, ~10-15, at the end of compression for all the experiments with Ca^{2+} present in the subphase.

5.2.3 Interaction of NCRD SP-A and its mutant with lipid A monolayers

Although the N-terminal is required to associate SP-A trimers to higher oligomers (*101*) and the surfactant function of SP-A is collagen domain dependent (*118*), the CRD is the domain responsible for lipid binding (*105, 111, 119*). The crystal structure of a recombinant truncated protein was determined by our collaborators (*8*). The Δ1-80/N187S fragment of SP-A encompasses the neck region (residues 81-108) and the globular CRD (residues 111-228). The N187S substitution eliminates the only site of N-linked glycosylation in the CRD to facilitate crystallization. The NCRD SP-A forms a trimer in solution (*101*). The X-ray structure shows that four amino acids: Glu-195, Arg-197, Asn-214, and Asp-215 donate five oxygen ligands to the primary Ca^{2+} binding site in the CRD (*8*). Alanine mutagenesis of these four residues in our collaborator's lab showed interesting results. SP-A directly kills microorganisms by membrane permeabilization (*120*) and D215A augments the permeabilizing activity of the protein for E. coli and H. capsulatum (McCormack et al., unpublished data).

We further studied native NCRD SP-A and its point mutation D215A NCRD SP-A, in order to correlate their interfacial behavior with their structural differences and biological activities. These two proteins were compared by

Figure 5-7. Surface pressure increase caused by N187S/PL SP-A (black) and D215A/PL SP-A (red) injection to clean air/D_2O interface as a function of time.
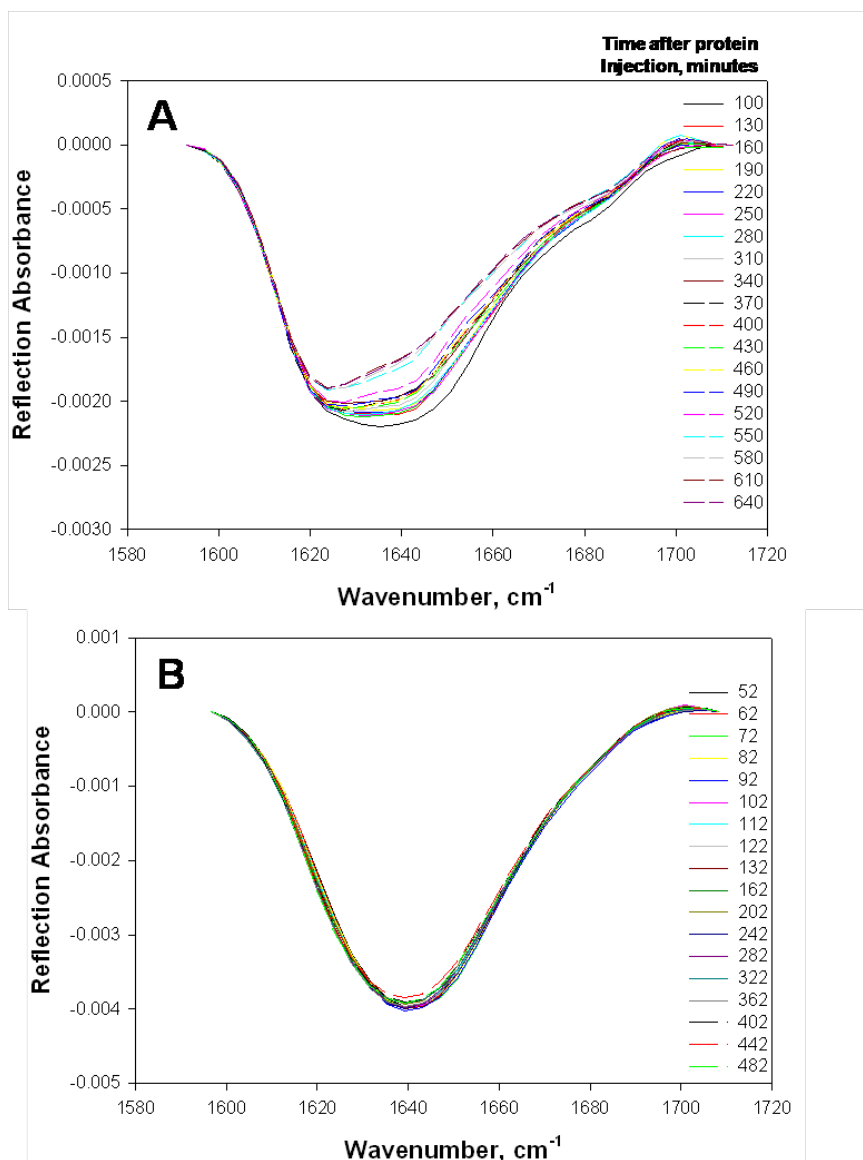
Figure 5-8. IRRAS spectra of the amide I region for N187S/PL SP-A (A) and D215A/PL SP-A (B) injection to clean air/D$_2$O interface. A series of spectra were taken after protein injection at the indicated time after injection.

Figure 5-9. (A) Integrated amide I peak area as a function of time for N187S/PL SP-A (black) and D215A/PL SP-A (red) injection to clean air/D_2O interface; (B) Bandwidth of amide I mode as a function of time for N187S/PL SP-A (black) and D215A/PL SP-A (red) injection to clean air/D_2O interface; A second trial for both proteins are shown as open circles in the correspondent colors.

injecting them onto clean air/water interfaces, and onto lipid A monolayers at surface pressures of 10 and 25 mN/m.

Figures 5-7 to 5-9 show the results for the two proteins injected onto a clean air/water surface. Native N187S SP-A produced a surface pressure increase of ~10 mN/m and an amide I band intensity of ~2.2 milliabsorbance units. The amide I intensity of N187S SP-A decreased with time in a time range of up to 10 hours. The band center frequency and band shape changed with time as well. D215A SP-A caused a greater surface pressure increase of ~14.5 mN/m and showed an amide I peak of ~4.0 milliabsorbance. D215A SP-A also demonstrated great stability at the air/water interface, and demonstrated no intensity decrease or band shape shift in 10 hours. Figure 5-9A compares the amide I intensity at the air/water interface. As already shown from the amide I region spectra, D215A SP-A had a stronger amide I band, and the amide I intensity remained stable over time. N187S SP-A was not as stable at the air/water surface, indicated by its decaying amide I intensity with time. Figure 5-9B plots the full width at half height of two proteins. The bandwidth of D215A SP-A was lower than that of the native protein.

As shown by X-Ray crystallography, the neck region of SP-A is composed of α helix and globular CRD includes three α helices and eleven short strands of β sheets. The resultant IR spectra is a broad band centered around ~1635 cm^{-1} intially for native NCRD SP-A and ~1640 cm^{-1} for D215A SP-A. The intensity decreases and band shape changes for native NCRD SP-A when exposed to the air/water interface revealed the secondary structure changes in SP-A. The amide
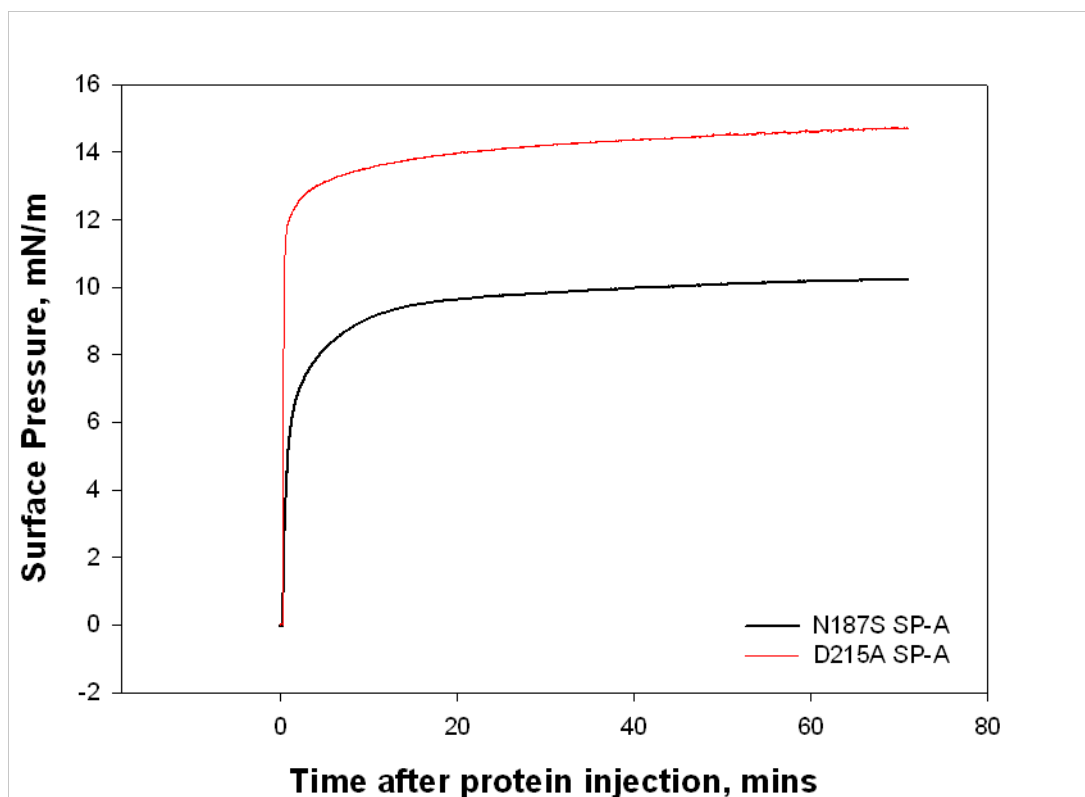
Figure 5-10. Surface pressure increase caused by N187S/PL SP-A (black) and D215A/PL SP-A (red) injection to lipid A monolayers at 10 mN/m on a Ca^{2+}-containing buffer as a function of time.

Figure 5-11. IRRAS spectra of the amide I region for N187S/PL SP-A (A) and D215A/PL SP-A (B) injection to lipid A monolayers at 10 mN/m. A series of spectra were taken after protein injection at the indicated time after injection.
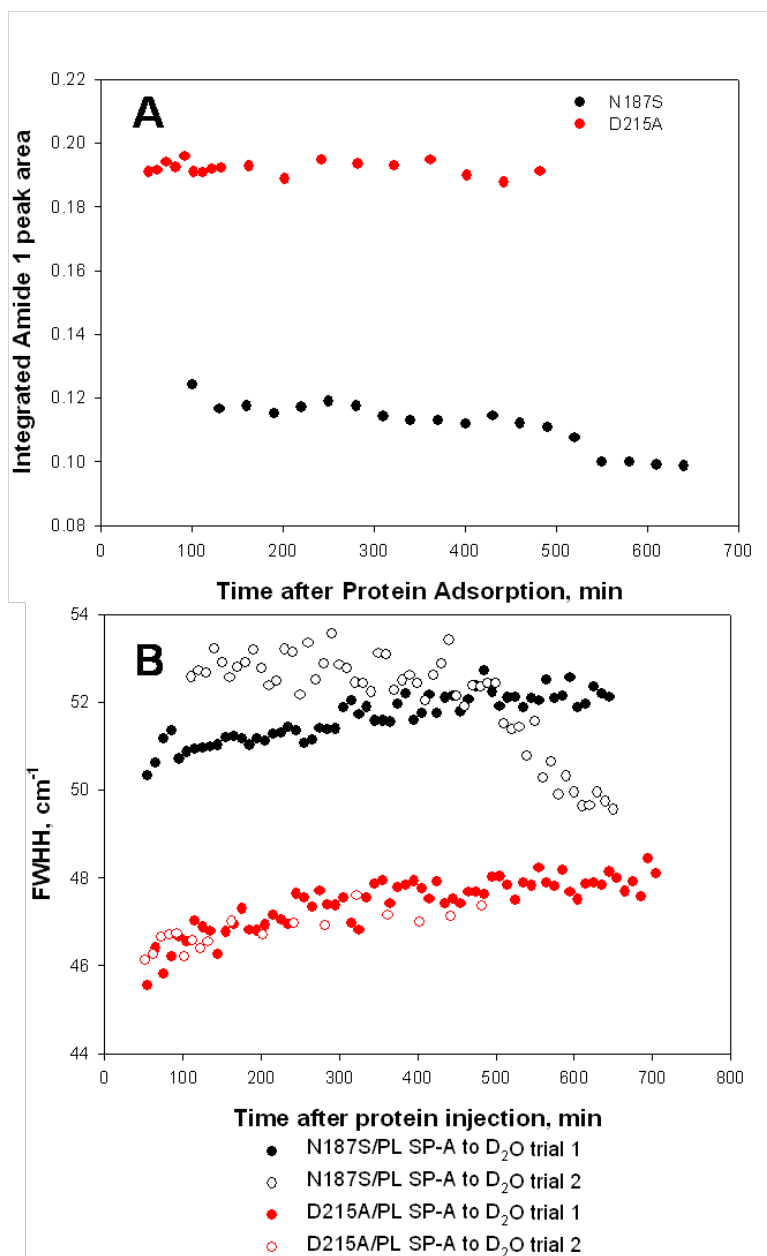
Figure 5-12. (A) Integrated amide I peak area as a function of time for N187S/PL SP-A (black) and D215A/PL SP-A (red) injection to lipid A monolayers at 10 mN/m; (B) Bandwidth of amide I mode as a function of time for N187S/PL SP-A (black) and D215A/PL SP-A (red) injection to lipid A monolayers at 10 mN/m; A second trial are shown as open circles in the correspondent colors.
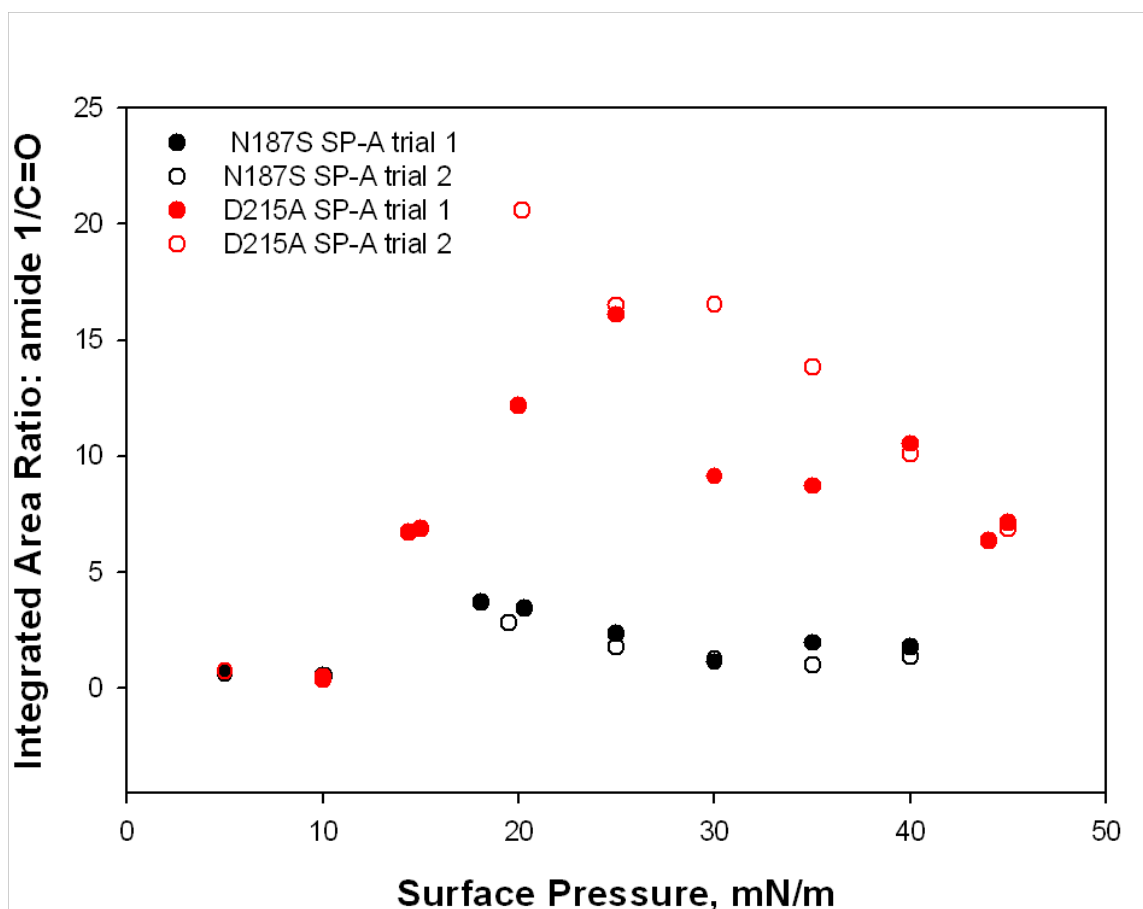
Figure 5-13. Integrated amide I /carbonyl peak area ratio as a function of surface pressure when compressed further after protein injection to lipid A monolayers at 10 mN/m (N187S/PL SP-A, black; and D215A/PL SP-A, red); A second trial for both proteins are shown as open circles in the correspondent colors.

I band center shifted to a lower frequency of ~1624 cm^{-1} and a shoulder started to appear at ~1686 cm^{-1} with time. These changes show an SP-A secondary structure with a greater proportion of β structure over time. D215A SP-A was able to retain its secondary structure at the air/water interface.

Next, D215A SP-A and NCRD SP-A were injected beneath preformed lipid A monolayers at a pressure 10 mN/m. The results are shown in Figures 5-10 to 5-12. N187S SP-A and D215A SP-A caused surface pressure increases of 9 and 14 mN/m. D215A still retained a bigger and more stable amide I peak, which was about 2.5 milliabsorbance as shown in Figure 5-11B. N187S SP-A (Figure 5-11A) showed an amide I peak of ~1.6 milliabsorbance, initially, which slowly decreased and changed shape with time. Amide I intensity (Figure 5-12A) and bandwidths (Figure 5-12B) are plotted for the two SP-A variants upon their injection onto lipid A monolayers at 10 mN/m. The intensity results are consistent with the observed spectra. The bandwidth of D215A SP-A mainly stayed the same over the time course while the bandwidth of NCRD SP-A, which was smaller when interacting with lipid A than at the air/water interface, increased over time. Figure 5-13 displays the amide I/carbonyl ratio when the lipid monolayer was compressed further, following SP-A injections. More D215A SP-A was involved in the monolayer than NCRD SP-A.

When proteins were injected beneath lipid A monolayers at a surface pressure of 25 mN/m, smaller surface pressure increases were observed than at surface pressures of 10 mN/m. The surface pressure increase of ~3.5 mN/m was
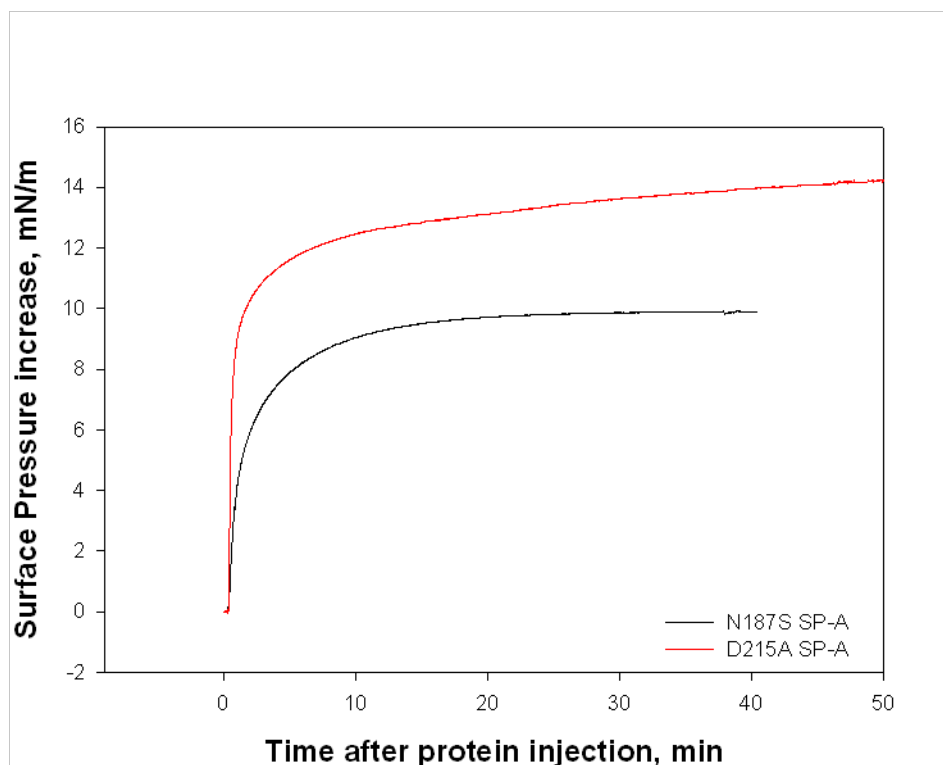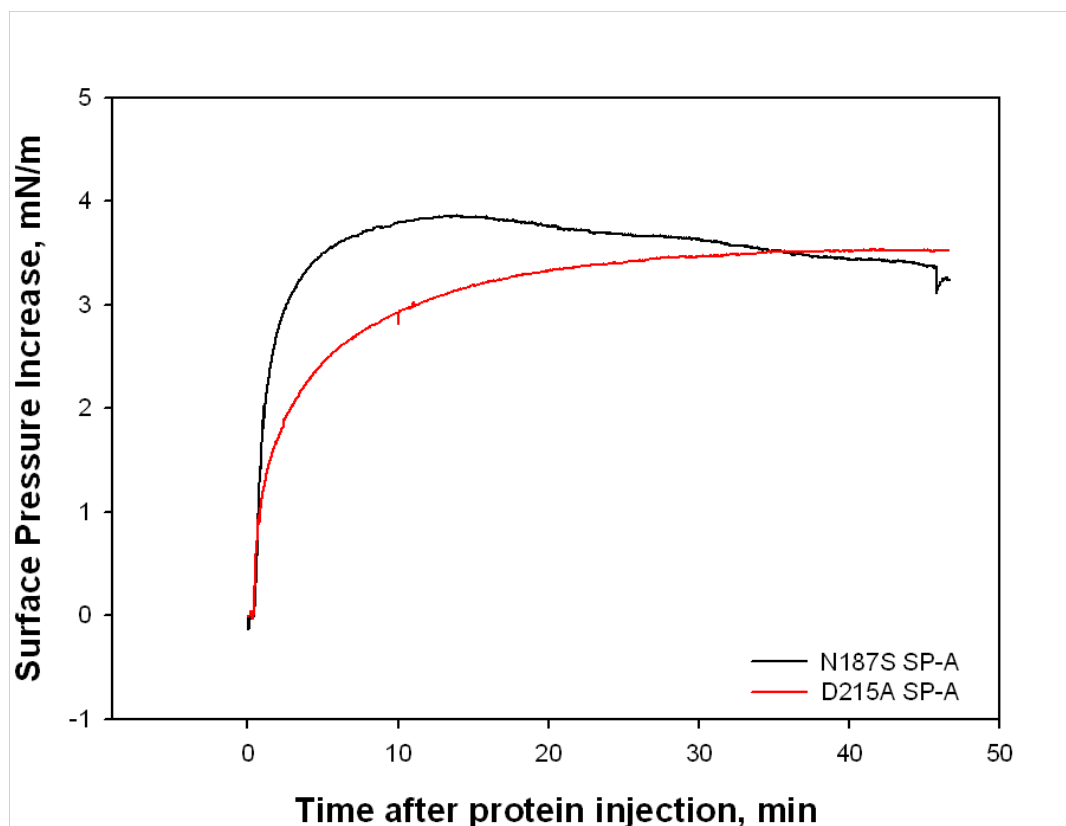
Figure 5-14. Surface pressure increase caused by N187S/PL SP-A (black) and D215A/PL SP-A (red) injection to lipid A monolayers at 25 mN/m on a Ca^{2+}-containing buffer as a function of time.
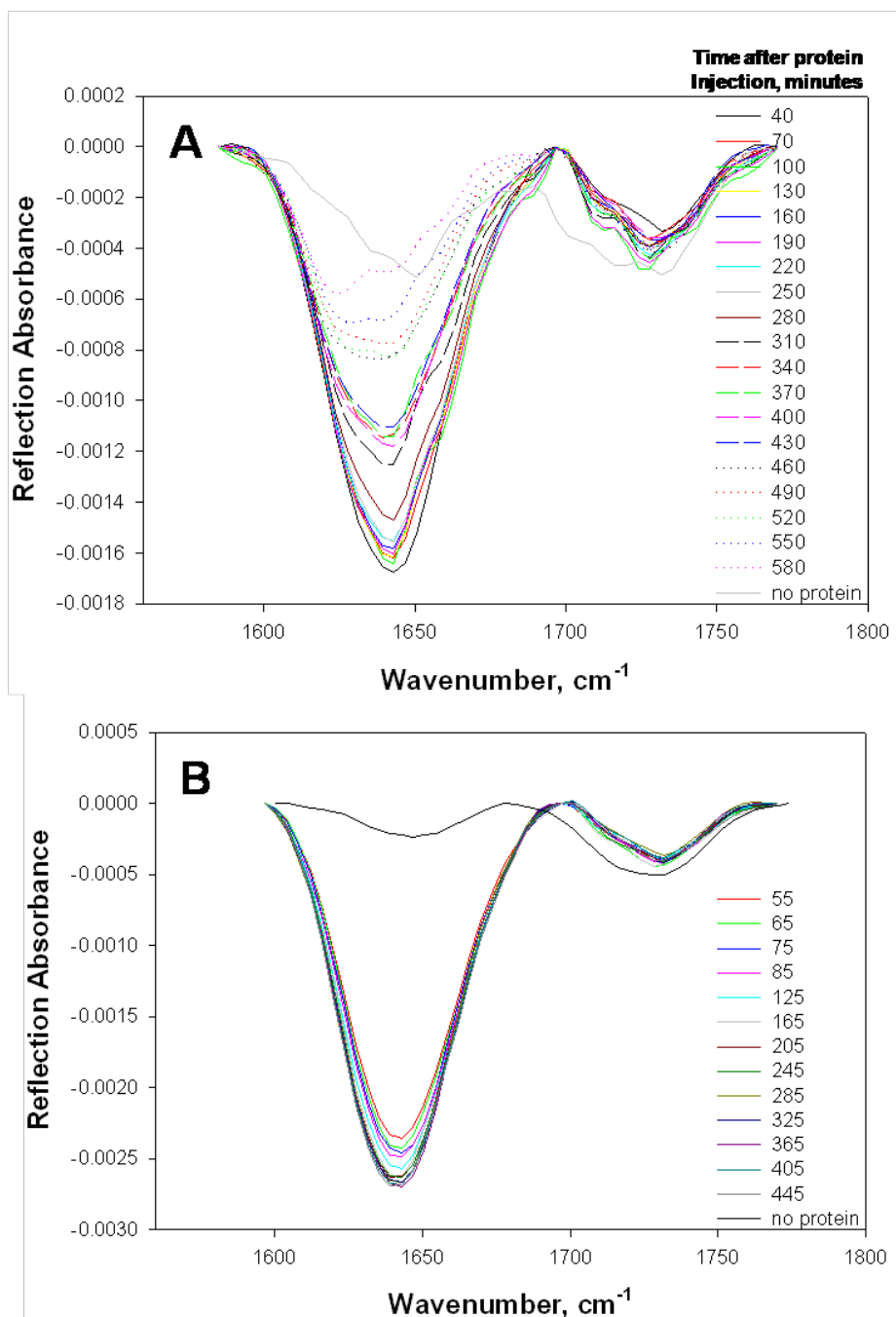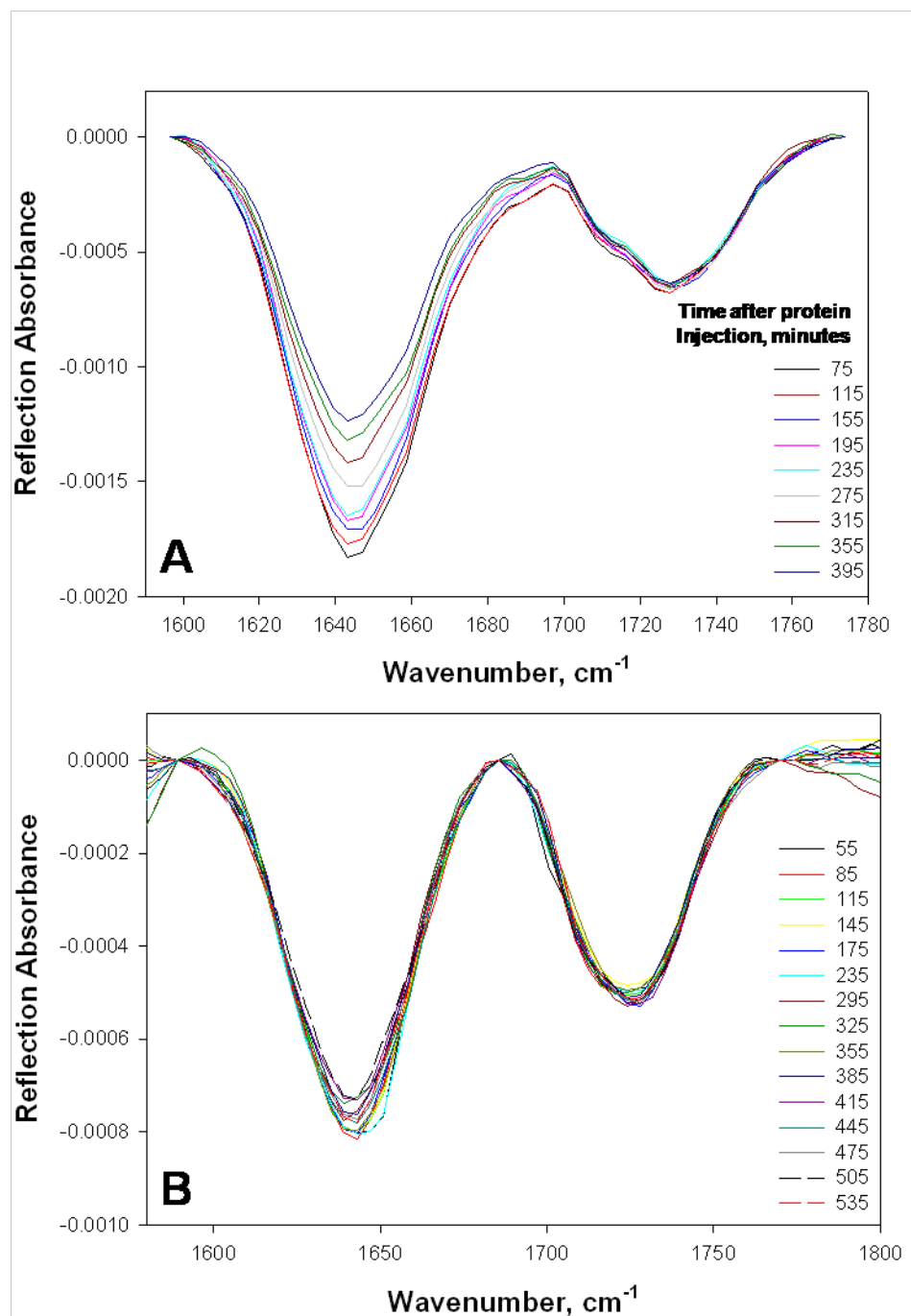
Figure 5-15. IRRAS spectra of the amide I region for N187S/PL SP-A (A) and

D215A/PL SP-A (B) injection to lipid A monolayers at 25 mN/m. A series of

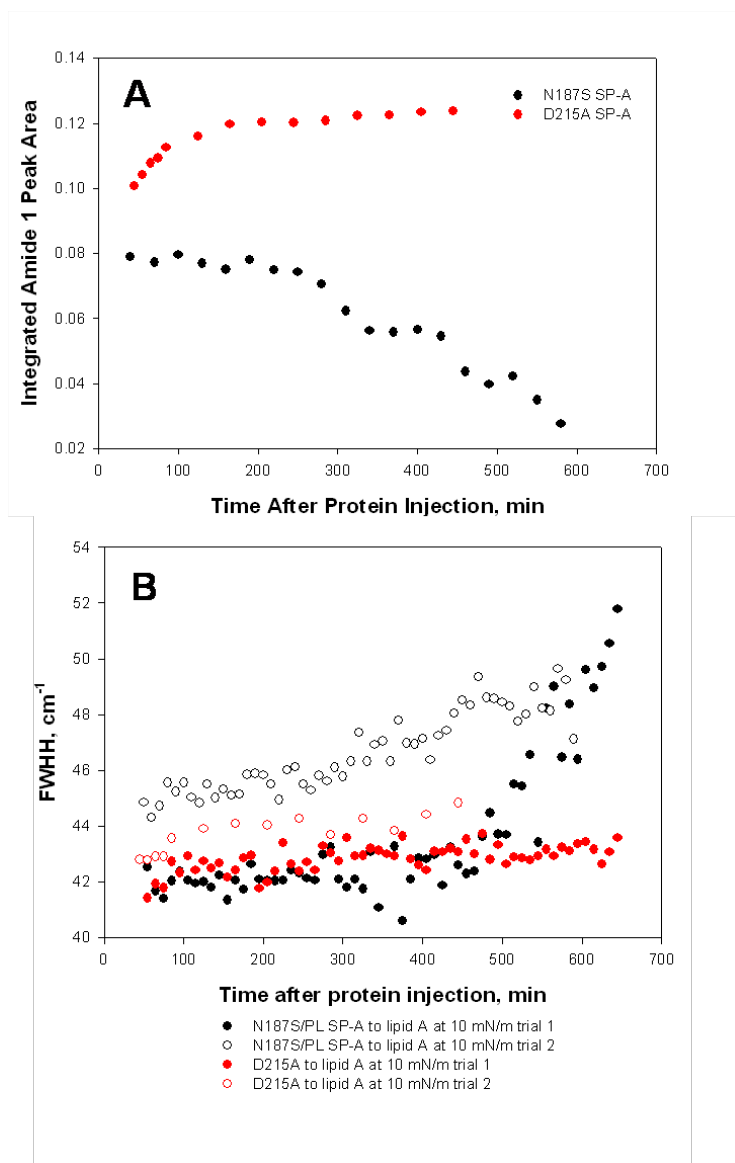spectra were taken after protein injection at the indicated time after injection.
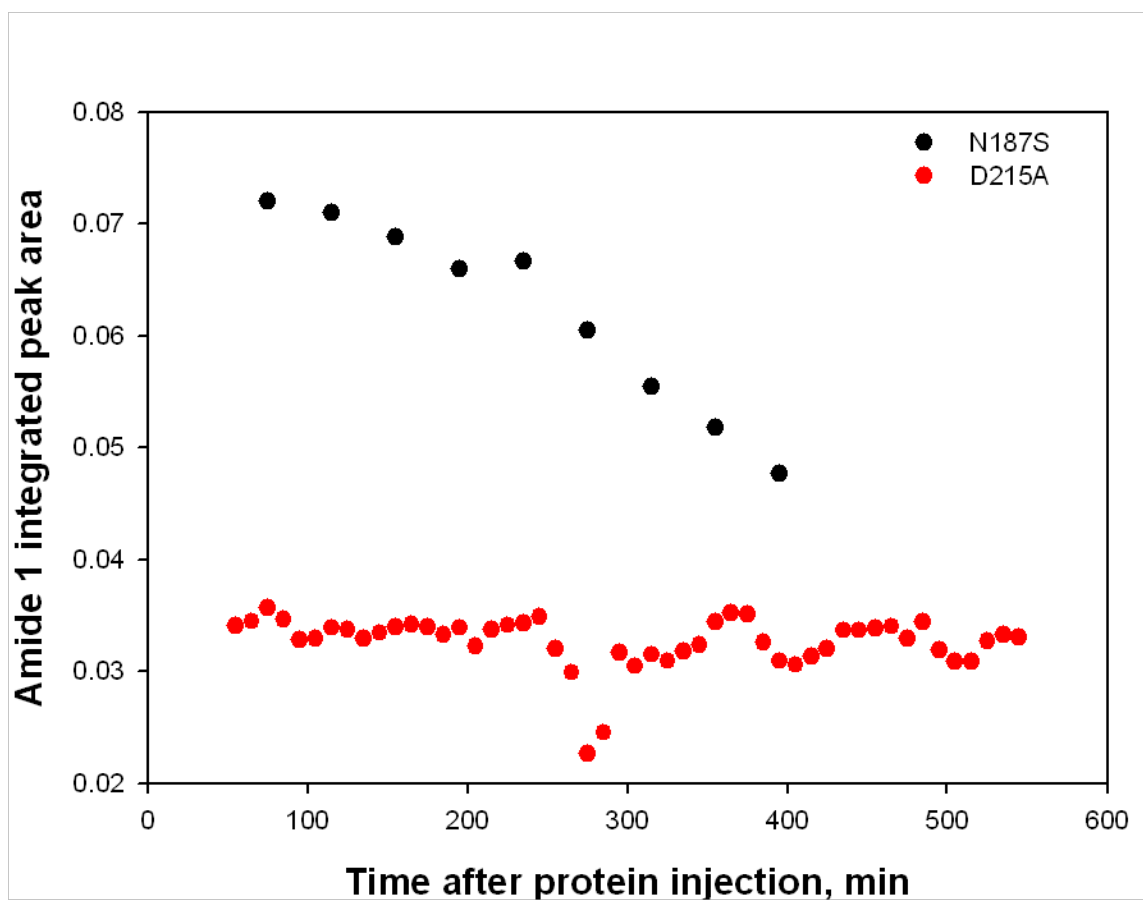
Figure 5-16. Integrated amide I peak area as a function of time for N187S/PL SP-A (black) and D215A/PL SP-A (red) injection to lipid A monolayers at 25 mN/m;

about the same for both proteins as shown in Figure 5-14. Their amide I peak intensities detected were also smaller than with lipid A monolayer at a surface pressure of 10 mN/m. As shown in Figure 5-15, N187S SP-A had an initial amide I peak intensity of 1.8 milliabsorbance, which decreased to 1.2 milliabsorbance over 6.5 hr. At a surface pressure of 25mN, the amide I band shape remained essentially unchanged for D215A SP-A, which was ~0.8 milliabsorbance and stable over ~9 hr of measurements. The stability of the amide I band is more clearly shown in Figure 5-16.

5.3 Discussion

In this chapter, IRRAS was used together with surface pressure-molecular area isotherms to study the SP-A/lipid A interaction in physiologically relevant environments. Results for Ca^{2+} mediated SP-A/lipid A interaction, acyl chain involvement in such interaction and comparison of the stability of two NCRD SP-A mutants were presented. The results can be partially rationalized in the context of SPA's proposed mode of action. Limitations of current experimental setup and further possible experimental directions are also considered.

SP-A/lipid interaction was studied in a biologically relevant monolayer state. Lipid monolayers at the air/water interface with hydrophilic protein injected underneath it are possibly one of the best ways to mimic the pathogen recognition process in the lung. SP-A exists in the aqueous sub-phase between the surfactant lipid monolayer and alveolar cell membranes in the alveoli. The

airborne pathogens contact pulmonary host defense surfactants at the air/water interface in the alveoli. Lipid A and R7 LPS are derivatives of LPS, which are the essential components of Gram-negative bacterial outer membranes (*121*). In monolayer experiments, useful physical properties of the system can be easily controlled, including monolayer lipid selection, surface pressure, protein concentration, subphase composition, temperature, pH, etc.

Surface pressure-molecular area isotherms have traditionally been combined with monolayer studies and surface pressure has been used to quantify the amount of protein adsorbed to the monolayer (*19, 122*). However, our results with the intensity measurement of amide I band from SP-A raise questions as to the validity of this approach. When SP-A was injected beneath a lipid A monolayer at 10 mN/m, the same pressure increase was observed both with and without Ca^{2+} present in the subphase, but dramatically larger amide I intensities were detected for the monolayers floating above the Ca^{2+} subphase. Similar discrepancies have also been observed by others. Clifton et al. studied a water-soluble protein found in wheat (puroindoline-b (Pin-b) and two mutants) with surface pressure and external reflectance Fourier transform infrared (ER-FTIR) spectroscopy (*123*). They found that when injecting these proteins beneath DPPG monolayers, the same amide I intensity was detected despite different surface pressure increases caused by each of them. It is believed that surface pressure measurement monitors only the surface properties, and 50% molecular surface coverage may be required before a change in surface pressure is detected when globular proteins were adsorbed to air/water interface (*124*). With

lipid monolayers present at the air/water interface, surface measurements can only detect proteins that penetrate through lipid layers and insert at the air/water interface. It is not sensitive to proteins that adsorb underneath monolayers.

In explaining the current results for SP-A/lipid A interaction, it is possible that SP-A was not only adsorbed to the available air/water interface in the presence of subphase Ca^{2+}, it was also adsorbed beneath lipid A monolayer. This portion of SP-A did not affect the surface and was not detected by surface pressure. It is reasonable to speculate that the protein adsorbed underneath lipid monolayers. Gidalevitz et al. studied the interaction of the antimicrobial peptide protegrin-a (PG-1) with biomembranes (*125*). Their X-ray reflectivity data demonstrated that PG-1 not only inserted into DPPG membrane monolayer but also adsorbed to its surface. Similarly, Garcia-Verdugo et al. observed SP-A aggregation underneath the lipid layer at the air/water interface by fluorescence (*112*). The smaller amide I band of SP-A on an EDTA-containing subphase could also be rationalized by protein denaturation and dissociation from the surface as well as by specific changes in protein orientation not detectable by s-polarized light used in the experiment. However, as shown by the NCRD SP-A stability results, the protein denaturation happened over a much longer time course than the 45-60 minutes used here. As for protein orientation, SP-A has such a complex structure with helical collagen, neck, and globular CRD domain that it is unlikely that certain orientations would align almost all the dipole moments from different oriented secondary structures perpendicular to the incident plane and thus not be detected by the s-polarized incidence to dramatically decrease the amide I

intensity. Even if such orientation was possible for SP-A/lipid A at EDTA-containing subphase, no physically logical reason could explain why SP-A would orient so differently both at the pure air/water interface and with lipid A monolayer in the presence of Ca^{2+}. Although no consensus results were arrived regarding the Ca^{2+} dependence of SP-A/lipid A interaction (*126, 127*), there was certainly no evidence showing Ca^{2+} blocking such interaction. Thus SP-A injected onto lipid A on an EDTA subphase should adopt an orientation either similar to that at a clean air/water interface (no specific protein/lipid interaction) or to that injected onto lipid A on Ca^{2+} subphase (possible specific protein/lipid interaction). But the latter two both showed much larger amide I intensities which were ~4.2-5.6 milliabsorbance units higher than the ~0.4 milliabsorbance unit observed in the absence of Ca^{2+}, after subtracting the contribution from the lipid A amide I band. To conclude the discussion, SP-A showed a Ca^{2+}-dependent, stronger and more specific (at least different) interaction with the lipid A monolayer. Considering the fact that the nonspecific adsorption of SP-A in the presence of lipid A monolayer at 10 mN/m also caused a surface pressure increase of ~5 mN/m, it is reasonable to assume that the specifically interacting SP-A is mainly adsorbed underneath the lipid A monolayer and not detectable by surface pressure changes. For the EDTA-containing subphase, SP-A was simply adsorbed nonspecifically to the available air/water interface. Such adsorption decreased the surface area available to lipid A molecules and increased the packing and conformation order of lipids to lead to a surface pressure increase. The 5 mN/m surface pressure increase along with 0.4 milliabsorbance in amide I intensity

resulted from such nonspecific adsorption could be used as baseline values to study other interactions.

The SP-A/lipid A interaction at different surface pressures and SP-A/R7 LPS interaction were studied to investigate regions of LPS recognized by SP-A. These experiments were done in the presence of subphase Ca^{2+}; the results are summarized in table 5-1. Comparing the interaction with lipid A, SP-A/R7 LPS showed 3.2 mN/m less surface pressure increase, and a 1.6 milliabsorbance weaker amide I band. Since R7 LPS has a larger headgroup than lipid A, there is less air/water interface available on R7 LPS monolayer at 10 mN/m than on lipid A monolayer. Thus less SP-A would be adsorbed to air/water interface at R7 LPS monolayer, so a smaller surface pressure increase was observed. The nonspecifically adsorbed SP-A only accounted for less than ~0.4 milliabsorbance unit (which is the amount of SP-A nonspecifically adsorbed to lipid A monolayer) decrease, the rest of 1.2 milliabsorbance was due to a smaller amount of SP-A interacting with R7. Similarly, for lipid A monolayers at 25 mN/m, more than ~1.5 milliabsorbance units in amide I intensity decrease is attributed to less protein specifically interacting with lipid A at higher surface pressure. Thus less SP-A interacts with R7 than lipid A at same surface pressure, and less with lipid A at lower surface pressures than at higher surface pressures. R7 headgroups have the same sugar composition as lipid A, and lipid A has higher headgroup concentrations at higher surface pressures. As a result, the acyl chains of R7 and lipid A at higher surface pressures are less accessible to protein than that of lipid A at lower surface pressures due to the interference caused by those larger

Table 5-1. Surface pressure increase and amide I intensity caused by SP-A injection to lipid monolayers

	Lipid A at 10 mN/m	R7 LPS at 10 mN/m	Lipid A at 25 mN/m
Surface pressure increase (mN/m)	5.4	2.2	1.0
Amide I intensity (miliabsorbance unit)	4.2	2.6	2.3

Table 5-2. Surface pressure increase and amide I intensity are caused both by SP-A nonspecifically adsorbed to the air/water interfaces and by SP-A specifically interacting with lipid monolayers.

Compared to Lipid A at 10 mN/m	R7 LPS at 10 mN/m	Lipid A at 25 mN/m
Difference in surface pressure increase	-3.2	-4.4
Difference in amide I Intensity	-1.6	-1.9
Amide I intensity difference accounted by less proteins nonspecifically adsorbed to the air/water interfaces	<0.4	<0.4
Amide I intensity difference accounted by less proteins specifically interacting with lipid monolayers	>1.2	>1.5

headgroup of R7 or closer packing at higher surface pressures. SP-A showed the strongest interaction with lipid A monolayers at 10 mN/m indicating that there are certain interactions between SP-A and the acyl chains of lipid A and R7 LPS. Since the lipid headgroups extend into the subphase and are the first to contact SP-A, the interaction between lipid headgroup and SP-A cannot be neglected. It is possible that SP-A first binds to the headgroups of lipid. It may then be followed by further interactions with the lipid acyl chains, and the latter interactions are very important.

The study on truncated proteins was intended to take advantage of the available X-ray crystallography data of SP-A. As noted earlier, NCRD SP-A is a rather complex globular protein. The amide I band resulting from its complex secondary structure has a broad contour, which shows only minor changes upon lipid binding. A modeling approach proposed by our group (*128*) is able to simulate the amide I band and subbands from individual secondary structure or domains of protein based on the three-dimensional structure obtained from X-ray or NMR. This amide I contour is a useful probe of 2-D protein conformation. Our simulation of SP-D showed that it had a neck tilt angle of 0-20° relative to the AIR/WATER surface when binding to an LPS monolayer while the tilt was ~90° in the absence of LPS (*116*). However this novel simulation approach could not be applied to NCRD SP-A/lipid systems. As shown by IRRAS spectra, native NCRD SP-A was not stable at air/water surface or when interacting with lipid A. The protein denatured with time. It is known that many proteins denature when exposed to the air/water interface due to adsorption and the unfolding process

resulting from the amphiphilic nature and marginal stability of globular proteins (*124*). Native NCRD SP-A is unstable at hydrophobic air/water interface. When the interface was covered with highly packed lipid A monolayer at 25 mN/m, NCRD SP-A stability is greatly enhanced. To determine protein conformation or orientation at interfaces, experimental data is needed to compare with simulation results. It takes up to 6 hours to collect the required data. With NCRD SP-A constantly going through conformation changes and denaturation, it is very difficult (if not impossible) to collect the data needed.

On the other hand, the point mutant D215A SP-A showed good stability at air/water interface independent of the presence of lipid monolayer. The higher stability of D215A at air/water interface might correlate with other findings in our collaborator's labs. Dr. McCormack found that the D215A mutant exhibits hyper-permeabilizing ability relative to wild type SP-A, while a series of other SP-A alanine mutants are mostly hypo-permeabilizing phenotypes (unpublished data).

Dr. Seaton's Lab has crystallized D215A and a hypo-permeabilizing E171A. These mutants exhibit structure differences in the loop region near the Ca^{2+} binding cite in the CRD. The loop formed by residues 198-203 sits between the primary and auxiliary sites in SP-A and is highly flexible in wild type SP-A (Figure 5-18, unpublished data). It is found that this loop has two alternate conformations, "closed" and "open". The two conformations appear to be interconvertible and are probably in equilibrium in wild type SP-A (Seaton, B., unpublished work). A more compact loop structure was observed in the preliminary D215A SP-A crystal structure and the loop stays further apart for
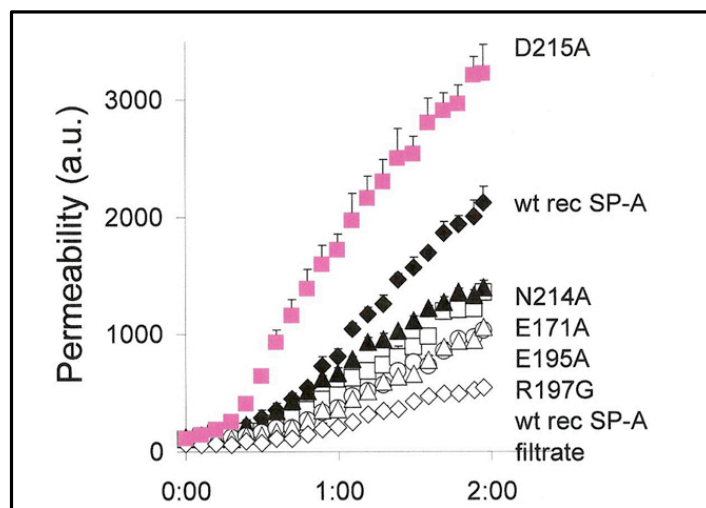
Figure 5-17. Permeabilization capabilites of NCRD mutants of SP-A
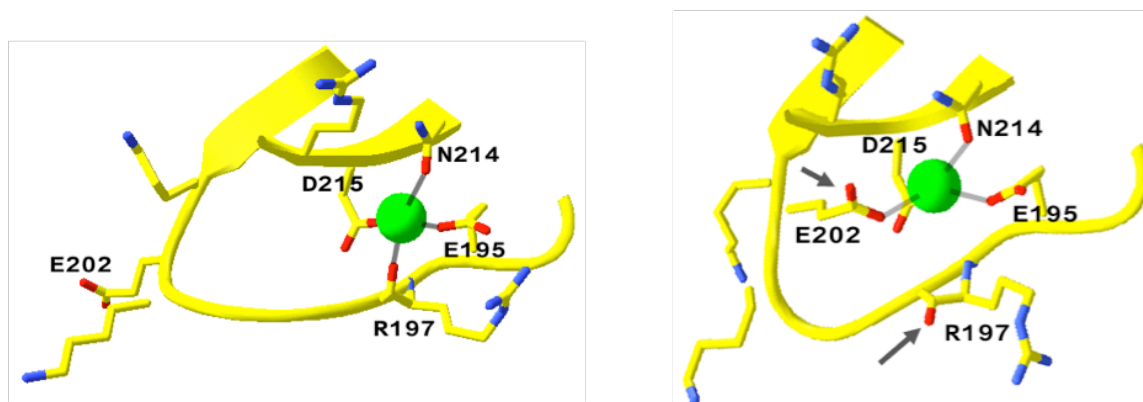
Figure 5-18. Alternate calcium coordination in SP-A: "open" (left) or "closed" (right) conformations.
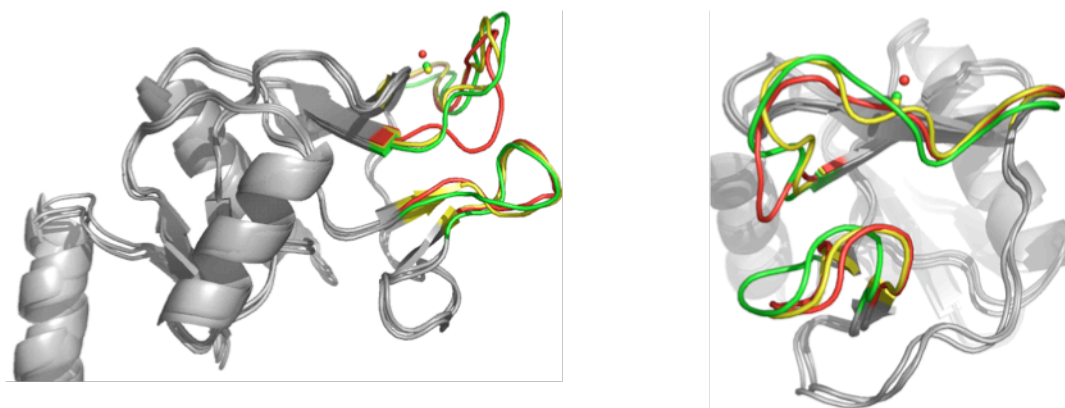
Figure 5-19. Superposition of crystal structures of SP-A NCRD monomers of WT and mutants highlight the significant conformational differences in the loop regions (upper is large loop). WT, yellow; D215A, red; E171A, green). Left: side view with part of neck helix shown, (perpendicular). Right: side view, 90° rotation around y axis from previous view. Small spheres denote lectin calcium ions.

E171A SP-A (Figure 5-19, unpublished data). This more compact loop structure might be the origin of higher physical stability and higher permeability characteristics of D215A SP-A.

In summary, this chapter showed preliminary results of SP-A/ligand interaction by IRRAS. It was clearly shown that SP-A/lipid A interacts in a Ca^{2+}-dependent manner and SP-A binds to lipid A probably by first binding to its head groups and further (possibly more importantly) interacting with acyl chains. A mutant of NCRD SP-A, D215A SP-A, was compared with its wild type counterpart and showed better stability at the interface and a stronger interaction with lipid A. The interfacial behavior of D215A might originate from its structure and leads to its hyper permeability effects. Nonspecific adsorption to the air/water interface even in the presence at lipid monolayers complicates the data interpretation of monolayer experiments. The lack of surface stability of NCRD SP-A places obstacles to simulation approach. More work with SP-A and NCRD SP-A will be carried out with (more expensive) bulk phase IR experiments.

References

1. Sun, S., Schiller, J. H., and Gazdar, A. F. (2007) Lung cancer in never smokers--a different disease, *Nat. Rev. Cancer 7*, 778-790.

2. Hawgood, S., and Clements, J. (1990) Pulmonary surfactant and its apoproteins, *J. Clin. Invest. 86*, 1-6.

3. Halliday, H. L. (2008) Surfactants: past, present and future, *J. Perinatol. 28*, S47-S56.

4. Rugonyi, S., Biswas, S. C., and Hall, S. B. (2008) The biophysical function of pulmonary surfactant, *Resp. Physiol. Neurobi. 163*, 244-255.

5. Creuwels, L., Vangolde, L., and Haagsman, H. (1997) The pulmonary surfactant system: Biochemical and clinical aspects, *Lung 175*, 1-39.

6. Wustneck, R., Perez-Gil, J., Wustneck, N., Cruz, A., Fainerman, V., and Pison, U. (2005) Interfacial properties of pulmonary surfactant layers, *Adv. Colloid Interfac. 117*, 33-58.

7. Perez-Gil, J., and Keough, K. (1998) Interfacial properties of surfactant proteins, *Biochim. Biophys. Acta-Mol. Basis Dis. 1408*, 203-217.

8. Head, J., Mealy, T., McCormack, F., and Seaton, B. (2003) Crystal structure of trimeric carbohydrate recognition and neck domains of surfactant protein A, *J. Biol. Chem. 278*, 43254-43260.

9. Wright, J. R. (2003) Pulmonary surfactant: a front line of lung host defense, *J. Clin. Invest. 111*, 1453-1455.

10. Voss, T., Eistetter, H., Schafer, K. P., and Engel, J. (1988) Macromolecular organization of natural and recombinant lung surfactant protein SP 28-36. Structural homology with the complement factor C1q, *J. Mol. Biol. 201*, 219-227.

11. Crouch, E., Persson, A., Chang, D., and Heuser, J. (1994) Molecular structure of pulmonary surfactant protein D (SP-D), *J. Biol. Chem. 269*, 17311-17319.

12. Johansson, J. (1998) Structure and properties of surfactant protein C, *Biochim. Biophys. Acta-Mol. Basis Dis. 1408*, 161-172.

13. Veldhuizen, E., and Haagsman, H. (2000) Role of pulmonary surfactant components in surface film formation and dynamics, *Biochim. Biophys. Acta-Biomembranes 1467*, 255-270.

14. Schurch, S., Green, F., and Bachofen, H. (1998) Formation and structure of surface films: captive bubble surfactometry, *Biochim. Biophys. Acta-Mol. Basis Dis. 1408*, 180-202.

15. Veldhuizen, R., Nag, K., Orgeig, S., and Possmayer, F. (1998) The role of lipids in pulmonary surfactant, *Biochim. Biophys. Acta-Mol. Basis Dis. 1408*, 90-108.

16. Goerke, J. (1998) Pulmonary surfactant: functions and molecular composition, *Biochim. Biophys. Acta-Mol. Basis Dis. 1408*, 79-89.

17. Schurch, S., Possmayer, F., Cheng, S., and Cockshutt, A. M. (1992) Pulmonary SP-A enhances adsorption and appears to induce surface sorting of lipid extract surfactant, *Am. J. Physiol. 263*, L210-L218.

18. Kuroki, Y., and Akino, T. (1991) Pulmonary surfactant protein A (SP-A) specifically binds dipalmitoylphosphatidylcholine, *J. Biol. Chem. 266*, 3068-3073.

19. Taneva, S., and Keough, K. (2000) Adsorption of pulmonary surfactant protein SP-A to monolayers of phospholipids containing hydrophobic surfactant protein SP-B or SP-C: Potential differential role for tertiary interaction of lipids, hydrophobic proteins, and SP-A, *Biochemistry 39*, 6083-6093.

20. Clements, J. A. (1962) Surface phenomena in relation to pulmonary function, *Physiologist 5*, 11-28.

21. Diemel, R. V., Snel, M. M., Waring, A. J., Walther, F. J., van Golde, L. M., Putz, G., Haagsman, H. P., and Batenburg, J. J. (2002) Multilayer formation upon compression of surfactant monolayers depends on protein concentration as well as lipid composition. An atomic force microscopy study, *J. Biol. Chem. 277*, 21179-21188.

22. Galla, H., Bourdos, N., von Nahmen, A., Amrein, M., and Sieber, M. (1998) The role of pulmonary surfactant protein C during the breathing cycle, *Thin Solid Films 327*, 632-635.

23. Wang, L., Cai, P., Galla, H., He, H., Flach, C., and Mendelsohn, R. (2005) Monolayer-multilayer transitions in a lung surfactant model: IR reflection-absorption spectroscopy and atomic force microscopy, *Eur. Biophys. J. 34*, 243-254.

24. Kingma, P., and Whitsett, J. (2006) In defense of the lung: surfactant protein A and surfactant protein D, *Curr. Opin. Pharmacol. 6*, 277-283.

25. Wright, J. (2005) Immunoregulatory functions of surfactant proteins, *Nat. Rev. Immunol. 5*, 58-68.

26. Kuroki, Y., Takahashi, M., and Nishitani, C. (2007) Pulmonary collectins in innate immunity of the lung, *Cell. Microbiol. 9*, 1871-1879.

27. Mccormack, F. X., and Whitsett, J. A. (2002) The pulmonary collectins, SP-A and SP-D, orchestrate innate immunity in the lung, *J. Clin. Invest. 109*, 707-712.

28. Wright, J. R., Borron, P., Brinker, K. G., and Folz, R. J. (2001) Surfactant Protein A: regulation of innate and adaptive immune responses in lung inflammation, *Am. J. Respir. Cell. Mol. Biol. 24*, 513-517.

29. Mingarro, I., Lukovic, D., Vilar, M., and Perez-Gil, J. (2008) Synthetic pulmonary surfactant preparations: New developments and future trends, *Curr. Med. Chem. 15*, 393-403.

30. Halliday, H. L. (1996) Natural vs synthetic surfactants in neonatal respiratory distress syndrome, *Drugs 51*, 226-237.

31.   Serrano, A. G., Cabre, E. J., Oviedo, J. M., Cruz, A., Gonzalez, B., Palacios, A., Estrada, P., and Perez-Gil, J. (2006) Production in Escherichia coli of a recombinant C-terminal truncated precursor of surfactant protein B (rproSP-B Delta C). Structure and interaction with lipid interfaces, *Biochim. Biophys. Acta 1758*, 1621-1632.

32.   Foot, N. J., Orgeig, S., Donnellan, S., Bertozzi, T., and Daniels, C. B. (2007) Positive selection in the N-terminal extramembrane domain of lung surfactant protein C (SP-C) in marine mammals, *J. Mol. Evol. 65*, 12-22.

33.   Kirshenbaum, K., Barron, A., Goldsmith, R., Armand, P., Bradley, E., Truong, K., Dill, K., Cohen, F., and Zuckermann, R. (1998) Sequence-specific polypeptoids: A diverse family of heteropolymers with stable secondary structure, *Proc. Natl. Acad. Sci. U.S.A. 95*, 4303-4308.

34.   Armand, P., Kirshenbaum, K., Goldsmith, R., Farr-Jones, S., Barron, A., Truong, K., Dill, K., Mierke, D., Cohen, F., Zuckermann, R., and Bradley, E. (1998) NMR determination of the major solution conformation of a peptoid pentamer with chiral side chains, *Proc. Natl. Acad. Sci. U.S.A. 95*, 4309-4314.

35.   Seurynck, S., Patch, J., and Barron, A. (2005) Simple, helical peptoid analogs of lung surfactant protein B, *Chem. Biol. 12*, 77-88.

36.   Brown, N. J., Wu, C. W., Seurynck-Servoss, S. L., and Barron, A. E. (2008) Effects of hydrophobic helix length and side chain chemistry on biomimicry in peptoid analogues of SP-C, *Biochemistry 47*, 1808-1818.

37.   Clements, J. A. (1957) Surface tension of lung extracts, *Proc. Soc. Exp. Biol. Med. 95*, 170-172.

38.   Kaganer, V., Mohwald, H., and Dutta, P. (1999) Structure and phase transitions in Langmuir monolayers, *Rev. Mod. Phys. 71*, 779-819.

39.   Enhorning, G. (1977) Pulsating bubble technique for evaluating pulmonary surfactant, *J. Appl. Physiol. 43*, 198-203.

40.   Banerjee, R. (2002) Surface chemistry of the lung surfactant system: Techniques for in vitro evaluation, *Curr. Sci. India 82*, 420-428.

41. Mendelsohn, R., Brauner, J., and Gericke, A. (1995) Externnal Infrared Reflection-Absorption Spectrometry monolayer films at the air-water-interface, *Annu. Rev. Phys. Chem. 46*, 305-334.

42. Gericke, A., Gadaleta, S., Brauner, J., and Mendelsohn, R. (1996) Characterization of biological samples by two-dimensional infrared spectroscopy: Simulation of frequency, bandwidth, and intensity changes, *Biospectroscopy 2*, 341-351.

43. Senak, L., Davies, M., and Mendelsohn, R. (1991) A quantitative IR study of hydrocarbon chain conformation in alkanes and phospholipids-CH2 wagging modes in disordered bilayer and HII phases, *J. Phys. Chem. 95*, 2565-2571.

44. Snyder, R., Liang, G., Strauss, H., and Mendelsohn, R. (1996) IR spectroscopic study of the structure and phase behavior of long-chain diacylphosphatidylcholines in the gel state, *Biophys. J. 71*, 3186-3198.

45. Moore, D. J., and Mendelsohn, R. (1994) Adaptation to altered growth temperatures in Acholeplasma laidlawii B: Fourier transform infrared studies of acyl chain conformational order in live cells, *Biochemistry 33*, 4080-4085.

46. Mendelsohn, R., Liang, G. L., Strauss, H. L., and Snyder, R. G. (1995) IR spectroscopic determination of gel state miscibility in long-chain phosphatidylcholine mixtures, *Biophys. J. 69*, 1987-1998.

47. Dluhy, R., and Cornell, D. (1985) In situ measurement of the infrared spectra of insoluble monolayers at the air-water interface, *J. Phys. Chem. 89*, 3195-3197.

48. Johansson, J., Curstedt, T., and Robertson, B. (1994) The proteins of the surfactant system, *Eur. Respir. J. 7*, 372-391.

49. Johansson, J., and Curstedt, T. (1997) Molecular structures and interactions of pulmonary surfactant components, *Eur. J. Biochem. 244*, 675-693.

50. Pastrana-Rios, B., Taneva, S., Keough, K. M., Mautone, A. J., and Mendelsohn, R. (1995) External reflection absorption infrared spectroscopy study of lung surfactant proteins SP-B and SP-C in phospholipid monolayers at the air/water interface, *Biophys. J. 69*, 2531-2540.

51. Pastrana-Rios, B., Flach, C., Brauner, J., Mautone, A., and Mendelsohn, R. (1994) A direct test of the squeexe-out hypothesis of lung surfactant function-External Reflection FT-IR at the air/water interface *Biochemistry 33*, 5121-5127.

52. Pison, U., Herold, R., and Schurch, S. (1996) The pulmonary surfactant system: Biological functions, components, physicochemical properties and alterations during lung disease, *Colloid. Surface. A 114*, 165-184.

53. Follows, D., Tiberg, F., Thomas, R. K., and Larsson, M. (2007) Multilayers at the surface of solutions of exogenous lung surfactant: direct observation by neutron reflection, *Biochim. Biophys. Acta 1768*, 228-235.

54. Cruz, A., Worthman, L. A., Serrano, A. G., Casals, C., Keough, K. M., and Perez-Gil, J. (2000) Microstructure and dynamic surface properties of surfactant protein SP-B/dipalmitoylphosphatidylcholine interfacial films spread from lipid-protein bilayers, *Eur Biophys J 29*, 204-213.

55. Cruz, A., Vazquez, L., Velez, M., and Perez-Gil, J. (2004) Effect of pulmonary surfactant protein SP-B on the micro- and nanostructure of phospholipid films, *Biophys. J. 86*, 308-320.

56. Bourdos, N., Kollmer, F., Benninghoven, A., Ross, M., Sieber, M., and Galla, H. J. (2000) Analysis of lung surfactant model systems with time-of-flight secondary ion mass spectrometry, *Biophys. J. 79*, 357-369.

57. Breitenstein, D., Batenburg, J. J., Hagenhoff, B., and Galla, H.-J. (2006) Lipid specificity of surfactant protein B studied by time-of-flight secondary ion mass spectrometry, *Biophys. J. 91*, 1347-1356.

58. Kramer, A., Wintergalen, A., Sieber, M., Galla, H., Amrein, M., and Guckenberger, R. (2000) Distribution of the surfactant-associated protein C within a lung surfactant model film investigated by near-field optical microscopy, *Biophys. J. 78*, 458-465.

59.   Malcharek, S., Hinz, A., Hilterhaus, L., and Galla, H. (2005) Multilayer structures in lipid monolayer films containing surfactant protein C: Effects of cholesterol and POPE, *Biophys. J. 88*, 2638-2649.

60.   Leonenko, Z., Gill, S., Baoukina, S., Monticelli, L., Doehner, J., Gunasekara, L., Felderer, F., Rodenstein, M., Eng, L. M., and Amrein, M. (2007) An elevated level of cholesterol impairs self-assembly of pulmonary surfactant into a functional film, *Biophys. J. 93*, 674-683.

61.   Wang, L., Cruz, A., Flach, C. R., Perez-Gil, J., and Mendelsohn, R. (2007) Langmuir-blodgett films formed by continuously varying surface pressure. Characterization by IR spectroscopy and epifluorescence microscopy, *Langmuir 23*, 4950-4958.

62.   Harbottle, R. R., Nag, K., McIntyre, N. S., Possmayer, F., and Petersen, N. O. (2003) Molecular organization revealed by time-of-flight secondary ion mass spectrometry of a clinically used extracted pulmonary surfactant, *Langmuir 19*, 3698-3704.

63.   Takamoto, D., Aydil, E., Zasadzinski, J., Ivanova, A., Schwartz, D., Yang, T., and Cremer, P. (2001) Stable ordering in Langmuir-Blodgett films, *Science 293*, 1292-1295.

64.   Cameron, D. G., Kauppinen, J. K., Moffatt, D. J., and Mantsch, H. H. (1982) Precision in Condensed Phase Vibrational Spectroscopy, *Appl. Spectrosc. 36*, 245-250.

65.   Rothschild, K. J., and Clark, N. A. (1979) Anomalous amide I infrared absorption of purple membrane, *Science 204*, 311-312.

66.   Schmidt, R., Steinhilber, W., Ruppert, C., Daum, C., Grimminger, F., Seeger, W., and Gunther, A. (2002) An ELISA technique for quantification of surfactant apoprotein (SP)-C in bronchoalveolar lavage fluid, *Am. J. Respir. Crit. Care Med. 165*, 470-474.

67.   Morrow, M. R., Taneva, S., Simatos, G. A., Allwood, L. A., and Keough, K. M. (1993) 2H NMR studies of the effect of pulmonary surfactant SP-C on the 1,2-dipalmitoyl-sn-glycero-3-phosphocholine headgroup: a model for transbilayer peptides in surfactant and biological membranes, *Biochemistry 32*, 11338-11344.

68.   Piknova, B., Schief, W. R., Vogel, V., Discher, B. M., and Hall, S. B. (2001) Discrepancy between phase behavior of lung surfactant phospholipids and the classical model of surfactant function, *Biophys. J. 81*, 2172-2180.

69.   Crane, J. M., and Hall, S. B. (2001) Rapid compression transforms interfacial monolayers of pulmonary surfactant, *Biophys. J. 80*, 1863-1872.

70.   Discher, B. M., Maloney, K. M., Grainger, D. W., Sousa, C. A., and Hall, S. B. (1999) Neutral lipids induce critical behavior in interfacial monolayers of pulmonary surfactant, *Biochemistry 38*, 374-383.

71.   Schief, W. R., Antia, M., Discher, B. M., Hall, S. B., and Vogel, V. (2003) Liquid-crystalline collapse of pulmonary surfactant monolayers, *Biophys J 84*, 3792-3806.

72.   Cochrane, C. G., Revak, S. D., Merritt, T. A., Heldt, G. P., Hallman, M., Cunningham, M. D., Easa, D., Pramanik, A., Edwards, D. K., and Alberts, M. S. (1996) The efficacy and safety of KL4-surfactant in preterm infants with respiratory distress syndrome, *Am. J. Respir. Crit. Care Med. 153*, 404-410.

73.   Cochrane, C. G., Revak, S. D., Merritt, T. A., Schraufstatter, I. U., Hoch, R. C., Henderson, C., Andersson, S., Takamori, H., and Oades, Z. G. (1998) Bronchoalveolar lavage with KL4-surfactant in models of meconium aspiration syndrome, *Pediatr. Res. 44*, 705-715.

74.   Walther, F. J., Waring, A. J., Sherman, M. A., Zasadzinski, J. A., and Gordon, L. M. (2007) Hydrophobic surfactant proteins and their analogues, *Neonatology 91*, 303-310.

75.   Wu, C., Seurynck, S., Lee, K., and Barron, A. (2003) Helical peptoid mimics of lung surfactant protein C, *Chem. Biol. 10*, 1057-1063.

76.   Wu, C., Sanborn, T., Zuckermann, R., and Barron, A. (2001) Peptoid oligomers with alpha-chiral, aromatic side chains: Effects of chain length on secondary structure, *J. Am. Chem. Soc. 123*, 2958-2963.

77.   Wu, C., Sanborn, T., Huang, K., Zuckermann, R., and Barron, A. (2001) Peptoid oligomers with alpha-chiral, aromatic side chains: Sequence requirements for the formation of stable peptoid helices, *J. Am. Chem. Soc. 123*, 6778-6784.

78.   von Nahmen, A., Schenk, M., Sieber, M., and Amrein, M. (1997) The structure of a model pulmonary surfactant as revealed by scanning force microscopy, *Biophys. J. 72*, 463-469.

79.   Ding, J., Takamoto, D., von Nahmen, A., Lipp, M., Lee, K., Waring, A., and Zasadzinski, J. (2001) Effects of lung surfactant proteins, SP-B and SP-C, and palmitic acid on monolayer stability, *Biophys J 80*, 2262-2272.

80.   Flach, C., Brauner, J., and Mendelsohn, R. (1993) Calcium-ion interactions with insoluble phospholipid monolayer films at the A/W interface-External reflection-absorption IR studies, *Biophys. J. 65*, 1994-2001.

81.   Flach, C., Brauner, J., Taylor, J., Baldwin, R., and Mendelsohn, R. (1994) External reflection FTIR of peptide monolayer films in-situ at the air/water interface-experimetnal design, spectra-structure correaltions, and effects of hydrogen-deuterium exchange, *Biophys. J. 67*, 402-410.

82.   Gericke, A., Flach, C. R., and Mendelsohn, R. (1997) Structure and orientation of lung surfactant SP-C and L-alpha-dipalmitoylphosphatidylcholine in aqueous monolayers, *Biophys. J. 73*, 492-499.

83.   Xu, Z., Brauner, J., Flach, C., and Mendelsohn, R. (2004) Orientation of peptides in aqueous monolayer films. Infrared reflection-absorption spectroscopy studies of a synthetic amphipathic beta-sheet, *Langmuir 20*, 3730-3733.

84.   Flach, C., Xu, Z., Bi, X., Brauner, J., and Mendelsohn, R. (2001) Improved IRRAS apparatus for studies of aqueous monolayer films: Determination of the orientation of each chain in a fatty-acid homogeneous ceramide 2, *Appl. Spectrosc. 55*, 1060-1066.

85.   Mao, G., Desai, J., Flach, C. R., and Mendelsohn, R. (2008) Structural characterization of the monolayer-multilayer transition in a pulmonary

surfactant model: IR studies of films transferred at continuously varying surface pressures, *Langmuir 24*, 2025-2034.

86. Cochrane, C. G., and Revak, S. D. (1991) Pulmonary surfactant protein B (SP-B): structure-function relationships, *Science 254*, 566-568.

87. Lal, M. K., and Sinha, S. K. (2008) Surfactant respiratory therapy using Surfaxin/sinapultide, *Ther. Adv. Respir. Dis. 2*, 339-344.

88. Takei, T., Hashimoto, Y., Ohtsubo, E., Sakai, K., and Ohkawa, H. (1996) Characterization of poly-leucine substituted analogues of the human surfactant protein SP-C, *Biol. Pharm. Bull. 19*, 1550-1555.

89. Otsubo, E., and Takei, T. (2002) Effects of the human pulmonary surfactant protein-C (SP-C), SP-CL16(6-28) on surface activities of surfactants with various phospholipids, *Biol. Pharm. Bull. 25*, 1303-1306.

90. Gupta, G., and Surolia, A. (2007) Collectins: sentinels of innate immunity, *Bioessays. 29*, 452-464.

91. Hussain, S. (2004) Role of surfactant protein A in the innate host defense and autoimmunity, *Autoimmunity 37*, 125-130.

92. Korfhagen, T., LeVine, A., and Whitsett, J. (1998) Surfactant protein A (SP-A) gene targeted mice, *Biochim. Biophys. Acta-Mol. Basis Dis. 1408*, 296-302.

93. McCormack, F. X. (2001) Functional mapping of surfactant protein A, *Pediatr. Pathol. Mol. M. 20*, 293-318.

94. Sano, H., and Kuroki, Y. (2005) The lung collectins, SP-A and SP-D, modulate pulmonary innate immunity, *Mol. Immunol. 42*, 279-287.

95. McCormack, F. X. (1998) Structure, processing and properties of surfactant protein A, *Biochim. Biophys. Acta 1408*, 109-131.

96.   Kishore, U., Wang, J., Hoppe, H., and Reid, K. (1996) The alpha-helical neck region of human lung surfactant protein D is essential for the binding of the carbohydrate recognition domains to lipopolysaccharides and phospholipids, *Biochem. J. 318*, 505-511.

97.   van de Wetering, J. K., van Golde, L. M., and Batenburg, J. J. (2004) Collectins: players of the innate immune system, *Eur. J. Biochem. 271*, 1229-1249.

98.   Korfhagen, T., Bruno, M., Ross, G., Huelsman, K., Ikegami, M., Jobe, A., Wert, S., Stripp, B., Morris, R., Glasser, S., Bachurski, C., Iwamoto, H., and Whitsett, J. (1996) Altered surfactant function and structure in SP-A gene targeted mice, *Proc. Natl. Acad. Sci. U.S.A. 93*, 9594-9599.

99.   Linke, M., Harris, C., Korfhagen, T., McCormack, F., Ashbaugh, A., Steele, P., Whitsett, J., and Walzer, P. (2001) Immunosuppressed surfactant protein A-deficient mice have increased susceptibility to Pneumocystis carinii infection, *J. Infect. Dis. 183*, 943-952.

100.   García-Verdugo, I., Sánchez-Barbero, F., Soldau, K., Tobias, P. S., and Casals, C. (2005) Interaction of SP-A (surfactant protein A) with bacterial rough lipopolysaccharide (Re-LPS), and effects of SP-A on the binding of Re-LPS to CD14 and LPS-binding protein, *Biochem. J. 391*, 115-124.

101.   McCormack, F., Damodarasamy, M., and Elhalwagi, B. (1999) Deletion mapping of N-terminal domains of surfactant protein A - The N-terminal segment is required for phospholipid aggregation and specific inhibition of surfactant secretion, *J. Biol. Chem. 274*, 3173-3181.

102.   McCormack, F. X., Festa, A. L., Andrews, R. P., Linke, M., and Walzer, P. D. (1997) The carbohydrate recognition domain of surfactant protein A mediates binding to the major surface glycoprotein of Pneumocystis carinii, *Biochemistry 36*, 8092-8099.

103.   Palaniyar, N., Ikegami, M., Korfhagen, T., Whitsett, J., and McCormack, F. (2001) Domains of surfactant protein A that affect protein oligomerization, lipid structure and surface tension, *Comp. Biochem. Phys. A 129*, 109-127.

104. Palaniyar, N., Zhang, L., Kuzmenko, A., Ikegami, M., Wan, S., Wu, H., Korfhagen, T., Whitsett, J., and McCormack, F. (2002) The role of pulmonary collectin N-terminal domains in surfactant structure, function, and homeostasis in vivo, *J. Biol. Chem. 277*, 26971-26979.

105. Kuroki, Y., McCormack, F., Ogasawara, Y., Mason, R., and Voelker, D. (1994) Epitope mapping for monoclonal-antibodies identifies functional domains of pulmonary surfactant protein-A that interact with lipids, *J. Biol. Chem. 269*, 29793-29800.

106. McCormack, F. X., Y, K., Stewart, J. J., Mason, R. J., and Voelker, D. R. (1994) Surfactant protein A amino acids Glu195 and Arg197 are essential for receptor binding, phospholipid aggregation, regulation of secretion, and the facilitated uptake of phospholipid by type II cells, *J. Biol. Chem. 269*, 29801-29807.

107. Pattanajitvilai, S., Kuroki, Y., Tsunezawa, W., McCormack, F. X., and Voelker, D. R. (1998) Mutational analysis of Arg197 of rat surfactant protein A. His197 creates specific lipid uptake defects, *J. Biol. Chem. 273*, 5702-5707.

108. Tsunezawa, W., Sano, H., Sohma, H., McCormack, F., Voelker, D., and KUROKI, Y. (1998) Site-directed mutagenesis of surfactant protein A reveals dissociation of lipid aggregation and lipid uptake by alveolar type II cells, *Biochim. Biophys. Acta-Protein Struct. M. 1387*, 433-446.

109. Haagsman, H., Sargeant, T., Hauschka, P., Benson, B., and Hawgood, S. (1990) Binding of calcium to SP-A, a surfactant-associated protein, *Biochemistry 29*, 8894-8900.

110. Ridsdale, R. A., Palaniyar, N., Holterman, C. E., Inchley, K., Possmayer, F., and Harauz, G. (1999) Cation-mediated conformational variants of surfactant protein A, *Biochim. Biophys. Acta 1453*, 23-34.

111. Palaniyar, N., McCormack, F. X., Possmayer, F., and Harauz, G. (2000) Three-dimensional structure of rat surfactant protein A trimers in association with phospholipid monolayers, *Biochemistry 39*, 6310-6316.

112. García-Verdugo, I., Cañadas, O., Taneva, S. G., Keough, K. M. W., and Casals, C. (2007) Surfactant protein A forms extensive lattice-like

structures on 1,2-dipalmitoylphosphatidylcholine/rough-lipopolysaccharide-mixed monolayers, *Biophys. J. 93*, 3529-3540.

113. van de Wetering, J., van Eijk, M., van Golde, L., Hartung, T., van Strijp, J., and Batenburg, J. (2001) Characteristics of surfactant protein a and D binding to lipoteichoic acid and peptidoglycan, 2 major cell wall components of Gram-positive bacteria, *J. Infect. Dis. 184*, 1143-1151.

114. Wang, H., Head, J., Kosma, P., Brade, H., Mueller-Loennies, S., Sheikh, S., McDonald, B., Smith, K., Cafarella, T., Seaton, B., and Crouch, E. (2008) Recognition of heptoses and the inner core of bacterial lipopolysaccharides by surfactant protein D, *Biochemistry 47*, 710-720.

115. Kerth, A., Erbe, A., Dathe, M., and Blume, A. (2004) Infrared reflection absorption spectroscopy of amphipathic model peptides at the air/water interface, *Biophys. J. 86*, 3750-3758.

116. Wang, L., Brauner, J. W., Mao, G., Crouch, E., Seaton, B., Head, J., Smith, K., Flach, C. R., and Mendelsohn, R. (2008) Interaction of recombinant surfactant protein D with lipopolysaccharide: Conformation and orientation of bound protein by IRRAS and simulations, *Biochemistry 47*, 8103-8113.

117. Brandenburg, K., Funari, S. S., Koch, M. H., and Seydel, U. (1999) Investigation into the acyl chain packing of endotoxins and phospholipids under near physiological conditions by WAXS and FTIR spectroscopy, *J. Struct. Biol. 128*, 175-186.

118. Ikegami, M., Elhalwagi, B. M., Palaniyar, N., Dienger, K., Korfhagen, T., Whitsett, J. A., and McCormack, F. X. (2001) The collagen-like region of surfactant protein A (SP-A) is required for correction of surfactant structural and functional defects in the SP-A null mouse, *J. Biol. Chem. 276*, 38542-38548.

119. McCormack, F. X., Stewart, J., Voelker, D. R., and Damodarasamy, M. (1997) Alanine mutagenesis of surfactant protein A reveals that lipid binding and pH-dependent liposome aggregation are mediated by the carbohydrate recognition domain, *Biochemistry 36*, 13963-13971.

120. McCormack, F., Gibbons, R., Ward, S., Kuzmenko, A., Wu, H., and Deepe, G. (2003) Macrophage-independent fungicidal action of the pulmonary collectins, *J. Biol. Chem. 278*, 36250-36256.

121. Brandenburg, K., and Wiese, A. (2004) Endotoxins: Relationships between structure, function, and activity, *Curr. Top. Med. Chem. 4*, 1127-1146.

122. Lad, M. D., Birembaut, F., Frazier, R. A., and Green, R. J. (2005) Protein-lipid interactions at the air/water interface, *Phys. Chem. Chem. Phys. 7*, 3478-3485.

123. Clifton, L. A., Lad, M. D., Green, R. J., and Frazier, R. A. (2007) Single amino acid substitutions in puroindoline-b mutants influence lipid binding properties, *Biochemistry 46*, 2260-2266.

124. Tripp, B. C., Magda, J. J., and Andrade, J. D. (1995) Adsorption of Globular-Proteins at the Air/Water Interface as Measured Via Dynamic Surface-Tension - Concentration-Dependence, Mass-Transfer Considerations, and Adsorption-Kinetics, *J. Colloid Interf. Sci. 173*, 16-27.

125. Gidalevitz, D., Ishitsuka, Y., Muresan, A., Konovalov, O., Waring, A., Lehrer, R., and Lee, K. (2003) Interaction of antimicrobial peptide protegrin with biomembranes, *Proc. Natl. Acad. Sci. U.S.A. 100*, 6302-6307.

126. Kalina, M., Socher, R., Rotem, R., and Naor, Z. (1995) Ultrastructural localization of protein kinase C in human sperm, *J. Histochem. Cytochem. 43*, 439-445.

127. Sano, H., Chiba, H., Iwaki, D., Sohma, H., Voelker, D. R., and Kuroki, Y. (2000) Surfactant proteins A and D bind CD14 by different mechanisms, *J. Biol. Chem. 275*, 22442-22451.

128. Brauner, J., Flach, C., and Mendelsohn, R. (2005) Quantitative reconstruction of the amide I contour in the IR spectra of globular proteins: From structure to spectrum, *J. Am. Chem. Soc. 127*, 100-109.

Curriculum Vitae

1983	Born April 14th in Inner Mongolia, China.
1997-2000	Wulanhaote First High School, Inner Mongolia, China.
2000-2004	B. S. in Chemistry, Peking University, Beijing, China.
2003-2004	Research in surface and colloid chemistry, Peking University, China.
2004-2010	Ph. D. in Chemistry, Rutgers University, Newark, New Jersey.
2004-2006	Teaching assistant, Department of Chemistry, Rutgers University.
2007-2010	Graduate assistant, Graduate School-Newark, Rutgers University.
2007	Article: Lu, T., Han, F., **Mao, Guangru**, Lin, G., Huang, J., Huang, X., Wang, Y., Fu, H., "Effect of Hydrocarbon Parts of the Polar Headgroup on Surfactant Aggregates in Gemini and Bola Surfactant Solutions." *Langmuir,* 23, 2932-2936.
2008	Article: **Mao, Guangru**, Desai, J., Flach, C. R., Mendelsohn, R., "Structural Characterization of the Monolayer-Multilayer Transition in a Pulmonary Surfactant Model: IR Studies of Films Transferred at Continuously Varying Surface Pressures." *Langmuir,* 24, 2025-2034.
2008	Article: Wang, L., Brauner, J. W., **Mao, Guangru**, Crouch, E., Seaton, B., Head, J., Smith, K., Flach, C. R., Mendelsohn, R., "Interaction of Recombinant Surfactant Protein D with Lipopolysaccharide: Conformation and Orientation of Bound Protein by IRRAS and Simulations." *Biochemistry,* 47, 8103-8113.
2010	Article: Mendelsohn, R., **Mao, Guangru,** Flach, C. R., "Infrared Reflection-Absorption Spectroscopy: Principles and Applications to Lipid-Protein Interaction in Langmuir Films." Biochimica et Biophysica Acta, 1798, 788-800.